R. & M. No. 3538


MINISTRY OF TECHNOLOGY



AERONAUTICAL RESEARCH COUNCIL
REPORTS AND MEMORANDA

# Measurements of the Performance of a Turbo-jet Engine with Reheat (Rolls Royce RA28R Avon) in High-speed Flight and under Simulated Conditions in Test Beds

By A. A. WOODFIELD, B.Sc. (Eng.), A.C.G.I., ANN CRONIN and GLYNIS VORLEY

LONDON: HER MAJESTY'S STATIONERY OFFICE
1968
PRICE £1 8*s.* 0*d.* NET

# Measurements of the Performance of a Turbo-jet Engine with Reheat (Rolls Royce RA28R Avon) in High-speed Flight and under Simulated Conditions in Test Beds

By A. A. WOODFIELD, B.Sc. (Eng.), A.C.G.I., ANN CRONIN and GLYNIS VORLEY

*Reports and Memoranda No.* 3538*
*February*, 1966

*Summary.*

The performance of a turbo-jet engine has been measured, and alternative methods of determining gross thrust and air mass flow calibrated in a ground level static test bed and an altitude test bed simulating flight conditions. The agreement between the two test beds is very good. It is shown that if it is necessary to extrapolate calibrations to flight conditions, this may be made most accurately in terms of 'effective areas'.

The preferred method of measuring gross thrust in flight is that based on the final nozzle static pressure measurements. The measurements of air mass flow required to convert gross thrust to net thrust are subject to quite large random errors, but the method based on the measurements from the transition section between the turbine and jet pipe is easiest to apply, and it should be possible to improve its accuracy. Using these methods, random errors of the order $\pm 4$ per cent for net thrust determination can be expected.

Comparison of 'non-dimensional' performance measured in flight, and in the test beds, was good for non-reheat conditions, but significant differences were noted for the reheat results. It is believed that these differences were due to the effects of the intake on the reheat fuel control unit in flight. The accuracy of net thrust in flight determined by the 'non-dimensional' method is of the same order as that based on the detailed calibrations for the non-reheat conditions, but would have a systematic error of 10 per cent for reheat conditions.

LIST OF CONTENTS



*Replaces R.A.E. Tech. Report No. 66 060—A.R.C. 27 873.

LIST OF CONTENTS—*continued*

1. *Introduction.*

One of the most important quantities required in the determination of the aerodynamic drag from flight tests on aircraft is the engine net thrust. For turbo-jet engines the net thrust is deduced from the difference between the gross thrust and the momentum of the air entering the engine, the latter being determined from measurements of air mass flow. The gross thrust and mass flow are usually obtained from measurements of total and static pressure and total temperature in the jet pipe close to the final nozzle; this requires the calibration of the engine on a test bed. Until relatively recently most of these calibrations were made in ground level static test beds. In this type of test bed it is not possible to simulate completely the conditions an engine experiences when installed in an aircraft flying at high speeds and altitudes, and thus it is necessary to extrapolate the calibration. The validity of this extrapolation must always be regarded with some doubt, particularly as the thrust of current turbo-jet engines is increasing the speed and altitude capability of aircraft and thus requiring a very large extrapolation of the calibration. More recently altitude test beds have become available that are able to simulate more closely flight conditions at high speed and altitude and in these cases extrapolation of the calibrations is not required. However, even in these test beds, it is not possible to simulate completely the conditions an engine experiences when installed in an aircraft. For example, in the 'connected-jet' type of altitude test bed air is usually even in these test beds, it is not possible to simulate completely the conditions an engine experiences when installed in an aircraft. For example, in the 'connected-jet' type of altitude test bed air is usually delivered to the compressor entry at uniform conditions and any flow distortions created by the intake are not represented; also the external flow is not correctly represented and this may affect conditions at the jet exit. In the 'free-jet' type of altitude test bed the air intake is represented and thus flight conditions are more closely simulated. No matter how carefully these test beds are designed it is important to check that the answers they produce are consistent with flight results. This type of exercise is very expensive as it involves a considerable amount of test bed and flight testing time and also requires very careful interpretation. Probably for these reasons such checks are seldom undertaken, but it is important that they are made periodically. This is particularly so when new generation engines are being tested, for example the current by-pass type, as they may possibly not have the same correlation as experienced with the earlier type of turbo-jet engine considered in this Report.

With this object in mind a series of flight and test-bed experiments have been made on a Rolls Royce RA28R Avon engine. This engine has been installed in the Fairey Delta 2 supersonic research aircraft, and, as the engine thrust has to be measured to obtain aircraft drag, the opportunity was taken to obtain more detailed engine measurements. The engine has been specially instrumented to provide two alternative methods of measuring gross thrust and three methods of measuring mass flow. Although the RA28R engine is not entirely representative of current engine designs, most of the results are thought to be relevant to turbo-jet engine in general. Nevertheless, it is important to make similar tests on current engine designs, as these are essential if the total aerodynamic drag of aircraft is to be measured in flight. The RA28R engine is equipped with reheat, and thus a useful opportunity was available to check methods of measuring thrust on this type of engine. The main difficulty in this case is obtaining the necessary measurements in the hot exhaust gas stream which is at more than 1500 deg C. At this temperature uncooled fixed pitot or temperature probes would not survive, and the provision of cooling is not practical in an aircraft installation. Only the use of static-pressure tappings is possible in the jet pipe and only the gross thrust can be obtained from these. However, an uncooled probe which traverses the jet efflux immediately downstream of the final nozzle can be used, and has been used in these tests to give values

of the pressures and temperatures in the jet. The sequence of the tests was,

(i) pre-flight ground level static tests, Glen test bed*

(ii) flight tests, Fairey Delta 2 aircraft

(iii) post-flight ground level static tests, Glen test bed

(iv) pre-altitude test bed ground level static tests, Glen test bed

(v) altitude tests, Cell 3 Altitude test bed*.

The first series of ground-level static tests has been reported in Ref. 1. The results of the five test series are compared in the present Report, which investigates the accuracy and consistency of the measurements obtained in the two test beds; compares the various methods used to measure gross thrust and air mass flow in flight, and compares the engine 'non-dimensional' performance as measured in the flight tests and in the test beds. The analysis of the traverse-probe measurements has presented certain difficulties, mainly due to the significant pressure measuring errors encountered when the flow is inclined relative to the pitot-static tube, as is the case for flight conditions of jet expansion, and also due to the asymmetric temperature distribution at the final nozzle, and thus only a limited analysis has been attempted at this stage. A more detailed analysis of the traverse probe measurements will be reported separately.

The results from thrustmeters installed to measure engine trunnion thrust in the flight tests[2] were wholly unsatisfactory, probably because of significant engine constraints produced by the jet pipe supports, and none of the results are presented.

## 2. *Description of the Engine and Test Beds.*

### 2.1. *The Engine.*

The engine tested, a Rolls Royce RA28R Avon, is a single spool axial compressor turbo-jet engine with reheat and powers the Fairey Delta 2 supersonic research aircraft, Fig. 1. A general view of the engine installed in the ground-level static test bed is shown in Fig. 2. Engine rating and geometric data are given in Table 1. The jet pipe has a two position final nozzle throat which is closed to its minimum area or opened to its maximum for non-reheat and reheat operation respectively, Fig. 3. The reheat fuel system is scheduled to maintain a constant turbine pressure ratio by the reheat fuel control unit; the pressure ratio setting on this control unit can be varied.

There is a limited control of thrust with reheat by throttling the engine, but in flight the reheat is automatically cancelled if the engine speed is reduced below 92·5 per cent (100 per cent = 8000 r.p.m.). Also a maximum-temperature controller is fitted which, together with the mechanical engine speed governor, prevents the engine from exceeding either the maximum jet pipe temperature of 685°C or the maximum speed of 101·2 per cent r.p.m. The maximum-temperature controller was not fitted for the ground tests.

The engine is fitted with variable incidence compressor inlet swirl vanes to prevent surging during engine accelerations at intermediate engine speeds. The vanes are automatically adjusted from $+25°$ to $-10°$ over an intermediate speed range, which is dependent on intake total temperature. At the standard sea-level static temperature of 288°K, the range is set from 81 per cent to 92 per cent r.p.m.

Ideally the vanes would operate within a fixed range of engine 'non-dimensional' speed, $N/\sqrt{T_{1_t}}$ ($N$ = engine speed, $T_{1_t}$ = intake total temperature). However, the control law only provides an approximation to this, giving adequate temperature compensation throughout the flight envelope.

The engine and jet-pipe instrumentation used in the tests is similar to that described in the earlier ground-level static-calibration report[1], and is listed in Table 2. Various pressures, temperatures and fuel flows were measured at the engine and jet-pipe reference planes defined in Fig. 4. In addition, the variation of the total and static pressure and total temperature of the jet efflux, immediately downstream of the final nozzle, was measured by a traversing probe. In the ground tests the instrumentation was connected to manometers and dial instruments in the usual manner, and, in the flight tests, to dial instruments on an automatic-observer panel.

*Details of these test beds are given in Sections 2.2 and 2.3.

2.2. *Ground-level Static Test Bed (The Glen Test Bed, N.G.T.E.).*

This test bed has been designed for the testing of engines under ground-level static conditions and is thus open to the atmosphere. Air enters the test bed through flow straightening and silencing splitter plates, and turbulence is reduced by a contraction before the test section. The engine, with a calibrated bellmouth intake, is mounted on a platform floating on oil bearings and constrained in the longitudinal direction by the thrust measuring weighbridge. A general view of the engine on the test bed is shown in Fig. 2. The air velocity through the test bed is less than 40 ft/sec at the maximum reheat thrust, the corresponding test-bed depression being approximately 0·5 inch of water. The jet efflux and induced air flow leave the test bed *via* a detuner.

The ambient pressure and temperature of the air at entry conditions, the mass flows of the air and fuel entering the engine, and the thrust were measured. Of these, the most important quantities are the thrust and air mass flow and although considerable care has been taken in their evaluation, some small residual errors may remain.

Following the normal test-bed practice the engine gross thrust has been assumed equal to the thrust measured by the weighbridge. This assumption is not necessarily valid and may introduce small errors of the order of 1 per cent. The measurement of thrust on the test bed is considered in more detail in Appendix A.

The air mass flow is deduced from the pressure drop in the calibrated bellmouth, and, as the bellmouth had been calibrated without the starter cable strut there may be a small but probably not significant change in the calibration.

2.3. *Altitude Test Bed (Cell 3, N.G.T.E.).*

This test bed has been designed to test engines under simulated flight conditions over a wide range of Mach number and altitude. It is of the connected jet type with air at nominally steady conditions piped directly to the compressor face and suction applied to the main body of the test bed. The engineering details of the test bed are described in Ref. 3, and the general arrangement of the test bed is shown in Fig. 5. Air is supplied to the plenum chamber and passes through a venturi air-flow measuring section to the engine. The engine, jet pipe and the final section of air delivery ducting are mounted on a platform supported on oil bearings and constrained in the longitudinal direction by thrust-measuring capsules. The connection between the fixed intake ducting and that mounted on the thrust-measuring platform is a slip joint of small radial clearance with the free ducting supported by leaf springs giving full vertical and lateral constraint and a minimum of longitudinal constraint. The thrust capsules were calibrated with this slip joint connected. Part of the air supply to the plenum chamber is diverted through the by-pass valves to provide cooling air for the exterior of the engine and jet pipe and to prevent the hot exhaust gases from recirculating into the body of the test bed. In these tests the velocity of the cooling air was only slightly higher than that in the ground-level static test bed, although the level of turbulence was considerably higher.

The instrumentation for measuring compressor entry conditions, air mass flow and thrust is similar to that used on the ground-level static test bed. The air mass flow is obtained from measurements of total and static pressures and total temperatures in the venturi measuring section (Fig. 5). The total pressure and temperature of the air entering the compressor is measured approximately four feet ahead of the compressor face in the 32 inch diameter parallel duct. The velocity distribution across this duct is measured approximately five feet ahead of the compressor. The resulting longitudinal thrust acting on the oil borne platform is obtained from the hydraulic load capsules. Two capsules are used with a preload applied to the system to eliminate backlash, as negative thrust conditions can occur at certain combinations of high ram ratio and low engine speeds. The engine gross thrust is obtained by correcting the measured thrust for intake momentum and pressure forces, including slip joint forces (*see* Appendix B). The thrust measuring system was calibrated at frequent intervals using a proving ring.

The static pressure in the cell was measured at three stations, one forward of the engine, one level with the compressor and one approximately ten feet forward of the jet pipe final nozzle.

3. *Test Conditions.*

3.1. *Flight Tests.*

The flight tests were made over a period of five years. The majority of the tests were at maximum engine speed and a nominal altitude of 40 000 ft with flight Mach numbers from 0·68 to 0·98 non-reheat and 0·85 to 1·64 with reheat. The envelope of Mach number and altitude covered is shown in Fig. 6. The tests were made under non-stablised flight conditions with average rates of change of total temperature and intake total pressure of 0·4 deg K/sec and 0·02 lb/(in.$^2$ sec) respectively and maximum rates of change of 1·0 deg K/sec and 0·05 lb/(in.$^2$ sec). With these low rates of change, the engine conditions will be the same as the steady state case. In the tests with reheat, variations of turbine pressure ratio from 3·0 to 3·7 occurred during the period of the flight tests due to unserviceability with a reheat fuel control unit and a gradual drift with time of the pressure ratio setting.

3.2. *Ground-level Static Test Bed.*

In these tests the intake and test-bed conditions were nominally constant, being dictated by the prevailing atmospheric conditions. The effects of engine speed and turbine pressure ratio were investigated. The engine speed was varied from 62·5 per cent to 100 per cent r.p.m. for non-reheat conditions and from 90 per cent to 100 per cent r.p.m. for reheat conditions. The turbine pressure ratio, as measured by the ratio of compressor delivery static pressure, $p_2$, to transition section static pressure, $p'_4$, was varied from 3·25 to 3·50, for reheat conditions, by adjusting the setting of the reheat fuel control unit.

Two series of tests were made after the completion of the flight tests. The first was the most comprehensive and included the tests at different turbine pressure ratios. The main aims of the tests were to measure any deterioration in performance that may have developed since the pre-flight tests[1], and to investigate the effects of turbine pressure-ratio variations to enable corrections to be applied to both flight and test-bed results. The results of this first series of tests are used for comparison with the flight and altitude test-bed results.

The second and briefer series of tests was made to confirm that no mechanical defects or performance differences were present prior to installation of the engine in the altitude test bed. At the start of this series the performance was about 3 per cent lower than in the first tests. This was caused by a considerable accumulation of dust on the blades of the first few stages of the compressor during storage of the engine between the two series of tests. After washing the compressor, the performance was restored to the same level as the first series. The results of this second series of tests are not included because of their limited scope and good agreement, after compressor washing, with the first series of tests.

3.3. *Altitude Test Bed.*

In these tests the following quantities were varied for both non-reheat and reheat conditions:

Engine speed.
Intake air total pressure.
Intake air total temperature.
Cell static pressure.

The reheat control unit turbine pressure ratio setting was not varied during these tests. The range of intake and test-bed conditions covered are given in Fig. 7. The engine speeds were from 80 per cent to 100 per cent r.p.m. non-reheat and 92·5 per cent to 100 per cent r.p.m. with reheat.

The purpose of the tests was to measure the performance and calibrate the engine with simulated flight conditions at 40 000 ft altitude. The majority of the tests were made at intake conditions simulating flight at Mach numbers from 0·7 to 1·8, Fig. 7a. For these tests the cell static pressure was set to give the jet efflux expansion that was measured in flight. This required higher pressures in the cell than the ambient static pressure for 40 000 ft of 2·7 lb/in$^2$, because the dynamic pressure of the external airflow in the test bed is much lower than the flight case (approximately 2 lb/ft$^2$ for the test bed, compared with up to 1400 lb/ft$^2$ in flight). The required cell pressure was initially calculated using the experimental

results of Lee[4] at transonic speeds and theoretical calculations of Love, *et al*[5], for other speeds. However, it was found from jet efflux traverse records, that the expansion was less than that experienced in flight. This was probably because the estimates made no allowances for base effects on the aircraft or the flow through the test bed. The cell pressures were thus reduced to bring the test-bed expansion conditions in line with the flight conditions.

Care was taken to represent the jet efflux expansion correctly as it was expected to effect the traverse probe results, which will be discussed in a further report, and possibly the final nozzle static-pressure calibration. However, since the final nozzle throat is choked for most of these tests, the variation of the expansion ratio should have no effect on other engine parameters. In order to establish the effects of varying jet expansion conditions, some tests, Fig. 7b, were made at nominally constant intake and engine speed conditions with various cell pressures (jet expansion being a function of cell static pressure).

4. *Method of Analysis.*

The net thrust of the engine, required for the determination of aircraft drag in flight, is obtained from the difference between the engine gross thrust and the free-stream momentum of the air mass flow entering the engine. To obtain measurements of gross thrust and air mass flow in flight, the engine internal measuring systems must first be calibrated against direct measurements of gross thrust and air mass flow in test beds. This Section first describes how the gross thrust and air mass flow are measured in the test beds, and then how these measurements are used to obtain the calibration factors required in the equations relating the internal pressure and temperature measurements to the gross thrust and air mass flow. Finally the methods of 'non-dimensionalizing' engine performance are stated.

Throughout the Section the numerical suffices refer to the engine measuring stations as shown in Fig. 4. These stations are:

Station 0 Free stream.
Station 1 Compressor entry.
Station 2 Compressor delivery.
Station 3 Turbine entry.
Station 4 Transition section, the parallel portion of jet pipe between the turbine exit diffuser and that prior to the reheat combustion section.
Station 5 Final nozzle.
Station 6 Jet exit.
Station 7 Probe traverse plane.

4.1. *Measurement of Gross Thrust and Air Mass Flow in the Test Beds.*

4.1.1. *Gross thrust.* Gross thrust is defined as the sum of the momentum and pressure forces at the jet exit plane

$$X_G = \frac{Q_6 V_6}{g} + (p_6 - p_0) A_6 \tag{1}$$

where

$X_G$ = gross thrust, lb

$Q_6$ = exit mass flow, lb/sec

$V_6$ = exit velocity, ft/sec

$g$ = gravitational acceleration, 32·2 ft/sec

$p_6$ = exit static pressure, lb/in.$^2$

$p_0$ = ambient static pressure, lb/in.$^2$

$A_6$ = exit area, in.$^2$

This cannot usually be measured directly. In the ground-level static tests the thrust measured is assumed equal to the gross thrust (*see* Section 2.2 and Appendix A). This could be subject to an error of approximately 1 per cent ($X_{G\,\text{measured}} \approx 0{\cdot}99\,X_G$). In the altitude test bed, the net thrust of the free system is measured, and the gross thrust is determined from the relation (*see* Appendix B).

$$X_G = X + \frac{Q_1 V_1}{g} + (p_1 - p_0)(A_s) \tag{2}$$

where

$X$ = measured thrust, lb

$A_s$ = area of duct, including slip joint flange, in.$^2$

$Q_1$ = compressor entry mass flow, lb/sec

$V_1$ = compressor entry velocity, ft/sec

$p_1$ = compressor entry static pressure, lb/in.$^2$

Since the present tests, the accuracy of the measurement of gross thrust in the altitude test bed has been improved by eliminating several small systematic errors amounting to a total of about +1 or 2 per cent gross thrust. The scatter of results is however only slightly reduced when compared with the results of this Report.

4.1.2. *Air mass flow.* The methods of measuring air mass flow were different on the two test beds. Appendix C gives full details of the methods.

On the ground-level static test bed a calibrated intake flare was fitted and air mass flow determined using the calibration equation derived from Appendix C, equation (27)

$$(Q_1)_c = 0{\cdot}985\sqrt{\frac{\Delta p_c\,(379{\cdot}68 - p_c)}{0{\cdot}488651}} \tag{3}$$

where $(Q_1)_c$ = air mass flow, lb/sec, corrected to ISA sea-level conditions

$\Delta p_c$ = differential pressure, inches of water, between test-bed static pressure and intake flare throat pressure, corrected to ISA sea-level conditions

As shown in Appendix C this approximate equation is accurate to within 2 parts in 10 000 for the intake conditions experienced on the ground-level test bed.

On the altitude test bed the mass flow was measured using the standard compressible flow equation for the mass flow in a duct

$$Q_1 = \frac{pA}{\sqrt{T_t}}\left(\frac{\gamma}{\gamma - 1}\right)\sqrt{\left\{\frac{2}{C_p}\left(\frac{p_t}{p}\right)^{\frac{\gamma-1}{\gamma}}\left[\left(\frac{p_t}{p}\right)^{\frac{\gamma-1}{\gamma}} - 1\right]\right\}} \tag{4}$$

where

$Q_1$ = mass flow, lb/sec

$p$ = static pressure, lb/in.$^2$

$p_t$ = total pressure, lb/in.$^2$

$T_t$ = total temperature, deg K

$A$ = cross sectional area, in.$^2$

$\gamma$ = ratio of gas specific heats

$C_p$ = gas specific heat at constant pressure, ft lb/slug °K

The pressures and temperatures were measured by multiple sensing points.

4.2. *Engine and Jet-pipe Calibrations.*

The engine and jet pipe were calibrated in the test beds to obtain the relations between the various pressure and temperature measurements and the gross thrust and air mass flow measured in the test beds. In most cases the calibrations define the effective areas at the various measuring stations, although in some cases the calibrations give a more direct measure of thrust or mass flow. These effective areas are the products of the hot geometric areas at the measuring stations and calibration factors, usually close to unity. The derivations of the equations relating the pressures and temperatures to the gross thrust and air mass flow are given in Ref. 1 and are summarised in Appendices D and E for gross thrust and air mass flow respectively. The equations are based on the assumptions

(1) One dimensional flow, i.e. conditions at any station are uniform.

(2) Adiabatic flow, i.e. no heat exchange through the duct wall.

(3) Continuous flow, i.e. no gas losses, with the exception of 2·5 per cent entry mass flow bled off at the last stage of the compressor.

(4) Homogeneous perfect gas, i.e. gas equations apply.

In practice none of these assumptions are completely valid and this results in the calibration factors differing from unity. The values of the specific heat at constant pressure, $C_p$, and the ratio of the specific heats, $\gamma$, used in the various equations are listed in Table 3.

Two equations relating the gross thrust to the internal pressure measurements are presented in Appendix D. The first is based on the static pressure measured in the final nozzle (Station 5, Fig. 4). The calibration factors for this method may be obtained either in terms of the effective area, $A_5$, or as a direct plot of the gross thrust to test-bed static-pressure ratio, $X_G/p_0$, as a function of the final nozzle static-pressure ratio, $p_5/p_0$; the thrust, $X_G/p_0$, is a function of $A_5$ and $p_5/p_0$ only. The second equation is based on the measured transition section (Station 4, Fig. 4) total pressure. In this case the gross thrust is a function of both the pressure ratio, $p'_{4_t}/p_0$, and the total pressure loss between the transition section and the jet exit, as well as the effective area of the jet exit, $A_6$. Thus, the calibration may only be given in terms of the effective area, $A_6$, if the total pressure loss is measured independently. This proved to be possible only for the ground-level static tests as the pressure difference was too small in the altitude tests. The traversing probe total pressure was used to obtain the final nozzle total pressure. However, because of the difficulty of measuring the total pressure loss, this transition section method has only been calibrated as a direct plot of $X_G/p_0$ as a function of $p'_{4_t}/p_0$.

Three equations relating air mass flow to internal measurements are presented in Appendix E. The most direct equation is based on measurements of the total and static pressures and the total temperature at the transition section (Station 4, Fig. 4) and the calibrating factor is obtained in terms of the effective areas $A_4$ and $A'_4$, corresponding to rake and wall measurements respectively. The other two equations are less direct. The first is based on the turbine nozzle guide vane (Station 3, Fig. 4) conditions, assumed choked, where the total pressure is measured, and the total temperature is obtained from the compressor and turbine work balance equation and the combustion temperature rise equation. The calibration factor is obtained in terms of the effective area, $A_3$. The second equation is based on the work balance and temperature rise equations only, the fuel-air ratio is calculated and the air mass flow obtained using the measured fuel mass flow. In this case the calibration factor is obtained by comparing the derived fuel-air ratio with that measured in the test beds.

Having obtained these calibrations, they are used to obtain measurements of gross thrust and air mass flow in flight using the equations of Appendices D and E together with the appropriate effective areas, or the direct calibration factors.

To compare the performance of the engine in flight with that measured in the test beds, it is necessary to know the total pressure at the compressor entry (Station 1, Fig. 4), $p_{1_t}$. This pressure is not measured

in flight, but has been derived from measurements of the compressor delivery static pressure, $p_2$. The pressure ratio, $p_2/p_{1_t}$, is a function of the non-dimensional engine speed, $N/\sqrt{T_{1_t}}$ ($N$ = engine speed, r.p.m., and $T_{1_t}$ = compressor entry total temperature) and turbine pressure ratio (reheat conditions only), and has been measured on the test beds as part of the calibration of the engine.

4.3. *Engine 'Non-dimensional' Performance Parameters.*

4.3.1. *Standard parameters.* The engine 'non-dimensional' performance parameters may be derived and, following the usual practice in engine analysis[6], are considered as functions of the non-dimensional engine speed, $N/\sqrt{T_{1_t}}$. All the 'non-dimensional' parameters used are only truly non-dimensional if the relevant areas, fuel calorific values, and gas constants are included. However, for a given engine operating in air and using a standard fuel these other terms are constant factors and do not affect the 'non-dimensional' parameters. The following parameters have been used in this report.

Gross thrust function defined as

$$\Phi = \left[\frac{X_G}{A_6 p_0} + 1\right] \Big/ \frac{p_{1_t}}{p_0} \tag{5}$$

where $X_G$ = gross thrust, lb

$A_6$ = final nozzle geometric area (non-reheat, 347 in.$^2$; reheat 498 in.$^2$)

$p_0$ = ambient static pressure, lb/in.$^2$

$p_{1_t}$ = compressor-entry total pressure, lb/in.$^2$

$p_{1_t}/p_0$ = ram ratio

Air mass flow function,

$$Q_1\sqrt{T_{1_t}}/p_{1_t}$$

where $Q_1$ = compressor-entry air mass flow, lb/sec

$T_{1_t}$ = compressor-entry total temperature, deg K

Fuel mass flow functions,

$$\text{engine, } Q_E/(p_{1_t}\sqrt{T_{1_t}}) \text{ and reheat, } Q_R/(p_{1_t}\sqrt{T_{1_t}})$$

where $Q_E$ = engine fuel flow, lb/hr

$Q_R$ = reheat fuel flow, lb/hr

Jet pipe temperature,

$$T_{4_t}/T_{1_t}$$

where $T_{4_t}$ = transition section total temperature, deg K

Compressor pressure ratio,

$$p_2/p_{1_t}$$

where $p_2$ = compressor delivery static pressure, lb/in$^2$

Compressor temperature ratio,

$$T_{2_t}/T_{1_t}$$

where $T_{2_t}$ = compressor-delivery total temperature, deg K

Turbine pressure ratio,

$$p_2/p'_4$$

where $p'_4$ = transition section static pressure, lb/in$^2$

The 'non-dimensional' engine speeds have been corrected, where necessary, for the operation of the compressor inlet swirl vanes. As described in Section 2.1, these vanes are not fully compensated to operate at constant values of $N/\sqrt{T_{1_t}}$. However, the engine manufacturer has prepared a chart, Fig. 8, based on the compressor characteristics, whereby the measured $N/\sqrt{T_{1_t}}$ in the swirl vane operating range may be corrected to an equivalent $N/\sqrt{T_{1_t}}$ corresponding to the swirl vanes being fully temperature compensated. The corrections are only required for the altitude test bed results at high intake total temperatures, and some of the non-reheat flight results at low engine speeds, as the remaining tests were made at engine speeds outside the operating range of the inlet swirl vanes.

4.3.2. *Correction of reheat results for turbine pressure ratio variation.* The tests with reheat covered a wide range of turbine pressure ratio, $p_2/p'_4$, and, as many of the engine parameters are very sensitive to changes in this ratio, the results have all been corrected to a common ratio of $p_2/p'_4 = 3{\cdot}43$. The value chosen is arbitrary, but corresponds to the condition at maximum engine speed in the ground-level static tests without reheat, and is also close to the majority of the reheat test conditions. In the ground-level static tests with reheat the setting of the reheat fuel-control unit, which determines $p_2/p'_4$, was deliberately varied to give values of $p_2/p'_4$ from 3·26 to 3·56. It was not possible to test at lower values of $p_2/p'_4$ as the limiting jet pipe temperature would be exceeded, and thus the results have been extrapolated to correct the results at the very low values of the ratio present in some of the flight tests. The corrections affect the gross thrust, $X_G$, reheat fuel flow, $Q_R$, engine fuel flow, $Q_E$, jet-pipe temperature, $T_{4_t}$, and, to a lesser degree, compressor delivery static pressure, $p_2$, and air mass flow, $Q_1$. The test bed results, showing the percentage change in the measured quantity as a function of the percentage change in the turbine pressure ratio from 3·43, are plotted in Fig. 9a to f. It has been necessary to make large extrapolations to correct some of the flight results. The extrapolation has been chosen such that the non-dimensional performance parameters (Section 4.3.1) become unique functions of the 'non-dimensional' engine speed. This was found to give extrapolations consistent with the measured test-bed data.

4.4. *Reheat Combustion Efficiency.*

The reheat combustion efficiency $\eta_R$ is defined as the ratio of the theoretical to the actual reheat fuel flow required to give the measured temperature rise across the reheat section, thus

$$\eta_R = Q_{R_{th}}/Q_R \,. \tag{6}$$

As the reheat temperature rise, $(T_{6_t} - T_{4_t})$, the jet pipe gas mass flow, $Q_4$, and the engine fuel-air ratio, $q$, are known, then the theoretical reheat fuel flow can be calculated directly, using

$$Q_{R_{th}} = Q_4 (H_6 - C_{p_4} T_{4_t})/(\text{E.C.V.}) \tag{7}$$

where $H_6$ = the total heat per lb at the jet exit temperature $T_{6_t}$ and engine fuel-air ratio, $q$

$C_{p_4}$ = Specific heat at constant pressure at transition-pipe temperature, $T_{4_t}$, and fuel-air ratio, $q$

E.C.V. = reheat fuel effective calorific value at temperature $T_{6_t}$

Values of $H_6$, $C_{p_4}$ and E.C.V. are obtained from the standard tables of Fielding and Topps[7]. In many engine tests the value of the jet exit temperature with reheat must be obtained indirectly, however in these tests the temperature was measured directly by the jet efflux traverse probe in the test beds and in flight.

## 5. *Results and Discussion.*

### 5.1. *Comparison of Ground-level Static Tests Before and After the Flight Tests.*

The non-reheat performance of the engine before and after the flight tests is compared in Figs. 10 and 11 for gross thrust and air mass flow respectively. The engine was tested in the same test bed for both the pre-flight[1], and the post flight cases. The agreement between the gross thrust measurements from the two tests is very good. Within the small scatter, it is not possible to distinguish any difference in the results. In the case of the air mass-flow measurements the present tests give results about $1\frac{1}{2}$ per cent lower than the pre-flight tests[1], but the general scatter of both sets of results suggests that this difference is not significant. The reheat thrust performance has not been compared, as the large effects of turbine pressure-ratio differences caused by different reheat fuel control-unit settings make direct comparisons impossible. The reheat air mass flow is the same as in the non-reheat case. The engine characteristics have been assumed to remain constant during both the flight tests and the N.G.T.E. altitude tests that concluded the test series because of this good agreement between the pre-flight and post-flight results.

### 5.2. *Calibration of the Engine and Jet Pipe.*

Using the methods described in Section 4.2 (and Appendices D and E) the calibrations for the engine and jet pipe have been obtained from the ground level static and altitude test-bed results. The agreement between the calibrations from the two test beds is very good in every case and, except when reheat and non-reheat results are presented separately, different symbols are not used. This good agreement between the two different sets of test-bed results gives confidence that the measurements of gross thrust and air mass flow, on which the calibrations primarily depend, are accurate.

5.2.1. *Effective areas.* The effective area calibrations are shown in Figs. 12 to 14 for the turbine nozzle guide vane, $A_3$, transition section, $A_4$ and $A'_4$, and final nozzle, $A_5$, areas respectively.

Fig. 12 shows that the turbine nozzle guide vane effective area, $A_3$, is constant for the range of engine conditions tested and has a value of 134 in.$^2$, which agrees very well with the earlier calibration[1], but is slightly higher than the calculated hot geometric area of 130·8 in.$^2$. The scatter of results is $\pm 4$ per cent for non-reheat and $\pm 2$ per cent with reheat, but is better than might have been expected, as Appendix E shows that the determination of $A_3$ depends on the measurement of 5 separate quantities. The cause of the greater scatter in the non-reheat tests may be due to the wider range of engine r.p.m. and turbine pressure-ratio conditions covered in the non-reheat tests.

Fig. 13 shows the two transition section effective areas, $A_4$ and $A'_4$, based on the rake and wall measurements respectively. The areas are constant for most conditions, with a small decrease at pressure ratios below 1·6. The mean areas are 469 in.$^2$ and 472 in.$^2$ for $A_4$ and $A'_4$ respectively, compared with a hot

geometric area of 454·2 in.$^2$. The scatter is about $\pm 3{\cdot}5$ per cent, and thus the difference in areas between $A_4$ and $A'_4$ is not significant. The value of $A'_4$ is about 2 per cent lower than the pre-flight calibration[1] ($A'_4$ is called $A''_4$ in Ref. 1). It was not possible to determine $A_4$ (called $A'_4$) satisfactorily in the tests of Ref. 1 because of a leak from the pitot rake. The 2 per cent difference between the pre-flight and post-flight calibrations of $A'_4$ is unlikely to be related to the $1\frac{1}{2}$ per cent difference in measured air mass flow (Fig. 11) for the two tests, as there is no difference between the pre- and post-flight calibrations of $A_3$, which also depends on the measured air mass flow. The most probable cause is minor surface distortions in the transition section affecting the static pressure measurements.

The variation of the final nozzle effective area, $A_5$, with final nozzle pressure ratio, $p_5/p_0$, is shown in Fig. 14a and b for the non-reheat and reheat results respectively. The agreement between results from both the ground level and altitude test beds is very good, although the scatter of the altitude results is somewhat greater. This increased scatter is possibly due to both the wider range of conditions tested and the smaller values of thrust and pressures present under altitude conditions. Both non-reheat and reheat effective areas vary considerably at low pressure ratios, but at high pressure ratios these areas agree with the calculated hot geometric area of 562·9 in.$^2$ to within $\frac{1}{2}$ per cent. The non-reheat value of $A_5$ does not become constant until the pressure ratio is greater than 2·8 which compares with the maximum value reached in the ground level tests of 2.1. Both values are significantly greater than the one-dimensional throat choking value of 1·65.

The present ground-level calibration gives non-reheat values of $A_5$ about 4 per cent higher than the earlier calibration[1]. This difference is not present in the reheat results, Fig. 14b, and it was shown in Fig. 10 that the non-reheat thrust is the same for both tests. Thus, the most probable explanation is a change in the ovality of the jet exit area with the movable eyelids in the closed, non-reheat position (Fig. 3). This would affect the local static pressure measured at the static tappings without changing the overall jet exit area, and thus the thrust would remain constant. For the reheat effective area, $A_5$, Fig. 14b, the value is constant above a pressure ratio of 2·3 compared with the nominal choking and maximum ground-level test ratios of 1·37 and 1·7 respectively. Agreement with the earlier calibration[1] is good. An altitude test bed calibration must be obtained to define the area $A_5$ under the flight conditions because of the variation of the effective areas at and above the low pressure ratios of the ground-level static test results. This is in contrast with the effective areas $A_3$ and $A_4$ which have constant values at all but the lowest pressure ratios. In the absence of an altitude test-bed calibration, an extrapolation of the ground-level results for $A_5$, assuming the area at high pressure ratios is equal to the hot geometric area, would be entirely satisfactory for the results of the present tests. However, further experimental justification is required before this method can be used with confidence for other tests.

The effect of varying the cell static pressure, $p_0$, whilst keeping the engine speed and intake conditions constant, was investigated for reheat conditions and is shown in Fig. 15. Within the scatter of results, there is no noticeable effect. The slight differences between the mean values of $A_3$ and $A_4$ in Fig. 15, and the means of Figs. 12 and 13a are a result of the small sample used in Fig. 15.

5.2.2. *Direct thrust-pressure calibrations.* As shown in Section 4.2 (and Appendix D) the thrust may be calibrated directly in terms of the relevant pressures.

Fig. 16 shows the variation of the gross thrust ratio, $X_G/p_0$, with transition section total pressure ratio, $p'_{4_t}/p_0$, for both non-reheat and reheat conditions. The agreement between the ground level and altitude tests is very good. There is some scatter in the altitude test results, but scarcely any in the ground-level test results; the mean lines through the results are very well defined. The calibrations are linear up to a pressure ratio of about 4 where there is a well defined kink in both reheat and non-reheat results. Above the kink the calibration is linear again with the same slope as for the lower pressure ratios. In the absence of tests in an altitude test bed, it has been common practice to assume that the one-dimensional theory applies, and thus the altitude performance can be obtained by extrapolating the ground-level tests results, above the one-dimensional choking pressure ratio, as a straight line. If this is done with the present results, Fig. 16 shows the extrapolation to give an error of 4 per cent above the kink pressure ratio of about 4·0. Fig. 17 shows the total pressure loss measured between the transition

section and the jet exit, the latter being obtained from traversing-probe results. This pressure loss is the difference between two relatively large quantities and since it was not measured directly, results for the ground-level test bed only are presented, as in the altitude test bed the difference was too small to obtain consistent results. The pressure loss consists of effects due to skin friction at the jet pipe wall, the drag of the reheat burner, and in the case of reheat, that due to the fundamental loss caused by burning fuel. The non-linear behaviour of the non-reheat curve suggests that the reheat-burner drag coefficient increases from a constant value at the higher jet pipe Mach numbers. Such a change in the reheat-burner drag coefficient could cause the kink in the non-reheat calibration of Fig. 16, which occurs at about the same pressure ratio. The general level of the pressure loss is about 6·5 per cent and 10·5 per cent for non-reheat and reheat respectively, the increase of 4 per cent being due to the fundamental burning loss. In view of the effect of the pressure loss on the direct thrust calibrations (Fig. 16), it is recommended that altitude test-bed results are essential in calibrating by this method, if large pressure losses occur between the measuring station and the jet exit.

Fig. 18 shows the variation of the thrust ratio $X_G/p_0$, with final nozzle static-pressure ratio, $p_5/p_0$, for both non-reheat and reheat conditions. The agreement between the ground level and altitude calibrations is very good and the scatter is very small. The calibrations do not show the kink that occurred in the transition section total-pressure calibration, Fig. 16, but the curves are not linear for pressure ratios less than 2·8 for non-reheat or 2·3 with reheat. Again the ground-level final-nozzle throat-choked results have been extrapolated on a linear basis, as is common in the absence of altitude tests. Using this extrapolation would give an overestimate of thrust by 6 per cent and 8 per cent at a pressure ratio of 5·0 for reheat and non-reheat respectively. The very large extrapolation of up to 10 times the range of the ground-level choked results makes accurate definition of the extrapolation very difficult, despite the very small scatter in the ground-level results. The main reason for the differences between the extrapolations and the altitude results is clear from a study of the effective-area curves of Fig. 14. Linear extrapolation of the ground-level choked results assumes the effective area to be constant once the final nozzle throat is choked, and Fig. 14 shows this assumption to be incorrect for the ground-level pressure ratios. In the absence of altitude tests it is more accurate to extrapolate the effective area assuming it is equal to the hot geometric area at high pressure ratios, unless the effective area is found to differ significantly from the hot geometric area.

It can be concluded that to obtain the best accuracy of thrust measurement in flight an altitude calibration is essential, particularly for the transition section method.

5.2.3. *Fuel-air ratio determination.* As shown in Section 4.2 (and Appendix E), one method of measuring air mass flow is from the calculated values of the engine fuel-air ratio. Comparison of the measured and derived fuel-air ratios for the test bed results are shown in Fig. 19a and b for non-reheat and reheat respectively. The mean values are 1·00 and 1·01 for non-reheat and reheat, with a corresponding scatter of $\pm 5$ per cent and $\pm 3$ per cent. These values agree with those of the earlier tests[1]. With this order of scatter it may be assumed that the derived fuel-air ratio is correct and thus the air mass flow may be obtained from fuel mass-flow measurements. The general scatter is of the same order as that for the effective areas, $A_3$, $A_4$ and $A'_4$ which may also be used for determining air mass flow.

5.2.4. *Compressor pressure ratio.* In Section 4.2 it is shown that the calibration of compressor pressure ratio $p_2/p_{1_t}$, as a function of 'non-dimensional' engine speed, $N/\sqrt{T_{1_t}}$, is required for the calculation of intake total pressure, $p_{1_t}$, in flight. This calibration is presented in Fig. 20 for all the tests. The agreement between the tests, both altitude and ground level, reheat and non-reheat, is good, after correcting the reheat results to the 'standard' turbine pressure-ratio conditions (Section 4.3.2.).

5.3. *Comparison of Various Flight Measurements of Gross Thrust and Air Mass Flow.*

5.3.1. *Gross thrust.* Two methods of measuring gross thrust are available in flight (*see* Appendix D),

not including the jet efflux traversing probe, which will be the subject of a separate report. The two methods are based on:

(i) Final nozzle static-pressure measurement.

(ii) Transition section total-pressure measurement. (Wall measurements only, pitot rake unserviceable.)

These thrusts are designated $X_{G_1}$ and $X_{G_2}$ respectively. Of the two methods, the first is the more direct, and has the calibration with the smaller scatter (Fig. 18, *c.f.* Fig. 16). For these reasons $X_{G_1}$ is used as the 'standard' thrust for the flight tests. However, as $X_{G_1}$ is not a direct measure of the gross thrust, but depends on a ground calibration, the possibility of a consistent error in the flight measurements cannot be ignored. It was hoped that the results of the jet efflux traverse probe, which is independent of the engine would enable any such error to be determined. However, the measuring difficulties with this probe (*see* Introduction) have prevented this check from being made at present. Comparison of the differences between the two measured values of thrust, $X_{G_1}$ and $X_{G_2}$, is shown in Fig. 21a and b for non-reheat and reheat respectively; 'non-dimensional' engine speed being used as an independent variable. Without reheat, Fig. 21a, the scatter of the results is considerable, but there is a consistent difference of thrust of +2·2 per cent with a standard deviation of 1·8 per cent. There is a slight, but probably not significant, tendency for the mean to decrease as $N/\sqrt{T_{1_t}}$ increases. With reheat, Fig. 21b, the scatter is less and the mean increases linearly from −2·5 per cent to +0·5 per cent over the $N/\sqrt{T_{1_t}}$ range. The standard deviation is 0·8 per cent. A possible reason for the increased scatter of the non-reheat results could be distortion of the jet exit area, with the movable 'eyelids' in the closed, non-reheat, position (Fig. 3). This was given as a possible cause of the differences in the final nozzle effective-area calibrations, $A_5$, (Fig. 14a). Another factor could be the wider range of true engine speed in the non-reheat tests. In the reheat conditions the eyelids are open and do not form the jet exit, and the true engine speed was nominally constant at 100 per cent. Because the reheat tests were at nominally constant altitude and engine speed, it is not possible to separate effects due to 'non-dimensional' engine speed changes or ram ratio, $p_{1_t}/p_0$, changes, as both these parameters are functions of Mach number only, under these conditions. Thus the trend of the thrust differences with reheat may be due to either effect. The range of $N/\sqrt{T_{1_t}}$ covered in Fig. 21b is equivalent to a Mach number range from 0·85 to 1·85.

The major difference between the test-bed and flight conditions that could affect the calibrations, and thus explain the differences between these two flight measurements of gross thrust, is the presence of the air intakes in flight. In the test beds the air is delivered to the engine in the most uniform manner possible, whereas in flight the intakes produce significant flow distortions. The two main effects produced by the flight intakes are:

(i) The velocity distribution (or total pressure distribution) at compressor entry is not uniform and depends on the flight and engine conditions (Mach number, incidence, and engine speed).

(ii) The air at the compressor entry has swirl, again dependent on the flight and engine conditions.

The most likely reason for the differences between the flight measurements of thrust deduced from the transition section and final nozzle is a change in the pressure distribution in these sections compared with test bed conditions, which would affect the calibrations. This is likely to occur in the transition section if either the pressure distribution or the swirl at the turbine exit is changed, producing a different flow past the exhaust cone support struts. Such changes in the transition section are not likely to persist at the final nozzle, because of the turbulent mixing zone downstream of the reheat burners. In fact both the poor intake pressure distribution and the intake swirl will have some effect on the turbine exit conditions. Refs. 8 to 11 consider effects of intake pressure distribution distortions, and indicate that the pressure distortion is negligible at turbine exit, although turbine efficiency, and thus swirl, may be slightly affected. The effects of intake swirl are not considered in the tests of Refs. 8 to 11, but it is believed that they have similar effects to pressure distortions. Thus there is a possibility of the transition section pressure distribution being affected by intake conditions with less likelihood of the final nozzle pressure

distribution being similarly affected, because of the mixing by the reheat burners. This is a further point in favour of the use of the final nozzle static-pressure method, $X_{G1}$, as the most reliable method of measuring thrust in flight. It would seem probable that the differences between the two measurements of thrust, $X_{G1}$ and $X_{G2}$, may be attributed to intake effects in flight affecting the calibration used for the transition pipe total pressure method, $X_{G2}$.

5.3.2. *Air mass flow.* Three methods are used for measuring air mass flow, $Q_1$, in flight (*see* Appendix E), not including the jet efflux traversing probe. The methods are:

(i) Transition section conditions, $Q_{11}$.

(ii) Turbine nozzle guide vane conditions, $Q_{12}$.

(iii) Fuel-air ratio calculation, $Q_{13}$.

The scatter in the calibrations of the three methods, Section 4.2, is of the same order, and thus it is not possible to select one method as the 'standard' for the flight results in terms of accuracy of measurement. However, the transition section method, $Q_{11}$, is the more direct and the easiest to install in most practical cases, and has thus been chosen as the 'standard' flight method for comparison purposes. The differences $(Q_{12}-Q_{11})$ and $(Q_{13}-Q_{11})$ are shown in Fig. 22a and b respectively for reheat conditions. The non-reheat results are not presented as they do not differ significantly from the reheat results. Although the scatter in Fig. 22a and b is considerable, the mean differences are small, and it is considered that there is no significant difference in the accuracy of the three methods. It seems probable that the presence of intake effects in flight does not affect the air mass-flow calibrations, unless all three methods are equally affected.

It is interesting to note, that, although the transition section method is the more direct and involves the measurement of fewer quantities, the accuracy of the results is no better. The reason for this is apparent, if the equation for mass flow is studied. In particular the simplified equation (22) for compressible flow obtained in Appendix C. This equation is

$$Q = A\lambda\sqrt{\left\{\frac{2}{RT_t}p(p_t-p)\right\}} \tag{22}$$

where $\lambda$ is a correction factor approximately equal to unity. In equation (23) the most critical term is $(p_t-p)$, which is generally less than 15 per cent of $p$ and depends on the measurement of both $p_t$ and $p$. Thus a 1 per cent error in either measurement will give an error of more than 4 per cent in the mass flow. It would appear more desirable to measure the static pressure, $p$, and the differential pressure, $(p_t-p)$, rather than $p$ and $p_t$ as in the present tests, if the best accuracy is to be obtained. The use of venturi pitots to obtain an increase in the magnitude of the apparent $(p_t-p)$ should also help. With the use of such methods the accuracy of the transition section method should be significantly improved.

5.4. *Determination of Mean Compressor Entry Total Pressure and Intake Pressure Recovery in Flight.*

As shown in Section 4.3.1, many of the 'non-dimensional' performance parameters, including those for gross thrust and air mass flow, contain the mean compressor entry total pressure, $p_{1_t}$. This pressure is measured directly in the test beds, but must be determined in flight using the test bed calibration of compressor pressure ratio, Fig. 20, and the compressor delivery pressure, $p_2$. Having obtained the value of $p_{1_t}$ in this manner, the intake pressure recovery $p_{1_t}/p_{0_t}$, may be calculated, using the value of free stream total pressure, $p_{0_t}$, measured in flight. Fig. 23 shows the intake pressure recovery for Mach numbers from 0·85 to 1·65 at 40 000 ft. The scatter of the results is considerable, probably due to the indirect method of measuring the pressure recovery. In level flight the pressure recovery is 0·89 up to a Mach number of 1·3 and falls to 0·80 at $M = 1{\cdot}6$. The agreement with model tests[12] at the same incidence is reasonable, the trends with Mach number being similar although the model tests predict about 0·02

higher pressure recovery. The effect of increasing the incidence in turning flight is to increase the pressure recovery, and this is also in agreement with the model tests[12].

5.5. *Comparison of 'Non-dimensional' Performance Measured in Flight and the Test Beds.*

Figs. 24 to 34 summarise the 'non-dimensional' performance measured in flight and in the ground level and altitude test beds. All the reheat results have been corrected to a 'standard' turbine pressure ratio, $p_2/p'_4$ of 3·43 using the correction curves of Fig. 9. The non-reheat results for gross thrust function, air mass-flow function, engine fuel-flow function, jet-pipe temperature ratio, and compressor-delivery temperature ratio are shown in Figs. 24 to 28. The corresponding reheat results and the reheat fuel-flow function are shown in Figs. 29 to 34. All the parameters are shown as functions of the 'non-dimensional' engine speed, $N/\sqrt{T_{1_t}}$.

5.5.1. *Non-reheat results.* The non-reheat performance measurements, Figs. 24 to 28, show a scatter of about $\pm 2$ per cent for the ground level results, and $\pm 3$ per cent for most of the altitude test bed and flight results. There is an increased scatter of $\pm 6$ per cent for the altitude test bed and flight values of the engine fuel flow function, Fig. 26, and $\pm 4$ per cent for the flight results of the air mass-flow function, Fig. 25. The agreement between the performance measured in flight and in the test beds is very good for all parameters, with the sole exception of the compressor delivery temperature ratio, Fig. 28. In this case, although results from the two test beds agree, the flight results are nearly 6 per cent higher, with a scatter of only $\pm 2$ per cent. Although compressor delivery temperature is difficult to measure, especially with only a few thermocouples, the difference is consistent with the effects of a distorted total-pressure distribution produced by the intake as noted in Refs. 8 to 11, where the presence of a low total-pressure area produced a rise in the compressor delivery total temperature in the corresponding delivery duct. The difference between the ground level and altitude test-bed results for the jet-pipe temperature ratio, Fig. 27, at low values of $N/\sqrt{T_{1_t}}$, is caused by the final nozzle throat being unchoked at these conditions in the ground level tests.

5.5.2. *Reheat results.* In general the reheat results, Figs. 29 to 34, have a scatter of about $\pm 2$ per cent, which is slightly reduced compared with the non-reheat results. However, in some cases the scatter is increased; for the flight measurements of air mass-flow function, Fig. 30, it is about $\pm 6$ per cent, and $\pm 5$ per cent for the reheat fuel-flow function from all three sources. In contrast with the non-reheat results, the agreement between results in flight and in the two test beds is not, in general, so good. There are two main aspects of these differences: firstly the rather unexpected differences between results from the two test beds, and secondly the differences between the results in flight and in the test beds, where the effect of large intake total-pressure distribution distortions in flight makes differences more likely. The following Table lists for each parameter the differences of the ground level test bed and flight results from the altitude test-bed results.

*Differences of the Ground-level Test Bed and Flight Results from the Altitude Test-bed Results with reheat*

| Fig. No. | Parameter | Differences, per cent | |
|---|---|---|---|
| | | Ground level test bed minus altitude test bed | Flight minus altitude test bed |
| 29 | Gross thrust function | −3 | −10 to −2 |
| 30 | Air mass-flow function | 0 | 0 to +3 |
| 31 | Engine fuel-flow function | −7 | −3 |
| 32 | Reheat fuel-flow function | −2 | −12 to −4 |
| 33 | Jet pipe temperature ratio | 0 | 0 |
| 34 | Compressor delivery temperature ratio | +3 to 0 | +3 |

It is not believed that these differences are a result of any consistent errors arising from the corrections for turbine pressure-ratio variations, as comparison of results, selected at the same turbine pressure ratio and 'non-dimensional' engine speed, for all three types of test show comparable differences.

Considering first the differences between results from the two test beds which are present in the gross thrust function, Fig. 29, the engine fuel-flow function, Fig. 31, and the compressor delivery temperature ratio, Fig. 34. The differences are not large, but are significant; the 3 per cent difference in gross thrust function being equivalent to a 5 per cent difference in gross thrust for a typical 40 000 ft flight condition.

Considering first the differences between results from the two test beds which are present in the gross thrust function, Fig. 29, the engine fuel-flow function, Fig. 31, and the compressor delivery temperature ratio, Fig. 34. The differences are not large, but are significant; the 3 per cent difference in gross thrust function being equivalent to a 5 per cent difference in gross thrust for a typical 40 000 ft flight condition.

The reason for these differences is not clear. Various possible explanations have been considered, but none can completely explain them. The points considered are:

(1) Errors in test-bed measurements, particularly gross thrust.

(2) Reynolds number effects on the compressor.

(3) Mechanical deterioration of the engine.

(4) Differences in the compressor entry total-pressure distributions.

The first is unlikely, because of the very good agreement between the thrust measurements in the two test beds shown in the direct thrust-pressure calibrations of Figs. 16 and 18. Tests by the engine manufacturer show no significant Reynolds number effects on the compressor for the range of conditions covered in the two test beds. Mechanical deterioration of the engine would be expected to produce a change in the jet-pipe temperature ratio and this is not evident in Fig. 33. Furthermore, all of these first three reasons should have a similar effect on the non-reheat results, and this is not evident. It is possible that the compressor entry total-pressure distribution was different in the two test beds.

Fig. 35 shows a typical distribution measured in the altitude test bed with less than 1 per cent distortion. No measurements are available for the ground level tests, and it may be possible that the presence of the engine mounting platform for a distance of approximately 8 ft ahead of, and only about 3 ft below, the intake could disturb the flow in the lower part of the bellmouth intake. Such an effect, if present, would be worse in the reheat condition because of the higher flow velocities induced through the test bed.

The most probable effect of disturbed intake flow would be to give a variation in the compressor delivery pressure, $p_2$, around the delivery ducting. This would cause the values of $p_2$ sensed by the instrumentation and the reheat control unit to differ as they are sensed at different positions, and thus the corrections to the reheat parameters for varying turbine pressure-ratio setting would be incorrect, as they are based on the instrumentation value of $p_2$. Such an error would have its largest effect on the gross thrust, and the engine and reheat fuel flows. Also the presence of intake flow distortion would tend to increase the compressor temperature ratio. The differences are in many ways consistent with such an error, but the relative magnitudes of the differences are not so consistent. If it is assumed that the error in gross thrust function of 3 per cent is due to incorrect values of $p_2/p'_4$, then the corresponding error in engine and reheat fuel flows should be 4 per cent and 10 per cent respectively, compared with the 7 per cent and 2 per cent observed. However, it does seem probable that at least some of the difference is caused by this effect, and in any future tests it is essential to measure the pressure that is used for the reheat fuel control-unit datum.

Although no full explanation can be given for the differences between the two test beds, the altitude test-bed results are considered to be more reliable, as intake conditions were more closely controlled and the tests were a closer simulation of flight conditions than in the ground level test bed.

Recent investigations by the National Gas Turbine Establishment[13] into the accuracy of gross thrust measurements in the Cell 3 altitude test bed suggest that there may be some small systematic errors which would tend to give values of gross thrust higher than the correct value. However, comparison of results from the Glen and Cell 3 test beds without reheat suggest that in the present tests any such errors are no greater than 1 per cent, or at the worst 2 per cent of gross thrust.

The considerable differences between the flight test and test-bed results, as listed earlier in Table 4, are considered next. In particular, the gross thrust and reheat fuel flow are smaller in flight. This may be consistent, but the thrust also depends on the reheat combustion efficiency. Fig. 36 shows a comparison of the reheat combustion efficiency measured in flight and in the two test beds as a function of the reheat gas/fuel ratio. The mean efficiency in the test beds is 70 to 80 per cent, whereas in flight it is 90 to 95 per cent. (Engine manufacturers' tests give 85 per cent). The gross thrust has been calculated from the reheat combustion efficiency, the air and fuel mass flows, and the jet-pipe temperature. The results of these calculations show reasonable agreement with the measured gross thrust in the test bed. However, the calculated gross thrust in flight is larger than in the test bed in contrast to the measured values where the flight thrust is lower. This implies that one of the three parameters: gross thrust, reheat fuel flow, or reheat combustion efficiency, measured in flight, is incorrect. It appears most likely that the reheat combustion efficiency is incorrect, as the measurement of jet exit temperature by the traversing probe requires considerable correction for the time lag in thermometer response, and also requires the assumption of axisymmetric temperature distribution. In particular, it appears unlikely that the distribution is axisymmetric, as the results from the probe are asymmetric. This asymmetry is worse in the test bed because of the weaker reheat setting, and this may explain some of the larger scatter in the test-bed results for reheat efficiency.

It seems probable that most of the differences between flight and test bed are related to the poor intake total-pressure distribution in flight[12], although further ground tests would be required to confirm this suggestion. It is probable that a considerable part of the differences in this case are caused by differences between the turbine pressure ratio measured by the instrumentation, and that sensed by the reheat fuel control unit, as these pressures are obtained from separate tappings. Such a difference would result in erroneous corrections for the variations in turbine pressure ratio which are an essential part of the 'non-dimensional' analysis of the reheat results. Refs. 8 to 11 show that distortions of intake pressure distributions are attenuated, but not eliminated at the compressor delivery section. Thus the static pressures, and hence the corrections for turbine pressure ratio, could well be affected by the poor pressure distribution in flight. An effect of this kind would explain the tendency for the differences between flight and test bed to increase as the $N/\sqrt{T_{1_t}}$ decreases : decreasing $N/\sqrt{T_{1_t}}$ being equivalent to increasing Mach number at the constant engine speed used for reheat tests in flight. Figs. 37 and 38—typical velocity distributions and maximum distortion values obtained in model tests on the intake, show that the level of distortion also increases with increasing Mach number (decreasing $N/\sqrt{T_{1_t}}$). Erroneous turbine pressure-ratio corrections could account for a significant part of the observed differences, and it is obviously essential in all future tests to measure any engine control law terms, such as turbine pressure ratio, directly.

### 5.6. *Comparison of Net Thrust Obtained from 'Non-dimensional' Characteristics and Engine Calibrations.*

A method frequently used for the determination of net thrust in flight, in the absence of detailed calibrations, is to use the 'non-dimensional' gross thrust and air mass-flow functions determined on the test bed. In this case it is only necessary in flight to measure, in addition to the normal aircraft performance parameters, engine speed and free stream total temperature. It is also necessary to know the intake total pressure, $p_{1_t}$. This parameter is difficult to measure in flight accurately, because the effects of intake velocity distortions require a pressure survey to give a reliable result. A more usual method is to estimate the intake total pressure from the intake efficiency deduced from model tests. If it is desired to avoid the reliance on model tests, $p_{1_t}$ can be obtained from a flight measurement of the compressor delivery pressure and a knowledge of the compressor characteristic. Because of the relative simplicity of this method, it is often used in preference to a calibration of the engine under representative flight conditions. From the comparisons of 'non-dimensional' performance in the present Report, it is possible to discuss the validity of the simpler method.

Considering first the non-reheat results, Figs. 24 and 25 show that the 'non-dimensional' method will give no consistent errors, but a random error of about $\pm 4$ per cent in net thrust will result from using either method. Although the calibration method has no advantages in the present tests, it should be remembered that the 'non-dimensional' method may be subject to systematic errors, examples being the accurate determination of free-stream conditions in flight and intake total pressure from model tests.

The presence of a systematic difference is well demonstrated by the reheat results of Fig. 29; the systematic error between flight and the altitude test bed is of the order of 6 per cent and this amounts to about 10 per cent in net thrust with a random error unchanged of about $\pm 4$ per cent. In this case the systematic error could have been eliminated if the operating pressures fed to the reheat fuel control unit had been measured, but this illustrates the traps that await the user of 'non-dimensional' data. Such occurrences are not so likely if internal measurements of pressures and temperatures are used together with test-bed calibrations, as described in this Report.

This random error of $\pm 4$ per cent in net thrust implies similar errors in aircraft performance calculated from the test-bed data and in the aerodynamic drag determined in flight from the thrust measurements. However, the error is mainly random and drag measurements will be improved by taking sufficient independent measurements to define the mean value to the required accuracy. The error is relatively large and any improvements would both reduce the number of measurements required to define the mean value and remove some of the uncertainties about only random errors being involved.

## 6. *Conclusions.*

Detailed tests have been made on an engine with reheat in flight and test beds and conclusions about the techniques and accuracy of thrust measurements are made. Although these conclusions are derived from tests on one particular engine, it is believed that they can have general application to other engines.

### 6.1. *Test-bed Calibrations.*

The agreement betwen the measurement of thrust and air mass flow in the ground-level static and altitude test beds is very good.

The effective areas of the turbine nozzle guide vane, $A_3$, Fig. 12, and the transition section, $A'_4$, Fig. 13, are constant over the range of conditions tested, and are about 3 per cent higher than the local hot geometric areas. $A'_4$ changed by about 2 per cent between the pre- and post-flight calibrations, probably due to surface distortions in the neighbourhood of the static-pressure tappings. The effective area of the final nozzle, $A_5$, Fig. 14, only becomes constant at pressure ratios significantly greater than choking and the maximum obtained in the ground-level static tests. At the higher pressure ratios, where $A_5$ is constant, it agrees with the hot geometric area to within $\frac{1}{2}$ per cent. The non-reheat value of $A_5$ changed about 4 per cent between the pre- and post-flight calibrations, probably due to a change in jet exit area ovality.

The thrust calibrations deduced from the transition section, Fig. 16, have a kink at a pressure ratio of about 4·0, and thus it would not be reliable to extrapolate the ground level test-bed measurements. Such an extrapolation would give an overestimate of about 4 per cent in thrust at higher pressure ratios. This kink is probably caused by a variation of the pressure loss between the transition section and the jet exit; the mean pressure loss is about 6·5 per cent non-reheat and 10·5 per cent reheat. The thrust calibrations derived from the final nozzle, Fig. 18, are not linear at low pressure ratios. Thus it would not be reliable to extrapolate from ground level test-bed measurements; an overestimate of about 7 per cent would result from such an extrapolation. It would be more reliable to extrapolate the effective area $A_5$ to the hot geometric area.

The fuel-air ratio method of determining air mass flow is as accurate as those based on the effective areas $A_3$ and $A_4$.

From the present tests it is concluded that ground level static test-bed calibrations are adequate for air mass-flow measurements, and may be adequate for gross thrust measurements using the final nozzle static-pressure method, if the final nozzle effective area can be assumed equal to the hot geometric area at high pressure ratios. The transition section total-pressure method of measuring gross thrust does, however, require an altitude test-bed calibration.

6.2. *Methods of Measuring Thrust and Mass Flow in Flight.*

Of the two methods of measuring gross thrust, that based on the final nozzle calibration is preferred to the transition section method. The reasons are that the method is more direct, the calibration has less scatter and is less liable to be affected by flight conditions. There are systematic differences between the thrusts derived from the two methods, Fig. 21, which amount to about 2 per cent non-reheat and from $-2{\cdot}5$ per cent to $+0{\cdot}5$ per cent reheat.

All three methods of measuring air mass flow, based on nozzle guide vane, transition section and fuel-air ratio, have random errors of the order of $\pm 6$ per cent, and there are no systematic differences, Fig. 22. However the transition section method is the easiest to apply, and it should be possible to improve the accuracy of this method.

6.3. *'Non-dimensional' Performance.*

Agreement between flight and model values of intake efficiency is reasonable, Fig. 23.

The agreement between flight and the two test beds for the 'non-dimensional' parameters for non-reheat conditions is very good, Figs. 24 to 28, with the exception of the compressor delivery temperature ratio which is affected in flight by the intake conditions. For reheat conditions, the agreement between flight and the two test beds is not so good, Figs. 29 to 34. The differences between the two test beds cannot be completely explained, but the altitude test-bed results are considered more reliable as conditions are more closely controlled and are a better representation of flight conditions. The major differences between the flight and altitude test-bed results are in the gross thrust and reheat fuel-flow functions which are about 8 per cent lower in flight. These differences are probably due to errors in the correction of the reheat results to a standard turbine pressure ratio. This possibility of error arises because the instrumentation and the reheat fuel-control unit, which maintains the turbine pressure ratio, sense the compressor delivery pressure at different positions on the engine circumference, and the pressure sensed by the reheat control unit was not measured. Thus, any flow distortions in the intake in flight could produce a variation of compressor delivery pressure around the circumference and corresponding errors in the corrections to the reheat results.

The use of 'non-dimensional' characteristics to determine net thrust gives a random error of about $\pm 4$ per cent which is similar to the results from direct calibrations. However, the 'non-dimensional' method is more susceptible to systematic errors. In the present tests, there is no systematic difference in the non-reheat results, but there is a systematic difference of about 10 per cent in the reheat results. These errors in thrust would imply similar errors in performance and drag measurements based on thrust.

7. *Acknowledgements.*

The authors wish to acknowledge the assistance given by the staff of the Engine Test Facility at the National Gas Turbine Establishment in both the operating of the two test beds and the initial computation of results. They would also like to acknowledge the co-operation of staff of both the National Gas Turbine Establishment and Rolls Royce Limited in discussing the results of these tests.

## LIST OF SYMBOLS

| | |
|---|---|
| $A$ | Area, inches$^2$ |
| $a$ | Sonic velocity, ft/sec |
| $C_p$ | Specific heat at constant pressure, ft lb/(slug. deg K) |
| $C_{p_{12}}$ | Mean specific heat at constant pressure between Stations 1 and 2, ft lb/(slug. deg K) |
| $C_{p_{34}}$ | Mean specific heat at constant pressure between Stations 3 and 4, ft lb/(slug. deg K) |
| $C_v$ | Specific heat at constant volume, ft lb/(slug. deg K) |
| $E.C.V.$ | Effective calorific value, chu/lb |
| $g$ | Gravitational acceleration, 32·2 ft/sec$^2$ |
| $H_6$ | Gas total heat per lb at Station 6, chu/lb |
| $M$ | Mach number |
| $N$ | Engine speed, r.p.m. |
| $p$ | Pressure, lb/in$^2$ |
| $\Delta p_c$ | Defined in equation (3) |
| $\Delta p_t$ | Defined in equation (33) |
| $Q$ | Gas mass flow rate, lb/sec |
| $Q_E$ | Engine fuel flow rate, lb/sec |
| $Q_R$ | Reheat fuel flow rate, lb/sec |
| $Q_{Rth}$ | Theoretical reheat fuel flow rate, lb/sec (equation (7)) |
| $q$ | Fuel-air ratio |
| $R$ | Gas constant, ft lb/(slug. deg K) |
| $T$ | Temperature, deg K |
| $V$ | Velocity, ft/sec |
| $X$ | Longitudinal thrust measured in the test beds, lb |
| $X_G$ | Gross thrust, lb |
| $X_{G_1}, X_{G_2}$ | Gross thrust determined in flight by methods 1 and 2, lb |
| $\alpha$ | Ratio $A_5/A_6$ |
| $\beta$ | Ratio $p_5/p_6$ |
| $\gamma$ | Ratio of specific heats, $C_p/C_v$ |
| $\eta_M$ | Mechanical efficiency of transmission between the turbine and the compressor |
| $\eta_R$ | Reheat combustion efficiency |
| $\lambda$ | Compressibility factor, gas mass-flow equations (Appendix C) |
| $\rho$ | Air density, slugs/ft$^3$ |
| $\Phi$ | Gross thrust function $\left[\frac{X_G}{A_6 p_0}+1\right] \Big/ \frac{p_{1_t}}{p_0}$ |

*Suffices*

| | |
|---|---|
| *B* | Base |
| *C* | Corrected to ISA sea-level conditions |
| *F* | Front (on the outside of bellmouth intake) |
| *int* | intake |
| *S* | Slip joint |
| *t* | Stagnation conditions |
| 0 | Upstream of engine at free-stream conditions |
| 1 | Compressor entry |
| 2 | Compressor delivery |
| 3 | Turbine entry |
| 4 | Transition section (rake measurements) |
| 4′ | Transition section (wall measurements) |
| 5 | Final nozzle |
| 6 | Jet exit |

---

## LIST OF REFERENCES


| *No.* | *Author(s)* | *Title, etc.* |
|---|---|---|
| 1 | R. Rose, F. W. Dee and A. E. Acethorpe .. | The test bed calibration of an Avon RA28 engine under both non-reheat and reheat conditions with comparison of thrust measurements by a swinging probe and various conventional methods. R.A.E. Tech. Note Aero 2861, A.R.C. 24 979. December 1962. |
| 2 | D. R. Andrews .. .. | Some notes on the instrumentation for measurement of gross and net thrust in flight on the Fairey ER103 aircraft. R.A.E. Tech. Note Aero No. 2548, 1958. |
| 3 | W. G. E. Lewis .. .. | Engine test facilities at the National Gas Turbine Establishment —Part II. N.G.T.E. M.296, A.R.C. 19430. April 1957. |
| 4 | G. Lee .. .. .. .. | An investigation of transonic flow fields surrounding hot and cold sonic jets. NASA TN D–853, 1961. |
| 5 | E. S. Love, C. E. Gringsby, L. P. Lee and M. J. Woodling .. | Experimental and theoretical studies of axisymmetric free jets. NASA TR–R–6. |

## LIST OF REFERENCES—*continued*


| *No.* | *Author(s)* | *Title, etc.* |
|---|---|---|
| 6 | A. W. Morley .. .. .. | Equilibrium running of the simple jet-turbine engine. *Jl. R. Aeronaut. Soc.*, Vol. 52, pp. 305–322. 1948. |
| 7 | D. Fielding and J. E. C. Topps .. .. | Thermodynamic data for the calculation of gas turbine performance. A.R.C. R. & M. No. 3099, June 1954. |
| 8 | E. W. Conrad and A. E. Sobolewski .. .. | Investigation of effects of inlet-air velocity distortion on performance of turbojet engine. NACA RM E 50G11, 1950. |
| 9 | C. L. Walker, J. N. Sivo and E. T. Jansen .. | Effect of unequal air-flow distribution from twin inlet ducts on performance of an axial-flow turbojet engine. NACA RM E 54E13, 1954. |
| 10 | S. C. Huntley, J. N. Sivo and C. L. Walker | Effect of circumferential total-pressure gradients typical of single-inlet duct installations on performance of an axial-flow turbojet engine. NACA RM E 54K26a, 1955. |
| 11 | I. D. Smith, W. M. Braithwaite and H. F. Calvert | Effect of inlet-air-flow distortions on steady-state performance of J65–B–3 turbojet engine. NACA RM E 55I09, 1956. |
| 12 | M. R. Pike .. .. .. | Fairey V air intake (RA28): A summary of wind tunnel tests on a 1/16th scale model in the Hucknall Supersonic Tunnel. Rolls Royce Ltd., Ref.: TAS/WFW.1/AM, 1957. Unpublished. |
| 13 | J. C. Ascough and Squadron Leader K. A. Campbell | Unpublished Ministry of Technology Work. |

## APPENDIX A

*Measurement of Gross Thrust in the Ground-level Static Test Bed* (*Section* 4.1.1)

A schematic arrangement of an engine with a bellmouth intake in the ground-level static test bed is shown in Fig. 39. In the working section small, but significant velocities are induced. Fig. 40 shows the simplified flow pattern used in the analysis. The pressure $p_0$ and velocity $V_0$ are assumed constant in most of the working section, as the velocity is small and the engine cross-sectional area is small compared with the working section area. However, the pressure $p_F$ acting on the outside of the bellmouth intake is variable, and will differ from $p_0$ because of the significant curvature of the bellmouth. Also the base pressure $p_B$ is different from $p_0$ as the local induced velocity is increased in this region by the flow into the detuner.

Applying the momentum equation to the control volume shown dotted in Fig. 40 gives

$$\int_0^{A_{\text{int}}} p_{\text{int}}\,dA - \int_{A_1}^{A_{\text{int}}} p_F\,dA - p_0(A_1 - A_B) - \int_{A_6}^{A_B} p_B\,dA - \int_0^{A_6} p_6\,dA + X + D$$

$$= \int_0^{A_6} \rho_6 V_6^2\,dA - \int_0^{A_{\text{int}}} \rho_{\text{int}} V_{\text{int}}^2\,dA \tag{8}$$

where $p_{\text{int}}$ = pressure at the entry to the bellmouth intake

$p_F$ = pressure on the outside of the bellmouth intake

$p_0$ = free-stream static pressure

$p_B$ = base pressure

$p_6$ = pressure at the final nozzle

$V_{\text{int}}$ = axial component of velocity at bellmouth intake

$V_6$ = axial component of velocity at the final nozzle

$X$ = force measured by the weighbridge

$D$ = skin-friction drag of the engine and mountings

$\rho$ = gas density

Gross thrust, $X_G$, is defined as the sum of the momentum and pressure forces at the final nozzle

$$X_G = \int_0^{A_6} \rho_6 V_6^2\,dA + \int_0^{A_6} p_6\,dA - p_0 A_6\,. \tag{9}$$

Equation (8) becomes:

$$X = X_G - D - \int_0^{A_{\text{int}}} \rho_{\text{int}} V_{\text{int}}^2\,dA + \int_0^{A_{\text{int}}} (p_0 - p_{\text{int}})\,dA - \int_{A_1}^{A_{\text{int}}} (p_0 - p_F)\,dA - \int_{A_6}^{A_B} (p_0 - p_B)\,dA\,. \tag{10}$$

The usual practice for ground-level static test beds is to assume that the gross thrust $X_G$ is equal to the measured thrust, $X$. This implies that all terms, except the first on the right hand side of equation (10), are negligible. For the present tests, estimates show that, in fact, the skin friction and profile drag, $D$, and the base drag are negligible. It is more difficult to estimate the magnitude of the remaining terms, but they may not be negligible as the mean velocity of the air entering the test bed is about 40 ft/sec and this will be increased at the bellmouth intake. If there is no region of separated flow at the lip of the bellmouth intake, it can be shown that the sum of the remaining terms may be expressed as

$$\int_0^{A_{\text{int}}} \rho_{\text{int}} V_{\text{int}}^2 \, dA - \int_0^{A_{\text{int}}} (p_0 - p_{\text{int}}) \, dA + \int_{A_1}^{A_{\text{int}}} (p_0 - p_F) \, dA = Q_1 V_0 \tag{11}$$

where $Q_1$ = air mass flow entering the engine

This can be evaluated and is found to represent approximately 1 per cent of the gross thrust. In practice a region of separated flow may well be present and the terms may only be obtained by pressure surveys. It is recommended that such surveys should be made in future tests.

## APPENDIX B

*Measurement of Gross Thrust in the Altitude Test Bed* (*Section* 4.1.1)

The external pressures acting on the engine in the altitude test bed are shown in the diagram, Fig. 41. Applying the momentum equation to the control volume gives:

$$\int_0^{A_S} p_1 \, dA - \int_0^{A_S} p_0 \, dA - \int_{A_B}^{A_1} p_0 \, dA - \int_{A_6}^{A_B} p_B \, dA - \int_0^{A_6} p_6 \, dA + X + D = \int_0^{A_6} \rho_6 V_6^2 \, dA - \int_0^{A_1} \rho_1 V_1^2 \, dA \tag{12}$$

where the pressures and forces are as defined in Appendix A with the addition of $p_1$ = pressure in the intake duct.
Using the definition of gross thrust, equation (9) of Appendix A, gives:

$$X = X_G - D - \int_0^{A_1} \rho_1 V_1^2 \, dA - \int_0^{A_S} (p_1 - p_0) \, dA - \int_{A_6}^{A_B} (p_0 - p_B) \, dA \, . \tag{13}$$

The measured pressures and velocities across the intake duct do not vary significantly, thus equation (13) becomes,

$$X = X_G - \frac{Q_1 V_1}{g} - (p_1 - p_0) A_S - D - \int_{A_6}^{A_B} (p_0 - p_B) \, dA \tag{14}$$

where $Q_1$ = mass flow of air in the intake duct

As in the case of the ground-level static test bed, the last two terms are negligible. Thus the gross thrust can be expressed in terms of measured quantities,

$$X_G = X + \frac{Q_1 V_1}{g} + (p_1 - p_0) A_S \, . \tag{15}$$

## APPENDIX C

*Measurement of Air Mass Flow in the Test Beds* (*Section* 4.1.2)

1. *General flow equation.*

The general flow equation may be obtained, using the equations for one-dimensional, adiabatic, isentropic flow as follows:

$$\text{Continuity} \qquad Q = \rho A V \tag{16}$$

$$\text{Gas equation} \qquad p = \rho R T \tag{17}$$

$$\text{Specific heats} \qquad R = C_p - C_v = C_p \frac{\gamma - 1}{\gamma} \tag{18}$$

$$\text{Energy equation} \qquad \frac{p_t}{p} = 1 + \frac{\gamma - 1}{2} M^2 \tag{19}$$

$$\text{Sonic velocity} \qquad a^2 = \gamma R T . \tag{20}$$

The general flow equation being

$$Q = \frac{pA}{\sqrt{T_t}} \left(\frac{\gamma}{\gamma - 1}\right) \sqrt{\left\{\frac{2}{C_p}\left(\frac{p_t}{p}\right)^{(\gamma-1)/\gamma} \left[\left(\frac{p_t}{p}\right)^{(\gamma-1)/\gamma} - 1\right]\right\}} \tag{21}$$

Equation (21) may be written as

$$Q = A\lambda \sqrt{\frac{2}{RT_t} p(p_t - p)} \tag{22}$$

where

$$\lambda = \sqrt{\frac{\frac{1}{2}\rho V^2}{(p_t - p)} \frac{T_t}{T}} \tag{23}$$

or

$$\lambda = \sqrt{\frac{\gamma}{(\gamma - 1)} \frac{p_t}{p_t - p} \left[\left(\frac{p_t}{p}\right)^{(\gamma-2)/\gamma} - \left(\frac{p_t}{p}\right)^{-1/\gamma}\right]}. \tag{23a}$$

The factor $\lambda$ represents the correction required to compensate for compressibility effects and is only slightly different from unity for low Mach numbers. For air, ($\gamma = 1{\cdot}4$), the difference is less than 1 per cent for Mach numbers less than 0·57. The variation of $\lambda$ with $(p_t - p)/p_t$ is shown in Fig. 42.

For normal ground-level static test bed conditions the equation (21) can be further simplified by rewriting as:

$$Q = A \sqrt{\frac{2\gamma p_t^2}{(\gamma - 1) RT_t} \left\{\left[1 - \left(\frac{p_t - p}{p_t}\right)\right]^{2/\gamma} - \left[1 - \left(\frac{p_t - p}{p_t}\right)\right]^{\frac{\gamma+1}{\gamma}}\right\}}. \tag{24}$$

The terms within the bracket may then be expanded using $\gamma = 7/5$. The coefficient of the cubic term in $(p_t - p)/p_t$ is found to be zero and assuming the affect of the higher power terms to be negligible for small values of $(p_t - p)/p_t$, the equation (24) becomes

$$Q = A\sqrt{\frac{2}{RT_t}\frac{p(15p - p_t)}{14}} \tag{25}$$

or writing

$$\Delta p = p_t - p \tag{26}$$

and substituting in equation (25)

$$Q = A\sqrt{\frac{2}{RT_t}\Delta p(p_t - \frac{15}{14}\Delta p)}. \tag{27}$$

The error involved in using equation (27) instead of the exact equation (21) is less than 2 parts in 10 000 for Mach numbers less than 0·57 (*c.f.* 100 parts in 10 000 using the incompressible equation, i.e. assuming $\lambda = 1{\cdot}0$ in equation (22)). Equation (27) is a convenient and simple expression for deriving the air mass flow.

2. *Altitude test-bed measurements.*

A venturi measuring section is used to obtain accurate measurements of the air mass flow entering the engine in the altitude test bed. The exact mass flow equation (21) has been used to calculate the flow. The appropriate discharge coefficient, determined from checks with pitot rakes, is included with the area term in the equation. A typical measured pressure distribution is shown in Fig. 43. No corrections have been applied for the small loss of mass flow through the slip joint downstream of the measuring section (Fig. 5), as this was calculated to be negligible.

3. *Ground level static test bed measurements.*

A calibrated bellmouth intake was used for these tests (Fig. 2), and equation (27) was used for the analysis, with a discharge coefficient obtained in earlier tests by Rolls Royce Ltd.

---

## APPENDIX D

*Gross Thrust Equations (Sections 4.2 and 5.3.1)*

Assuming one dimensional, adiabatic, continuous flow, the gross thrust can be expressed in terms of the jet exit pressures as

$$X_G = \left\{ p_6\left(\frac{2\gamma}{\gamma - 1}\right)\left[\left(\frac{p_{6_t}}{p_6}\right)^{\gamma - 1/\gamma} - 1\right] + (p_6 - p_0)\right\} A_6 \tag{28}$$

where the gross thrust is defined as the sum of momentum and pressure forces at the jet exit. For the two different conditions of final nozzle throat choked and unchoked, the equation (28) may be simplified.

*Final nozzle choked*, i.e.

$$\frac{p_{6_t}}{p_0} \geqslant \left(\frac{\gamma+1}{2}\right)^{\gamma/\gamma-1}.$$

Then

$$\left(\frac{p_{6_t}}{p_6}\right) = \left(\frac{\gamma+1}{2}\right)^{\gamma/\gamma-1}$$

and equation (28) becomes

$$\frac{X_G}{A_6\, p_0} = (\gamma+1)\left(\frac{2}{\gamma+1}\right)^{\gamma/\gamma-1}\left(\frac{p_{6_t}}{p_0}\right) - 1. \tag{29}$$

*Final nozzle unchoked*, i.e.

$$\frac{p_{6_t}}{p_0} < \left(\frac{\gamma+1}{2}\right)^{\gamma/\gamma-1}.$$

Then $p_6 = p_0$

and equation (28) becomes

$$\frac{X_G}{A_6\, p_0} = \frac{2\gamma}{(\gamma-1)}\left[\left(\frac{p_{6_t}}{p_0}\right)^{(\gamma-1)/\gamma} - 1\right]. \tag{30}$$

Using the above equations, two relations between gross thrust and the jet-pipe pressure measurements in the present tests may be obtained. Both are described in detail by Rose[1].

1. *Final nozzle static pressure method.*

It can be shown[1] that the static pressure in the final nozzle, $p_5$, is a function of the final nozzle pressures, $p_{6_t}$ and $p_6$, and the area ratio between the two stations $A_5/A_6\,(=\alpha)$. As shown above, the static pressure at the jet exit, $p_6$, is either a fixed proportion of the total pressure, $p_{6_t}$, (jet exit choked), or equal to the ambient static pressure, $p_0$, (exit unchoked). Thus $p_5$ can be obtained as a function of $p_{6_t}$ and $\alpha$ only. Equations (29) and (30) then become

*Choked*

$$\frac{X_G}{p_0} = \frac{A_5}{\alpha}\left[\frac{(\gamma+1)}{\beta}\left(\frac{p_5}{p_0}\right) - 1\right]. \tag{31}$$

*Unchoked*

$$\frac{X_G}{p_0} = \frac{2\gamma\,\alpha\,A_5}{(\gamma-1)}\left\{\frac{(p_5/p_0)^{2/\gamma} - (p_5/p_0)^{(\gamma+1)/\gamma}}{1-\alpha^2(p_5/p_0)^{2/\gamma}}\right\} \tag{32}$$

where $\beta$ in equation (31) is the ratio $p_5/p_6$ and is a function of $\alpha$ and $\gamma$ only, with a choked exit, i.e. it is constant for a given configuration.

In practice the assumptions used in deriving equations (31) and (32) will not be completely satisfied, and test bed measurements are used to obtain calibrations of the effective area, $A_5$, or a direct calibration of $X_G/p_0$ as a function of $p_5/p_0$. Flight measurements obtained using these calibrations are designated $X_{G_1}$.

2. *Transition section total pressure method.*

The transition section total pressure, $p'_{4_t}$, is related to the jet exit total pressure, $p_{6_t}$, by the equation

$$p_{6_t} = p'_{4_t}\left(1-\frac{\Delta p_t}{p'_{4_t}}\right) \tag{33}$$

where $\Delta p_t$ is the loss of total pressure between Stations 4 and 6. This loss of total pressure is mainly caused by the drag of the reheat burner system plus the combustion loss when reheat is burning. Using equation (33), equations (29) and (30) become

*Choked*

$$\frac{X_G}{p_0} = A_6\left\{(\gamma+1)\left(\frac{2}{\gamma+1}\right)^{(\gamma+1)/(\gamma-1)}\left(\frac{p'_{4_t}}{p_0}\right)\left(1-\frac{\Delta p_t}{p'_{4_t}}\right)-1\right\}. \tag{34}$$

*Unchoked*

$$\frac{X_G}{p_0} = \frac{2\gamma A_6}{(\gamma-1)}\left[\left\{\left(\frac{p'_{4_t}}{p_0}\right)\left(1-\frac{\Delta p_t}{p'_{4_t}}\right)\right\}^{(\gamma-1)/\gamma}-1\right]. \tag{35}$$

Thus, unlike the final nozzle static-pressure method, calibration of these transition section equations for the practical case is only possible if either an independent measurement of the jet-pipe pressure loss is made or this loss is assumed to be a function of $p'_{4_t}/p_0$ only. Usually, the latter assumption is made, although this is only true for constant ram ratio, $p_{1_t}/p_0$, conditions, but as the pressure loss is normally constant for most high ram ratio conditions a unique calibration of $X_G/p_0$ as a function of $p'_{4_t}/p_0$ may be obtained from the test bed. In the present tests, and those of Ref. 1, the jet-pipe pressure loss was measured independently by the jet-efflux traversing probe. However only the ground-level results were accurately defined, the altitude results having considerable scatter because of the smaller pressure difference, and, thus it has not been possible to calibrate in terms of the effective area, $A_6$. The flight measurement of gross thrust obtained using this method is designated $X_{G_2}$.

## APPENDIX E

### *Air Mass-flow Equations* (*Sections* 4.2 *and* 5.3.2)

Assuming one-dimensional, adiabatic flow, the gas mass flow at any station is given by (*see* Appendix C)

$$Q = \frac{pA}{\sqrt{T_t}}\sqrt{\frac{2}{C_p}}\sqrt{\left\{\left(\frac{p_t}{p}\right)^{(\gamma-1)/\gamma}\left[\left(\frac{p_t}{p}\right)^{(\gamma-1)/\gamma}-1\right]\right\}}. \tag{21}$$

The following three methods have been used to obtain the relations between internal pressures and temperatures and the air mass flow, as described in detail by Rose[1].

1. *Transition section method.*

In the transition section the total and static pressures and the total temperature are measured and the air mass flow may be calculated directly from the equation (21), or more simply, by applying the value of $\gamma$ for the transition section of 4/3, equation (21) may be explanded to give the approximate equation

$$Q_4 \approx A_4 \sqrt{\left\{\frac{2}{RT_{4_t}} \Delta p_4 \left(p_{4_t} - \frac{9}{8}\Delta p_4\right)\right\}} \tag{36}$$

where $\Delta p_4 = p_{4_t} - p_4$

Equation (36) is accurate to better than 0·1 per cent at the highest transition pipe Mach number and has been used for the calculations in this Report. The effective area $A_4$ (or $A'_4$) required to obtain measurements of air mass flow in flight is obtained from test-bed results where the mass flow is measured independently. The air mass flow entering the compressor is obtained from the mass flow in the transition section after subtracting the engine fuel mass flow and correcting for the 2·5 per cent of compressor air bled off for various purposes. The air mass flow obtained using this method in flight is designated $Q_{11}$.

2. *Turbine nozzle guide vane total pressure method.*

Flow through the turbine nozzle guide vanes is choked for most engine conditions and equation (21) reduces to

$$Q_3 = \frac{p_{3_t} A_3}{\sqrt{T_{3_t}}} \gamma \left(\frac{2}{(\gamma-1)}\right)^{\gamma/\gamma-1} \sqrt{\frac{(\gamma+1)}{2C_p(\gamma-1)}}. \tag{37}$$

The nozzle guide vane total pressure, $p_{3_t}$, is measured, and the turbine entry total temperature, $T_{3_t}$, is obtained by equating the compressor and turbine work using a mechanical efficiency for the transmission, $\eta_M$ of 99 per cent. The work equation is

$$Q_1 C_{p_{12}} (T_{2_t} - T_{1_t}) = Q_3 C_{p_{34}} (T_{3_t} - T_{4_t}) \eta_M \tag{38}$$

and substituting

$$Q_3 = 0{\cdot}975\, Q_1 + Q_E \text{ and } Q_E/0{\cdot}975\, Q_1 = q$$

where $q$ = fuel-air ratio.
Equation (38) becomes

$$C_{p_{12}} (T_{2_t} - T_{1_t}) = 0{\cdot}975\, C_{p_{34}} (T_{3_t} - T_{4_t}) (1+q) \eta_M . \tag{39}$$

In this equation the temperatures $T_{1_t}$, $T_{2_t}$ and $T_{4_t}$ are measured, and $T_{3_t}$ and $q$ are the unknowns. However, $q$ is related to the combustion temperature rise $(T_{3_t} - T_{2_t})$ and is not an independent parameter. Using an iterative method, *see* Ref. 1, the value of $T_{3_t}$ is obtained. From the independent measurements of air mass flow in the test beds, the effective area, $A_3$, can be determined. The flight measurements of air mass flow using this method, after correction for engine fuel flow and the 2·5 per cent bleed, are designated $Q_{12}$.

3. *Fuel-air ratio method.*

In the solution of equation (39) for turbine entry temperature, the fuel-air ratio is also derived. Thus from measurements of engine fuel flow the air mass flow in flight may be obtained. The values of the derived and the actual fuel-air ratio must first be compared in the test beds to evaluate the calibration factor which is close to unity. The air mass flow measured in flight using this method is designated $Q_{13}$.

TABLE 1

*Engine data*

| | |
|---|---|
| Type | Rolls Royce RA28R |
| Serial No. Engine | 7482 |
| Jet pipe | 653 |
| Rated static thrust at 100 per cent r.p.m. with parallel slave jet pipe and 20·8 inches diameter machined final nozzle | 10 550 lb |
| Static thrust at 100 per cent r.p.m. with reheat jet pipe No. 653 | 9 500 lb |
| Reheat static thrust at 100 per cent r.p.m. and $p_2/p'_4 = 3{\cdot}43$ | 12 250 lb |
| Geometric area of the turbine inlet throat (Station 3) | 130·8 $in^2$ |
| Geometric area of the transition pipe (Station 4) | 454·2 $in^2$ |
| Geometric area of the final nozzle (Station 5) | 562·9 $in^2$ |
| Geometric area of the jet exit (Station 6) nozzle closed | 360 $in^2$ |
| nozzle open | 504 $in^2$ |

*Note.*—All geometric areas calculated at the mean working temperature for the station.

TABLE 2

*Engine and jet pipe instrumentation*

| Symbol | Parameter | Method of measurement |
|---|---|---|
| $p_2$ | Compressor delivery static pressure | Single wall tapping in one of the outlet ducts. |
| $T_{2_t}$ | Compressor delivery total temperature | Four copper/constantan thermocouples; two in each of two outlet ducts (not the duct used for the pressure tapping). The couples were connected in parallel. |
| $p_{3_t}$ | Turbine inlet total pressure | Twelve holes, six drilled in the leading edges of each of two diametrically opposite nozzle guide vanes (Fig. 44); the pressures were manifolded to give a mean reading. |
| $p'_{4_t}$ | Transition section wall total pressure | Four pitot tubes equi-spaced around the wall of the pipe; the pressures were manifolded to give a mean reading. |
| $p_{4_t}$ | Transition section rake total pressure | An integrating rake of six total head probes placed on the centres of equal annular areas; the pressures were manifolded to give a mean reading. Figs. 45 and 46 show the instrumentation in the transition section*. |
| $p'_4$ | Transition section wall static pressure | Three wall tappings equi-spaced around the circumference of the pipe (Fig. 45); the pressures were manifolded. |
| $p_4$ | Transition section rake static pressure | A single static pressure probe at the centre of the pipe. |
| $T_{4_t}$ | Transition section rake total temperature | Three rakes of five chromel/alumel thermocouples placed on the centres of equal annular areas, and one thermocouple at the centre of the pipe (Figs. 45 and 46); the couples from each rake were connected in parallel. |
| $T'_{4_t}$ | Diffuser total temperature | Eight of the sixteen chromel/alumel thermocouples in wall tappings in the diffuser section connected in parallel. |

*During the ground level static tests of this report a leak was discovered and repaired in the transition section total-pressure rake. This leak was almost certainly present during the tests of Ref. 1 and the subsequent flight tests. Thus it has not been possible to use the measured transition section rake total pressure in analysing the flight tests.

TABLE 2—*continued*

| Symbol | Parameter | Method of measurement |
|---|---|---|
| $p_5$ | Final nozzle static pressure | A pair of diametrically opposite wall tappings 7·9 inches from the jet-pipe lip: the pressures were manifolded. |
| $N$ | Engine r.p.m. | Direct mechanical drive with standard tachometer. |
| $Q_E$ | Engine fuel flow rate | Temperature compensated volumetric flow meter, corrected for fuel specific gravity on test bed only. |
| $Q_R$ | Reheat fuel flow rate | As $Q_E$ above. |

In addition the following quantities were measured for engine control and monitoring purposes during the test-bed runs.

Inlet guide vane position (ground level static only)
Centre and rear bearing temperatures
Lubricating oil inlet temperature and pressure
Throttle position
Engine speed
Engine low pressure fuel supply pressure
Engine burner pressure
Jet-pipe temperature (eight thermocouples in the diffuser section)
Reheat turbo-pump air inlet pressure
Reheat turbo-pump fuel inlet pressure
Reheat burner pressure
Jet exit eyelid position
Jet pipe cooling annulus temperature
Jet pipe cooling annulus static pressure
Compressor case vibration: vertical and lateral

TABLE 3

*Values of $C_p$ and $\gamma$*

Using the data of Fielding and Topps[7], values of the specific heat at constant pressure and the ratio of the specific heats at various points in the engine have been estimated. For each particular point mean values of the temperature and fuel/air ratio have been assumed.

| Parameter | Nozzle guide vanes non-reheat or reheat | Transition section non-reheat or reheat | Final nozzle non-reheat | Final nozzle reheat |
|---|---|---|---|---|
| Mean temperature °K | 1200 | 950 | 950 | 1750 |
| Mean fuel/air ratio | 0·0167 | 0·0167 | 0·0167 | 0·0500 |
| $\gamma$ | 1·32 | 1·33 | 1·33 | 1·27 |
| $C_p$ ft lb/(slug. deg K) | 12890 | 12348 | 12348 | 14433 |

FIG. 1. Fairey Delta 2.

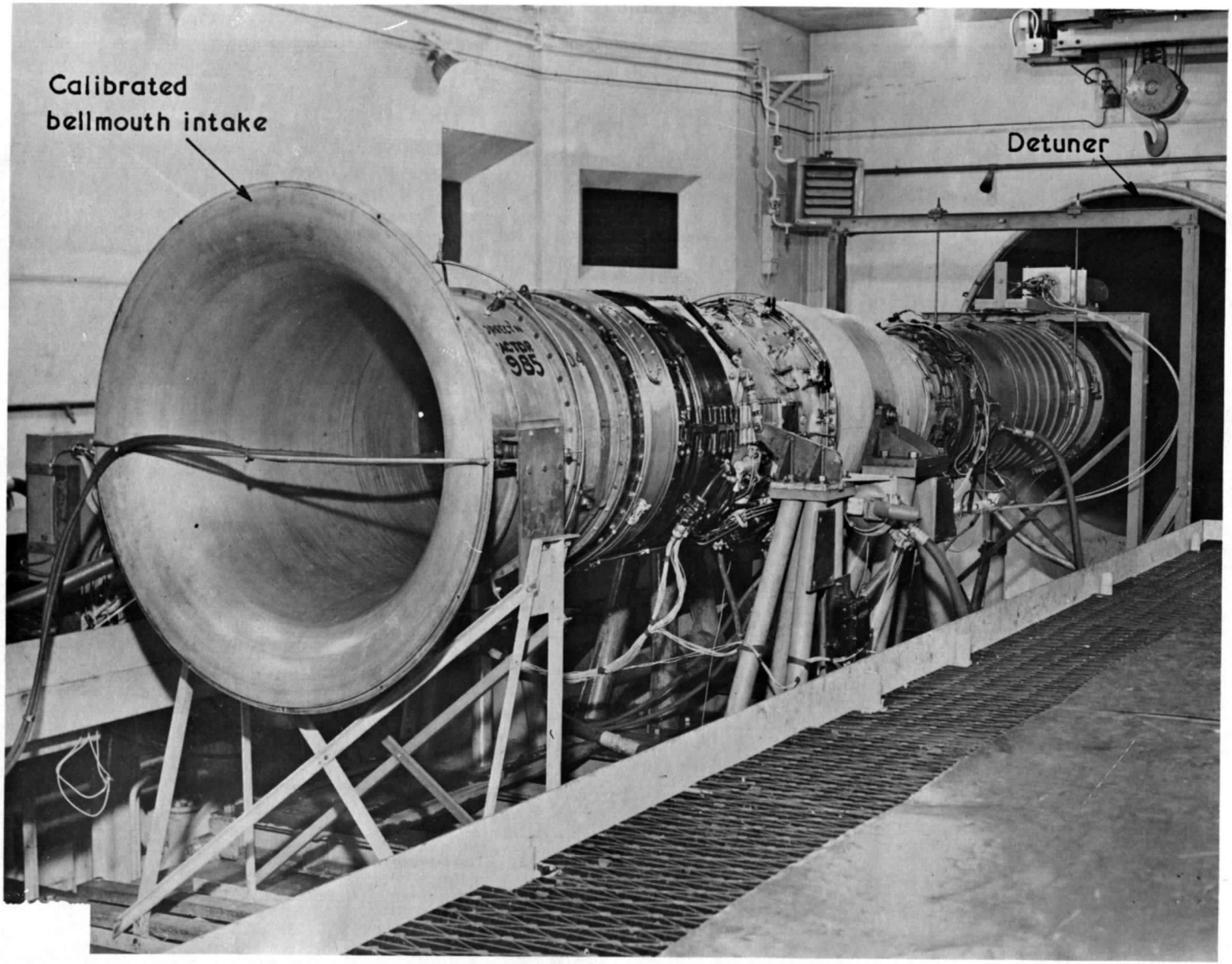


FIG. 2. Engine installed in the Glen ground-level static test bed, N.G.T.E.

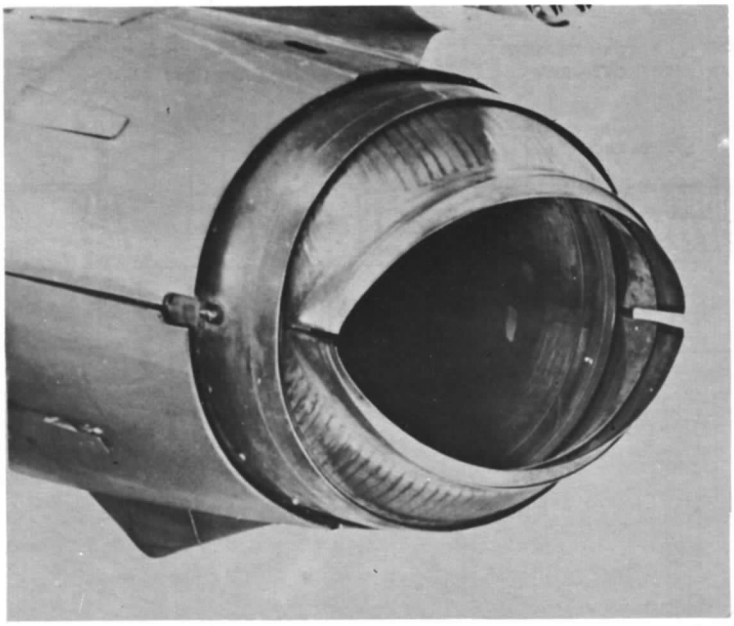

a. Non-reheat final nozzle

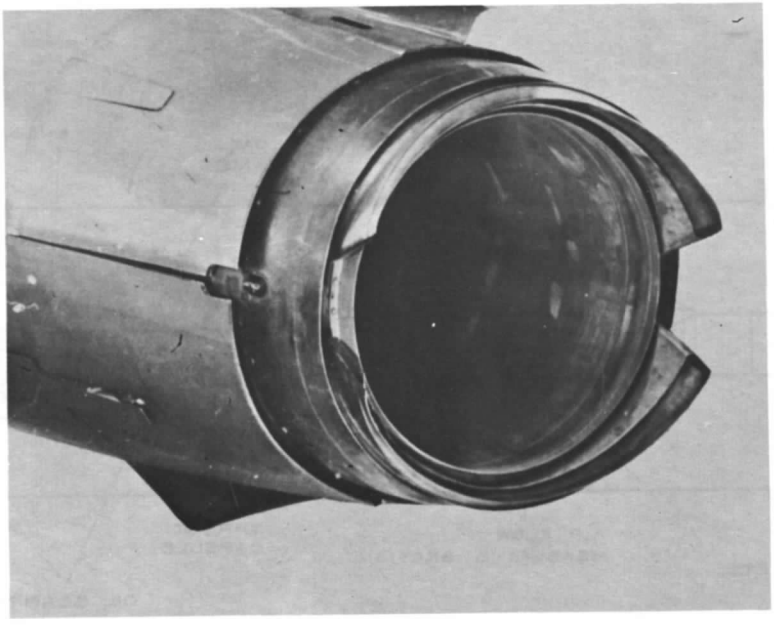

b, Reheat final nozzle

FIG. 3. Final nozzle in reheat and non-reheat positions.

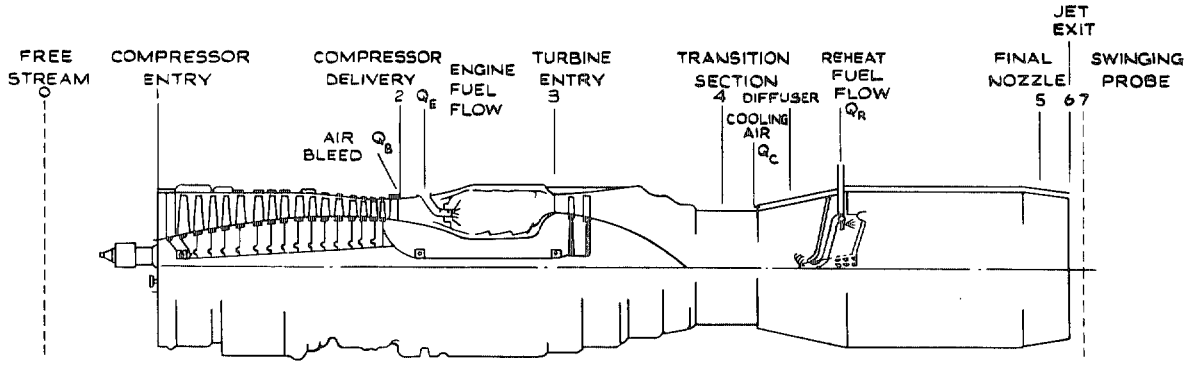


FIG. 4. Engine reference planes.

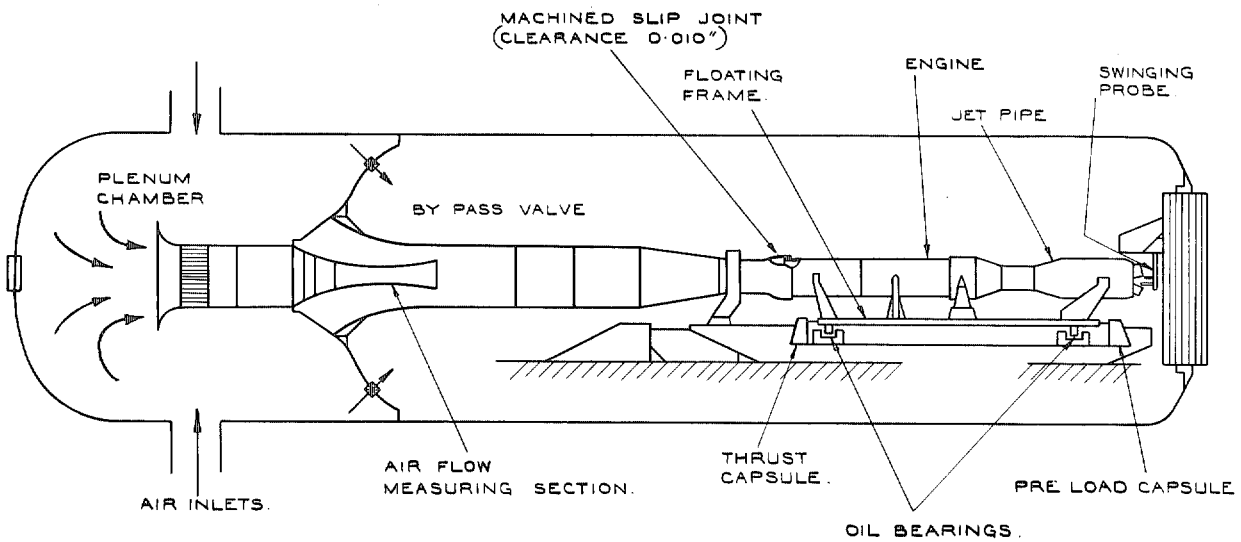


FIG. 5. Diagram of RA28 Avon installed in the N.G.T.E. cell 3 altitude test bed.

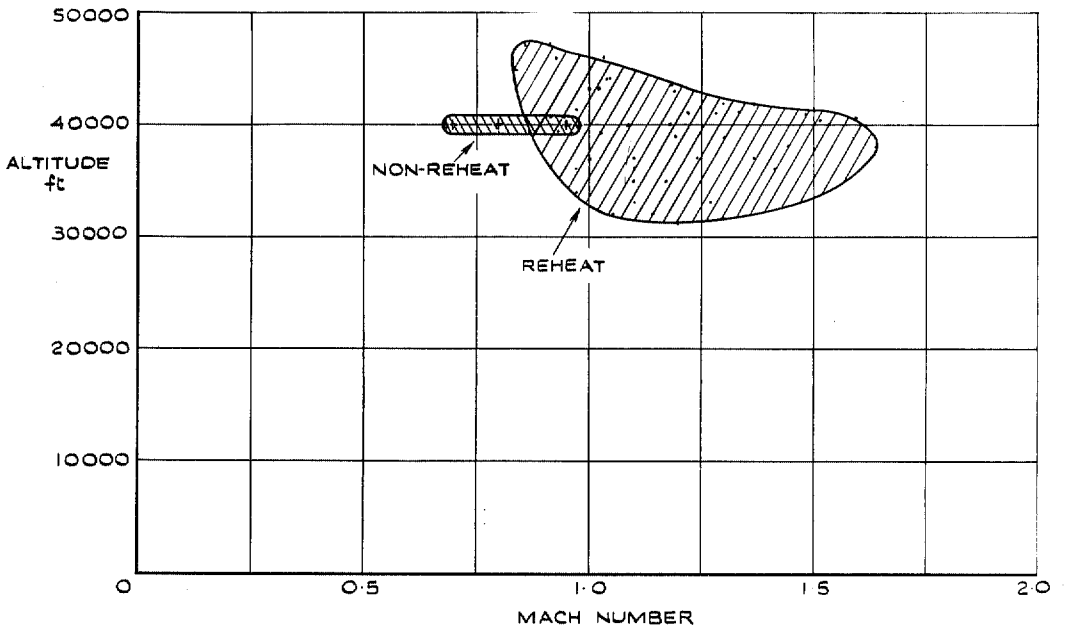


FIG. 6. Envelope of flight tests.

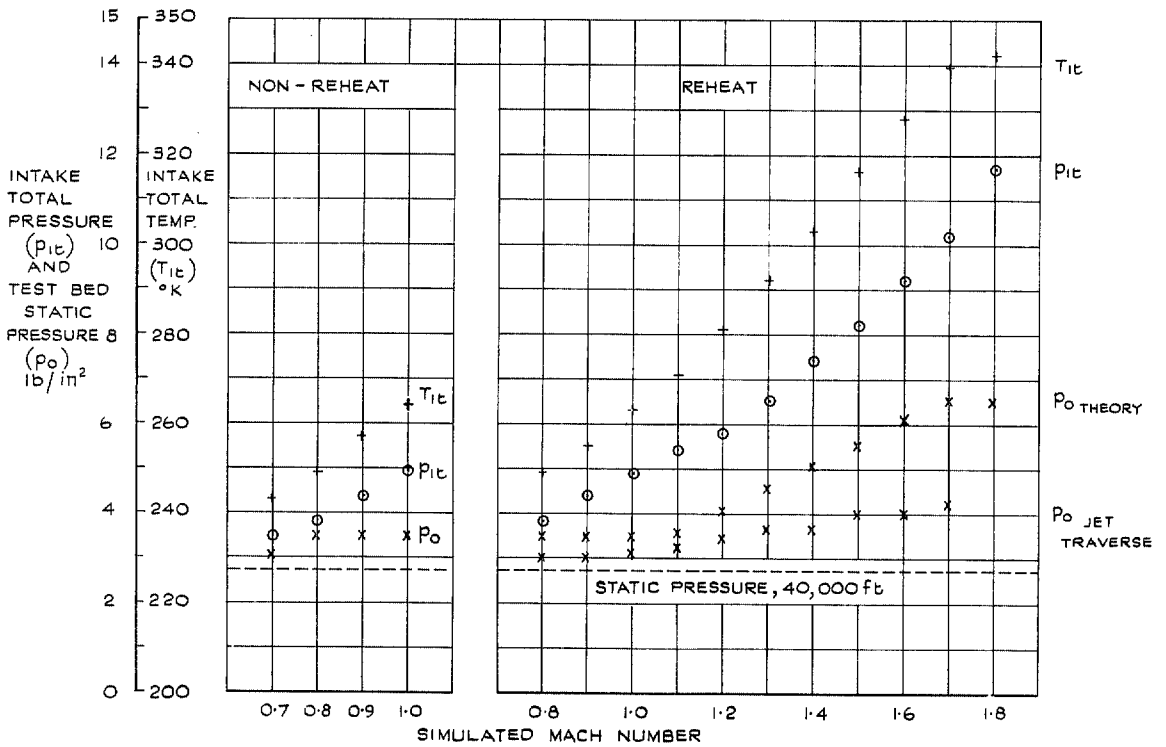


FIG. 7a. Intake and test-bed conditions for the altitude tests. Simulated flight conditions at 40,000 ft.

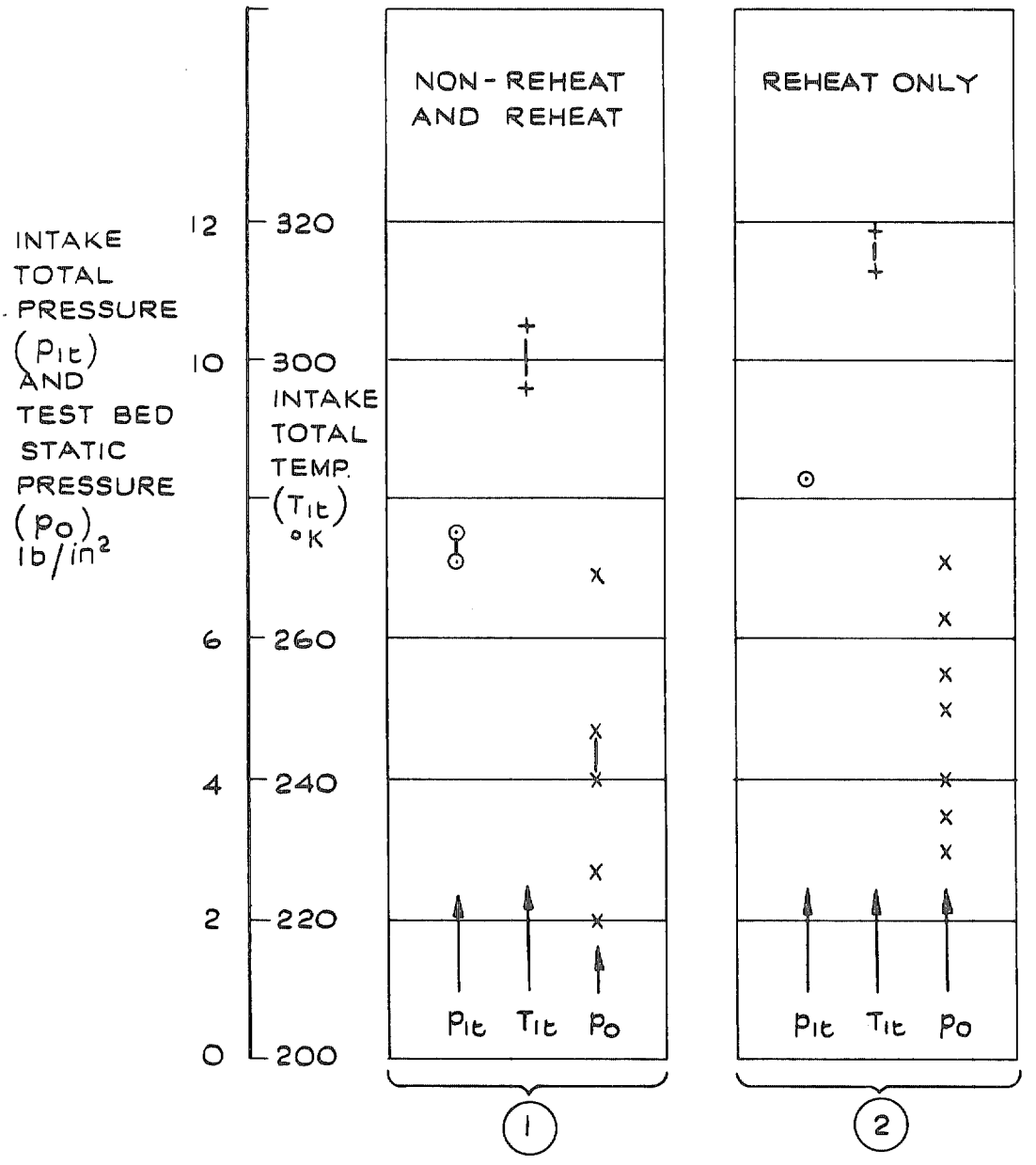


FIG. 7b. Intake and test bed conditions for the altitude tests.
Test bed pressure varied at nominally constant intake conditions.

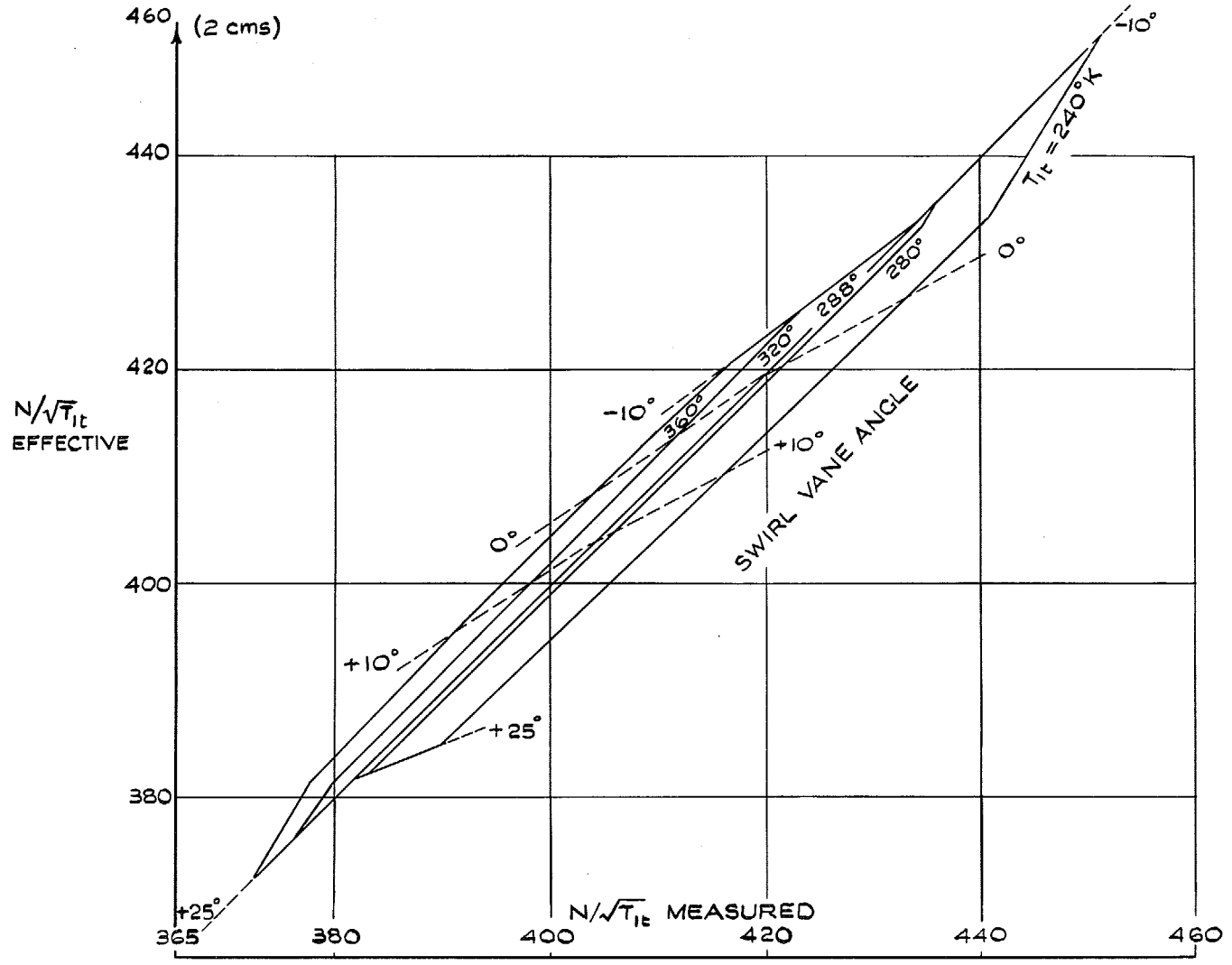


FIG. 8. Correction of engine speed for inlet swirl vane operation.

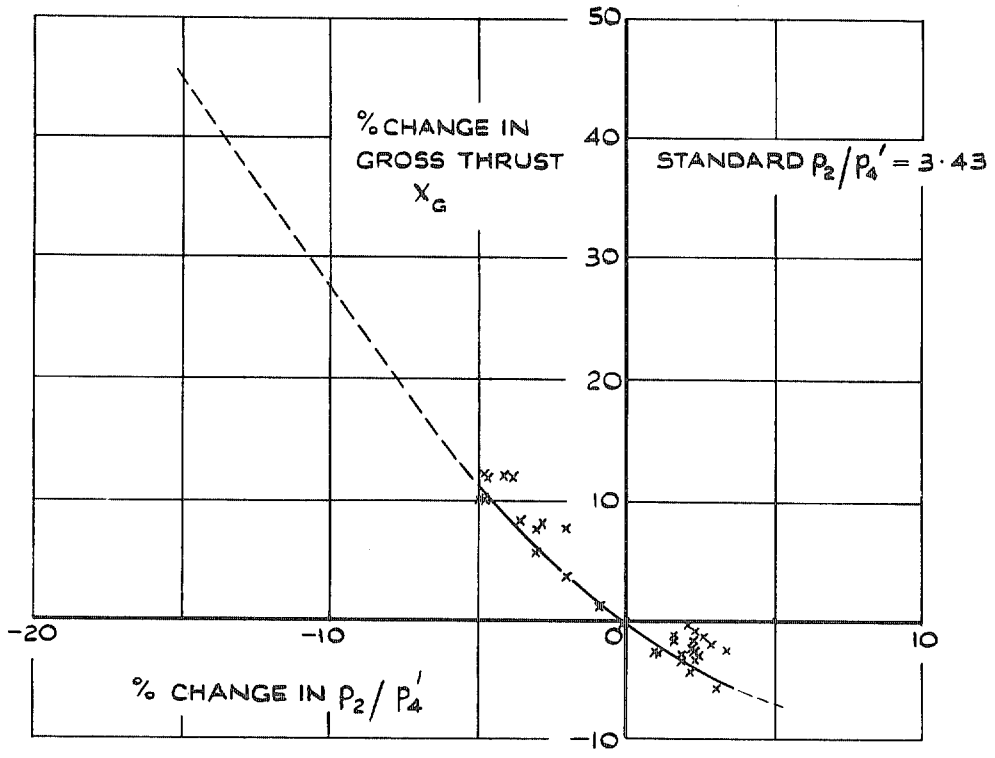


FIG. 9a. Reheat correction curves—gross thrust.

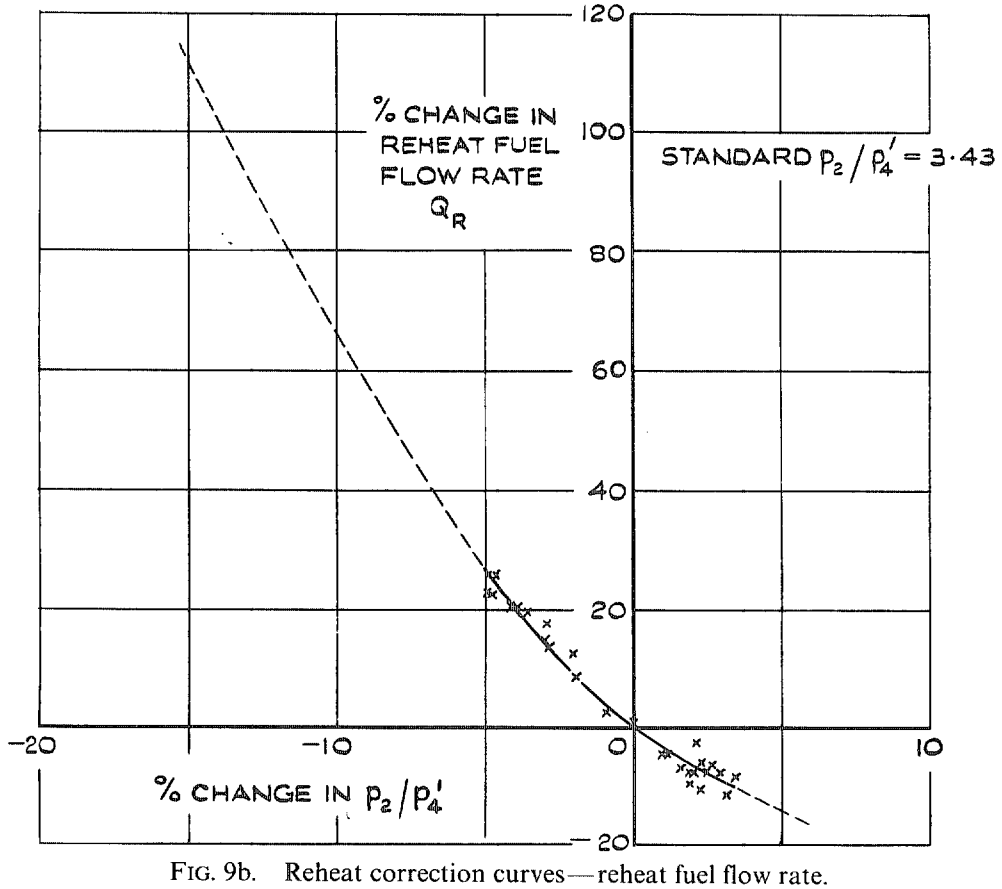


FIG. 9b. Reheat correction curves—reheat fuel flow rate.

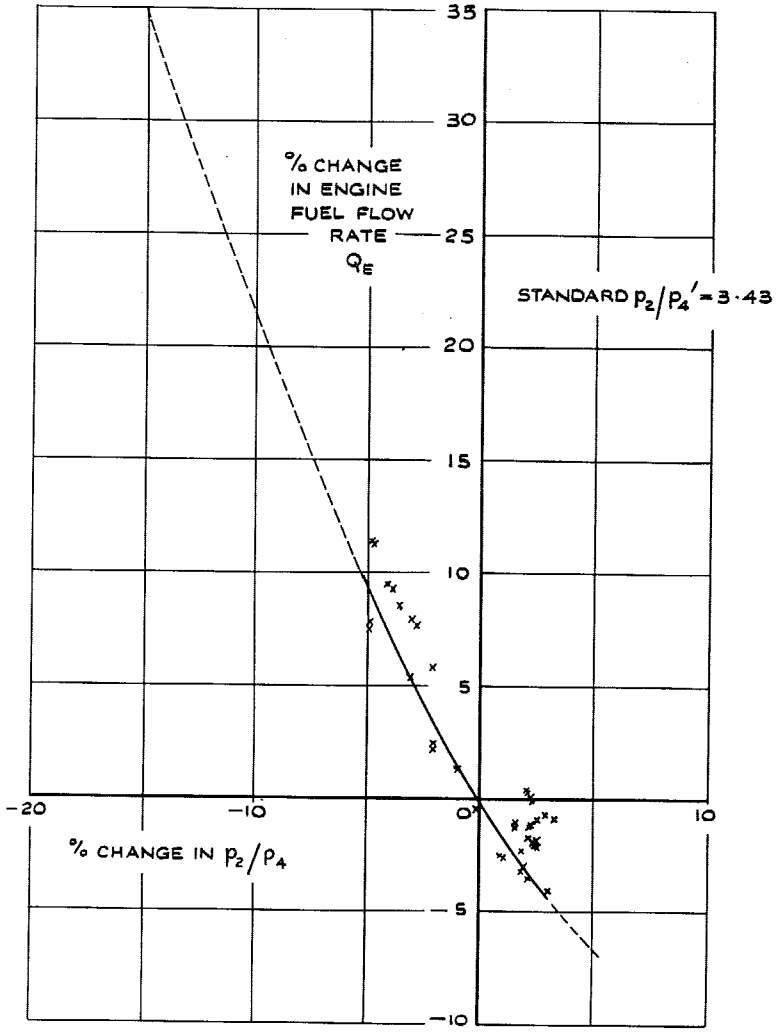


FIG. 9c. Reheat correction curves—engine fuel flow rate.

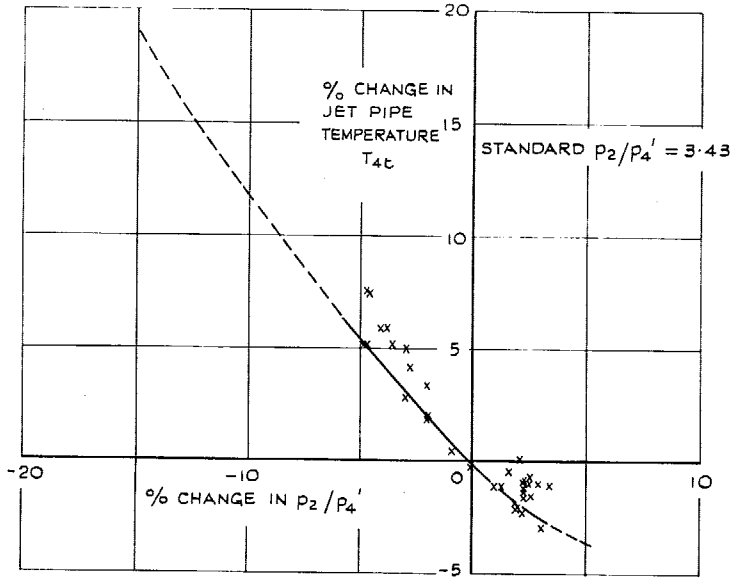


FIG. 9d. Reheat correction curves—jet pipe temperature.

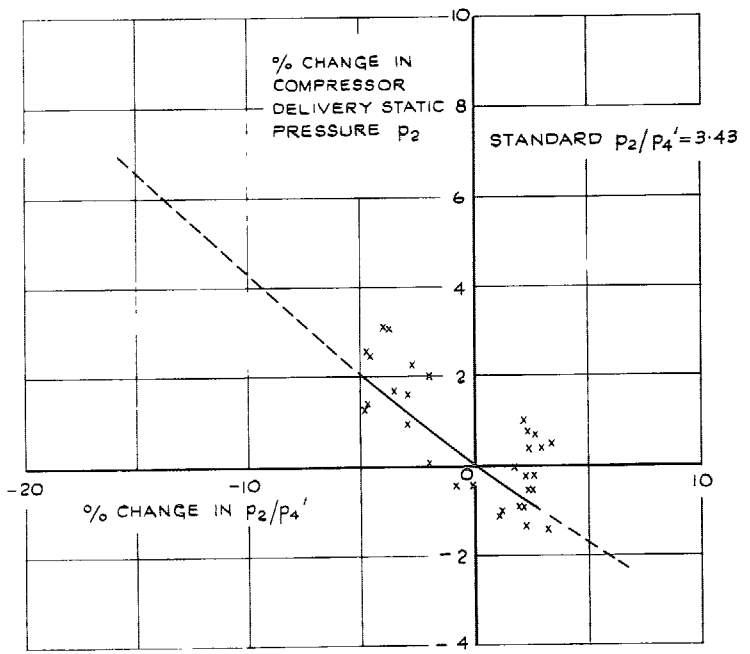


FIG. 9.e. Reheat correction curves—compressor delivery static pressure.

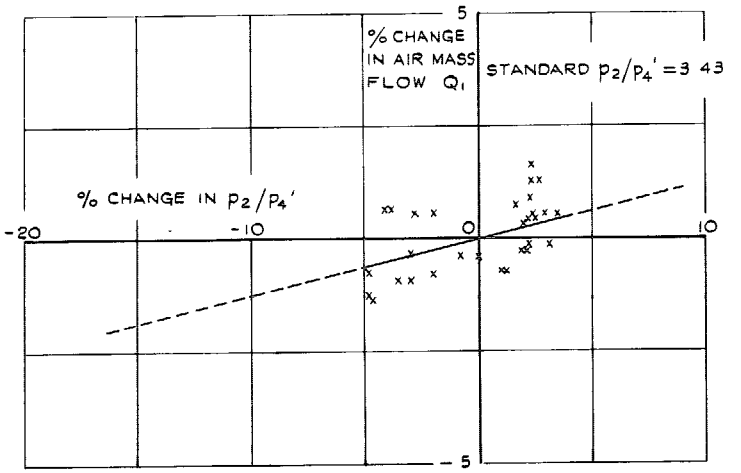


FIG. 9f. Reheat correction curves—air mass flow.

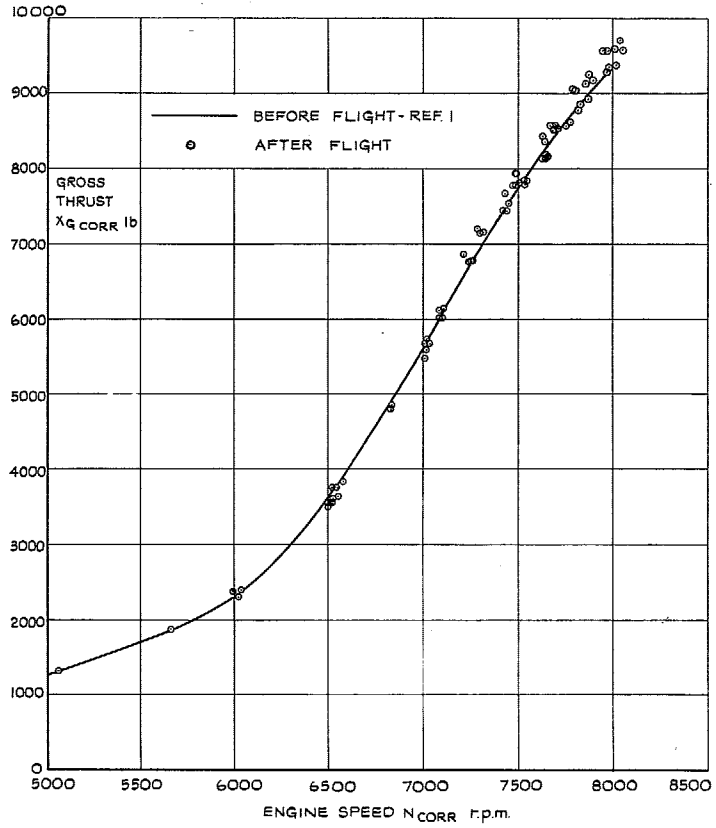


FIG. 10. Gross thrust variation with engine speed—before and after flight tests (non-reheat).

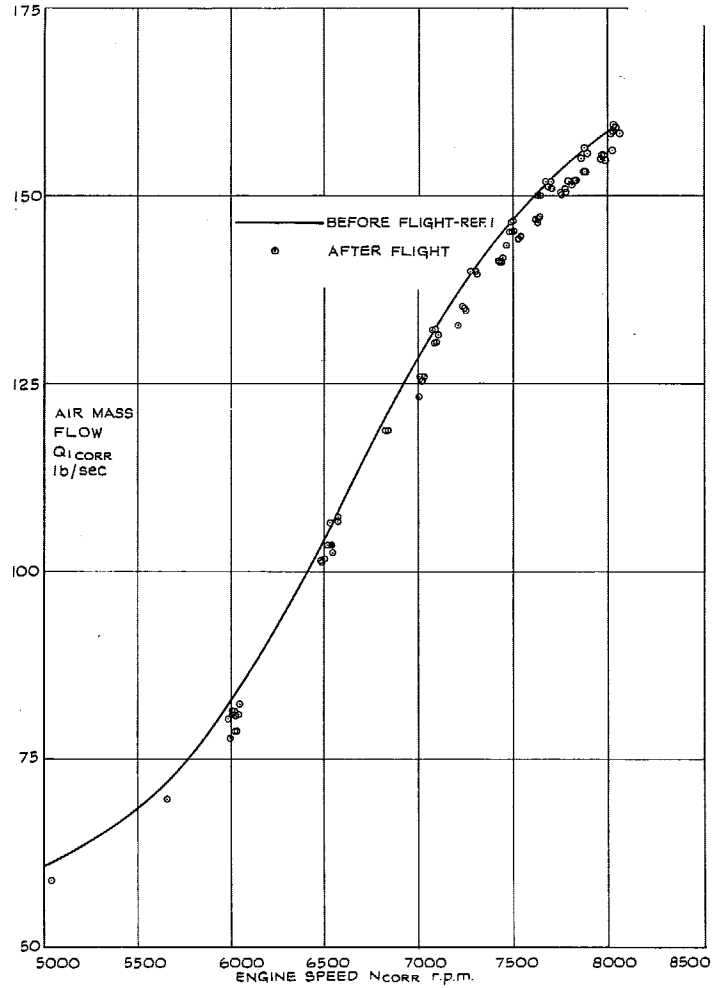


FIG. 11. Air mass-flow variation with engine speed—before and after flight tests (non-reheat).

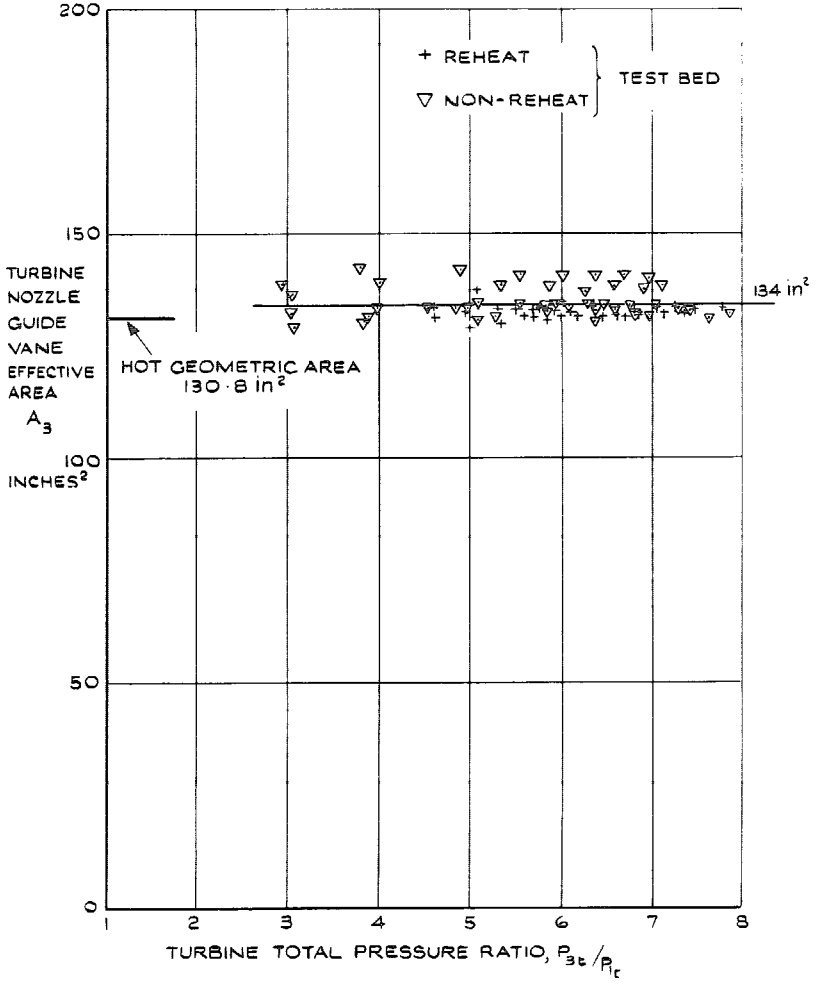


FIG. 12. Variation of turbine nozzle guide vane effective area with turbine total pressure ratio.

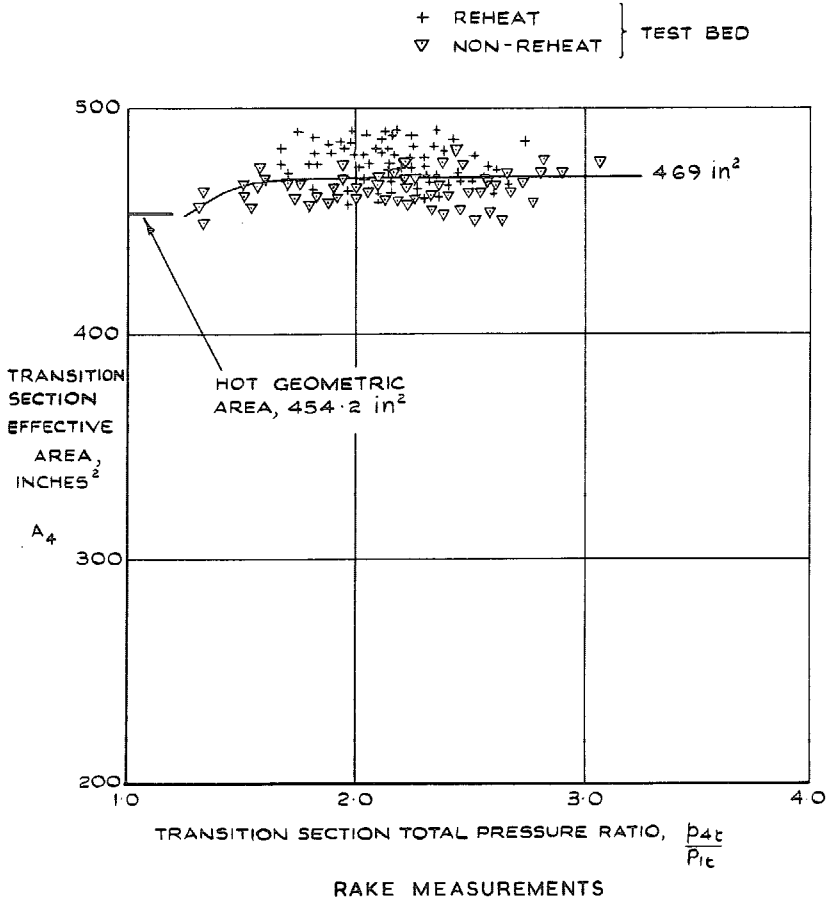


FIG. 13a. Variation of transition section effective areas with transition section total pressure ratios.

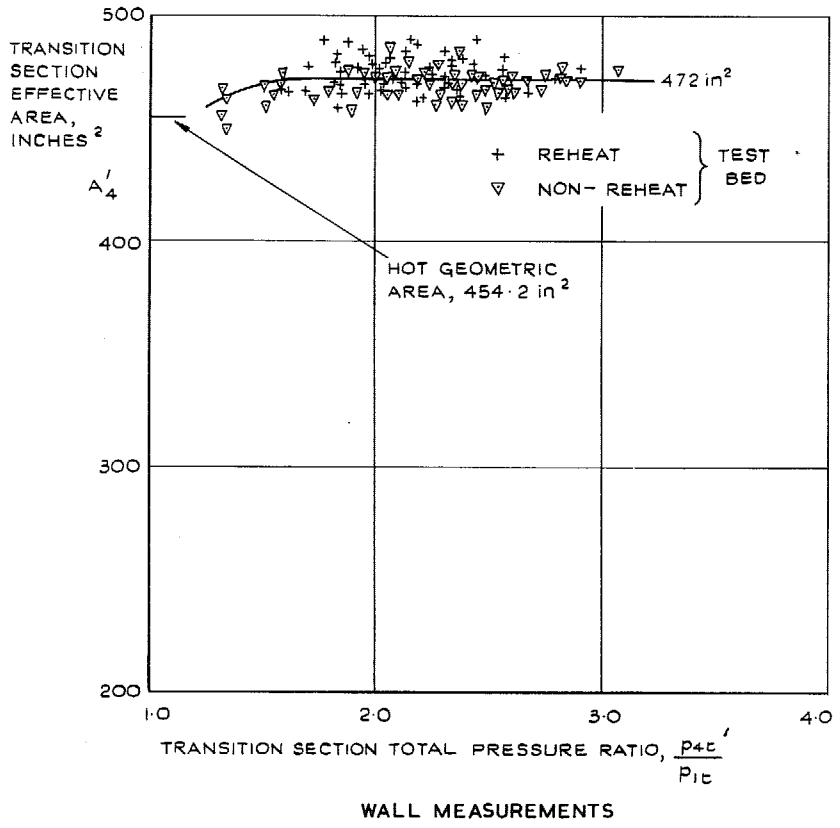


FIG. 13b. Variation of transition section effective areas with transition section total pressure ratios.

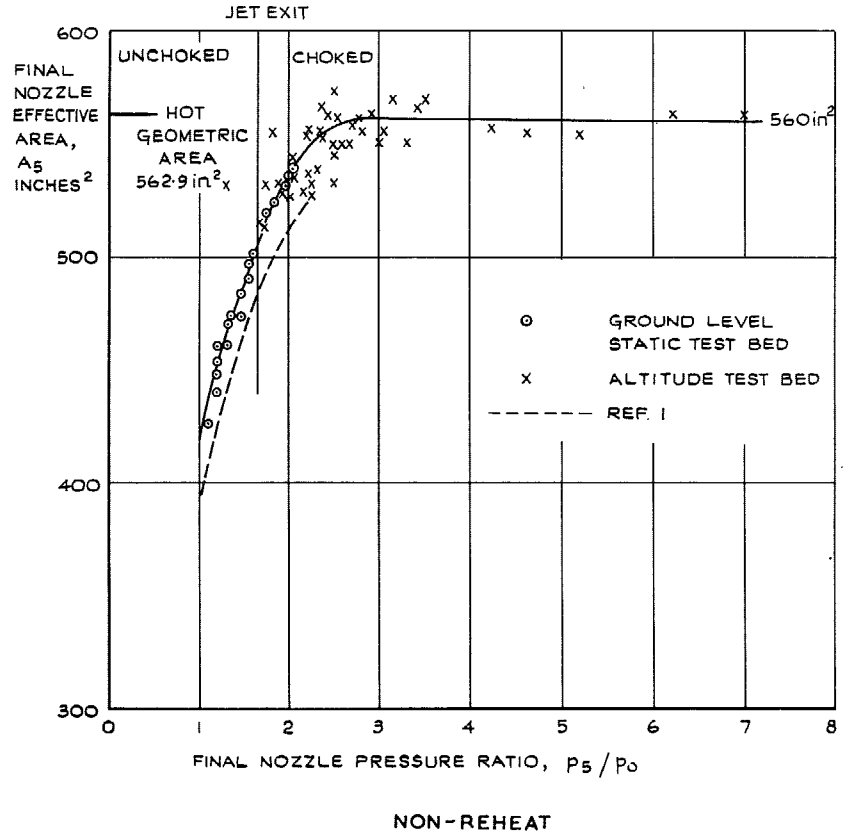


FIG. 14a. Variation of final nozzle effective area with nozzle pressure ratio.

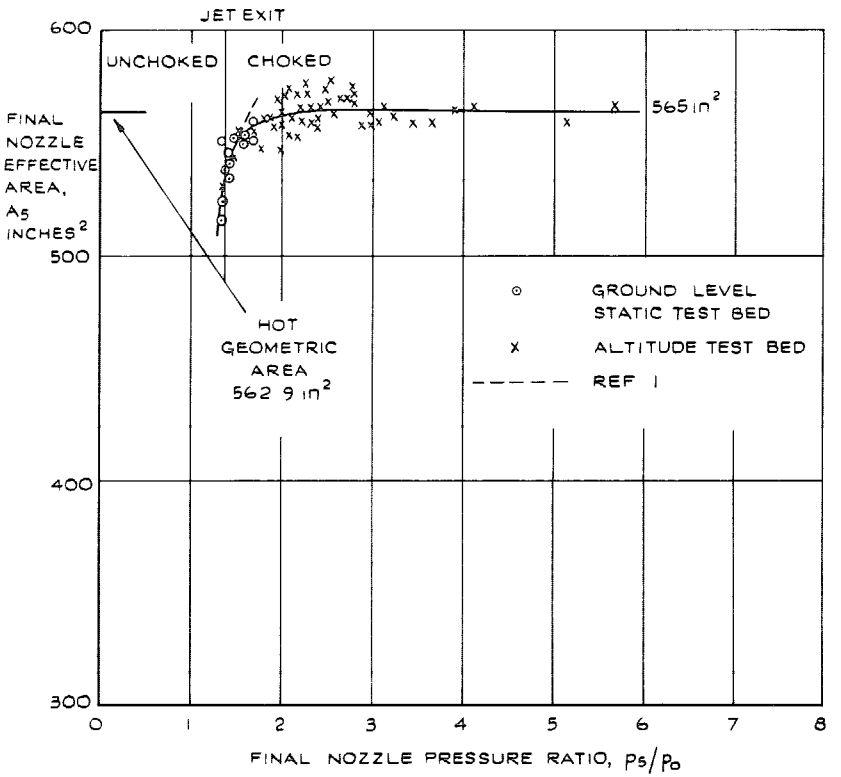


FIG. 14b. Variation of final nozzle effective area with nozzle pressure ratio.

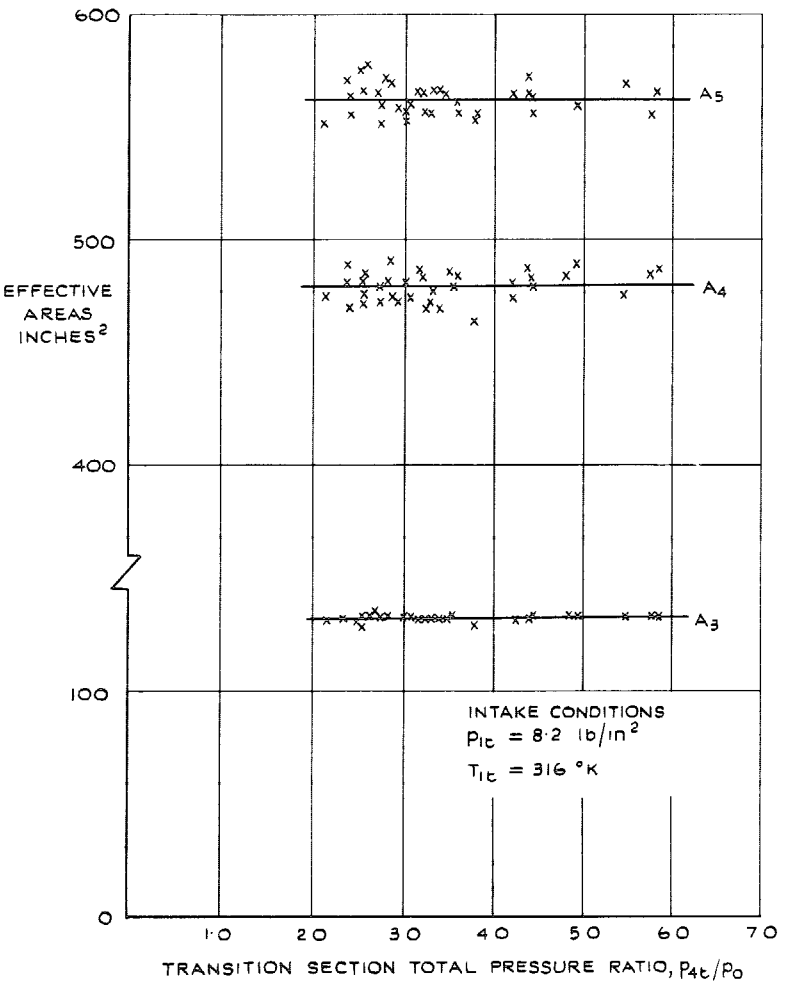


FIG. 15. Effect of cell static pressure on the effective areas at constant intake conditions—reheat.

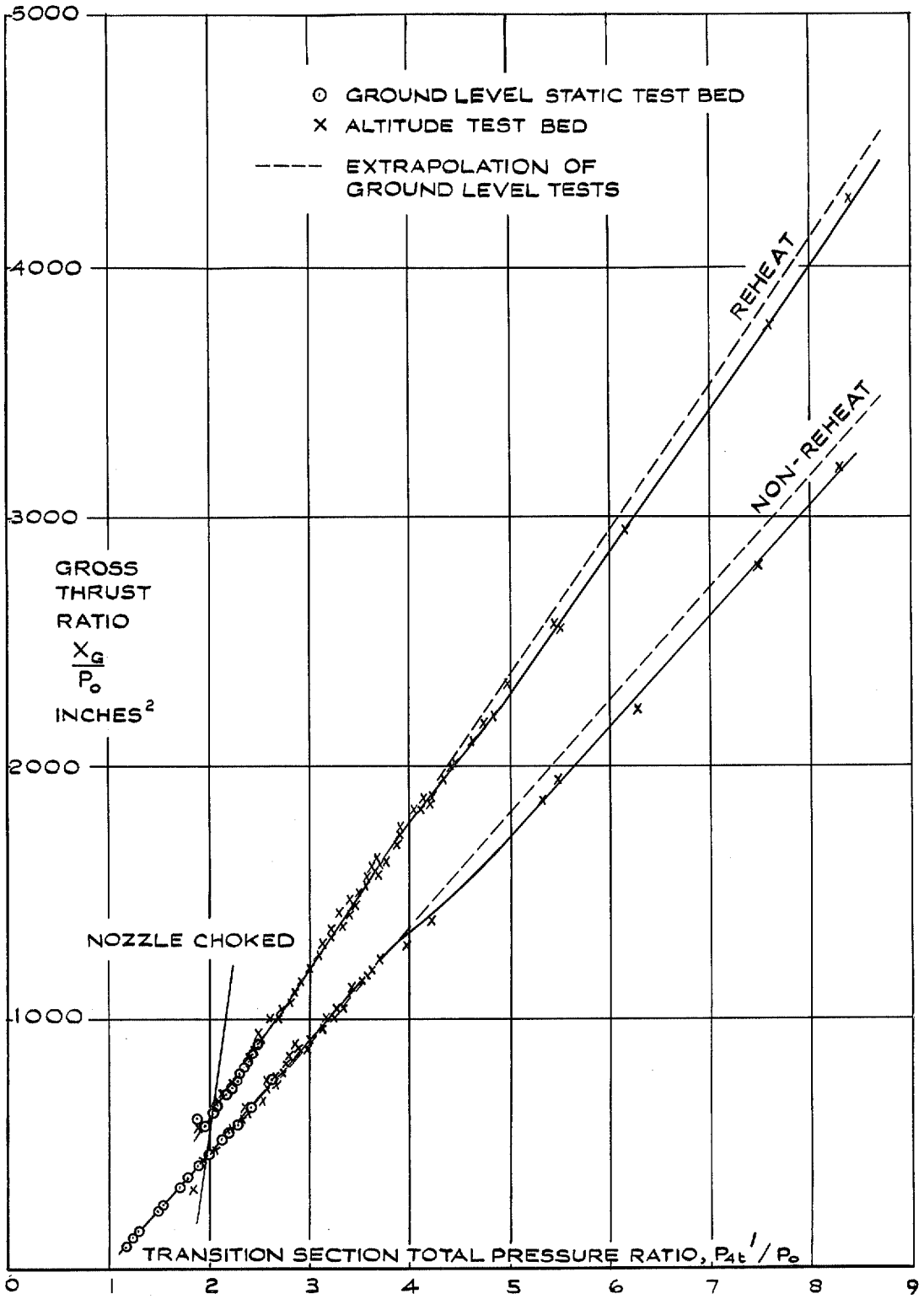


FIG. 16. Calibration of gross thrust against transition section total pressure ratio.

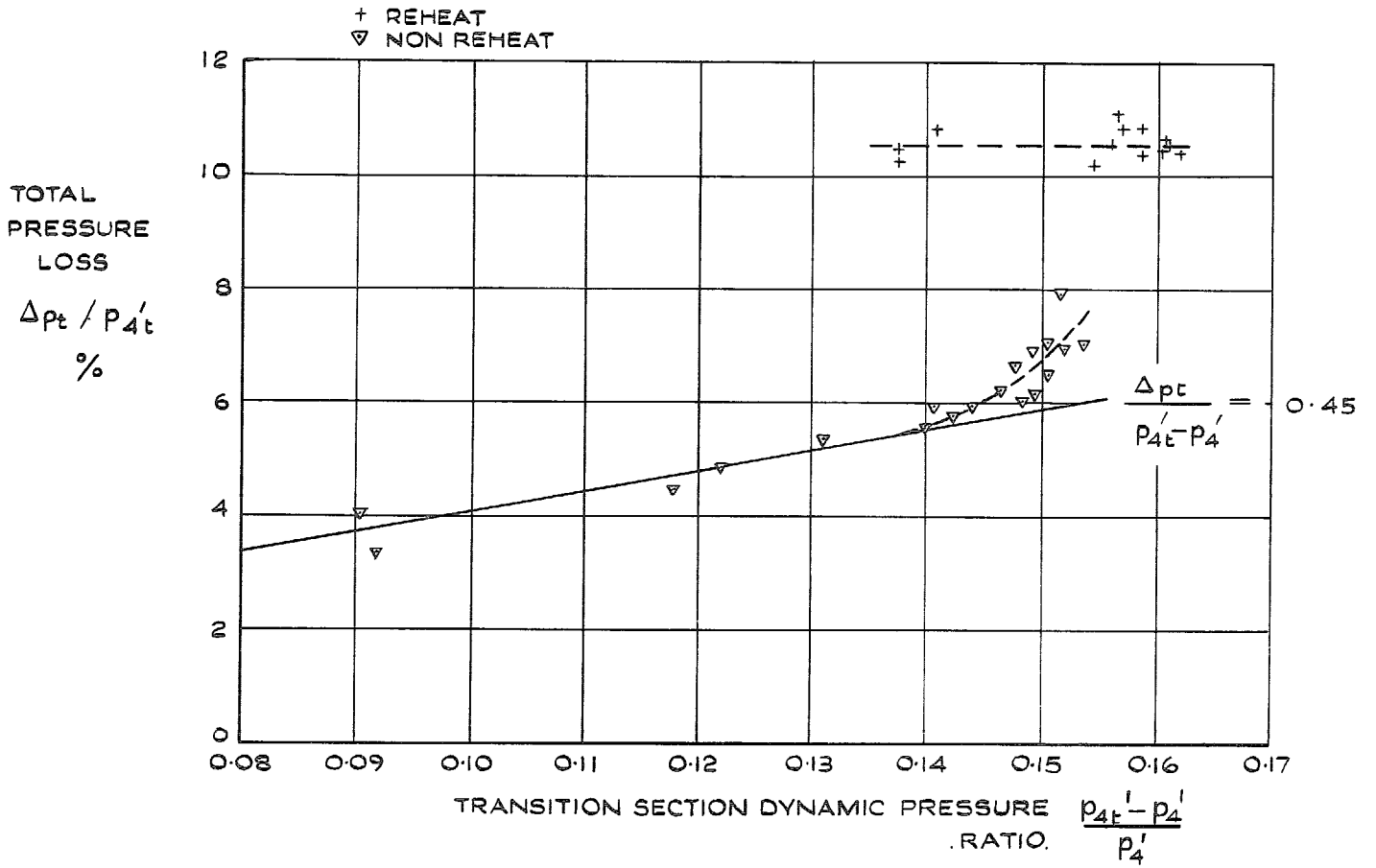


FIG. 17. Variation of total pressure loss with transition section dynamic pressure ratio measured in the ground-level test bed.

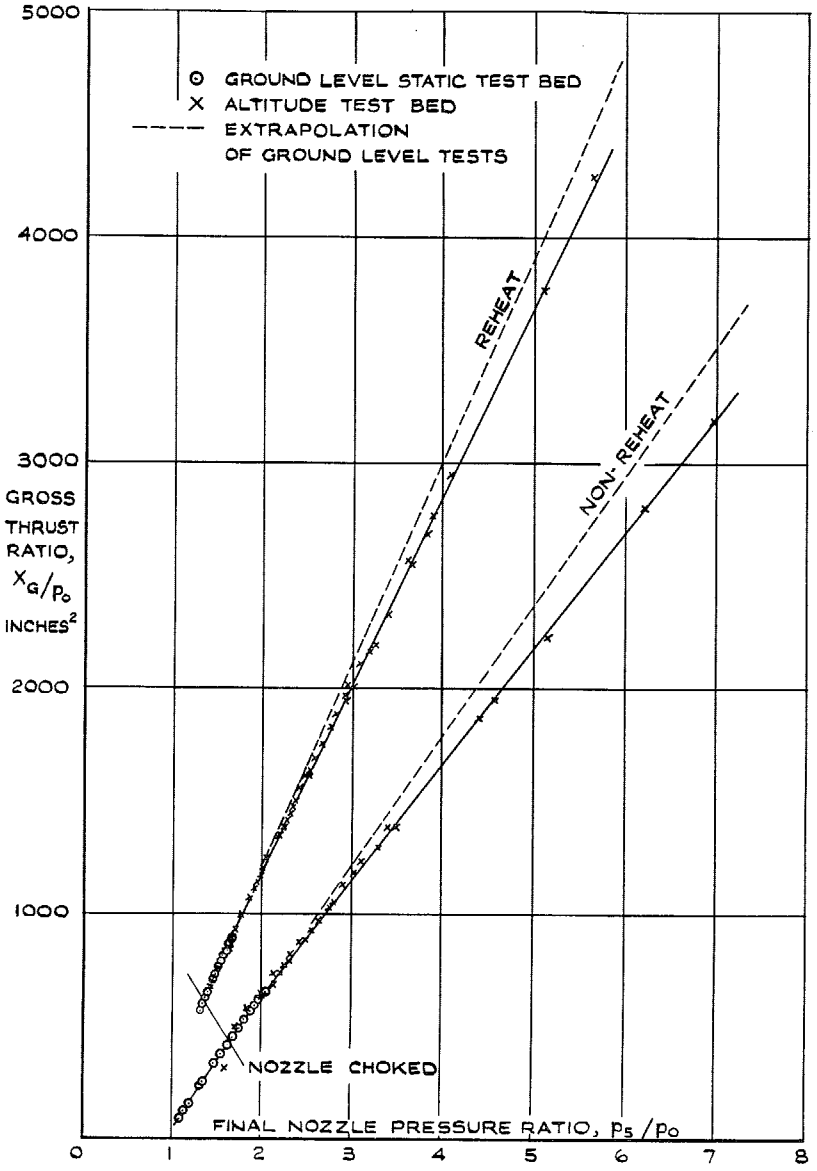


FIG. 18. Calibration of gross thrust against final nozzle pressure ratio.

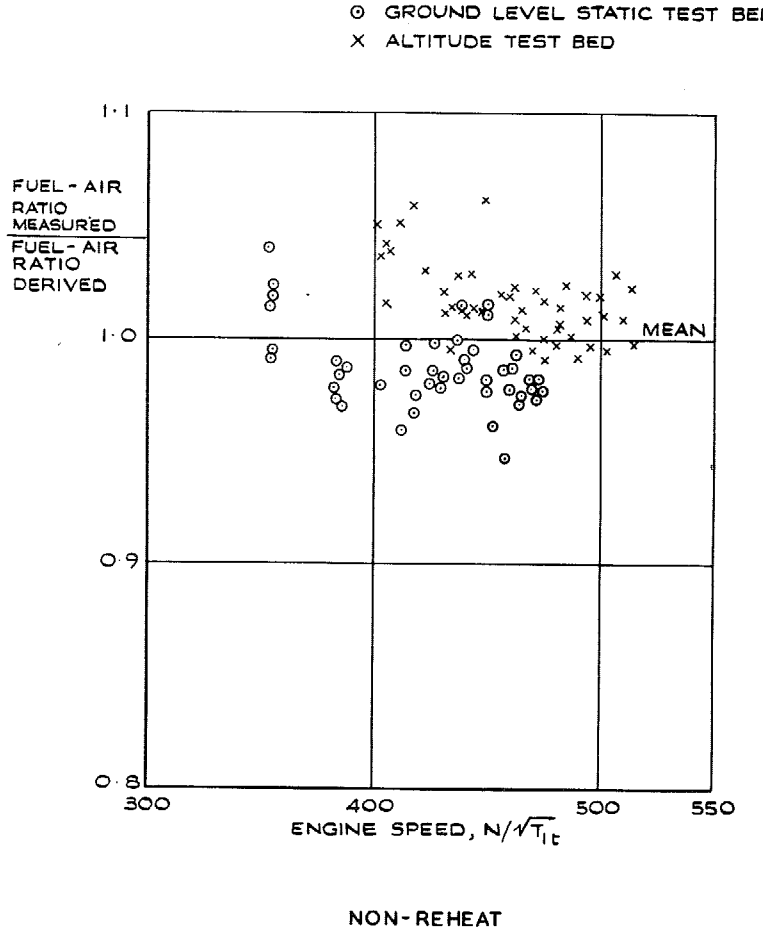


FIG. 19a. Comparison of fuel-air ratios measured and derived.

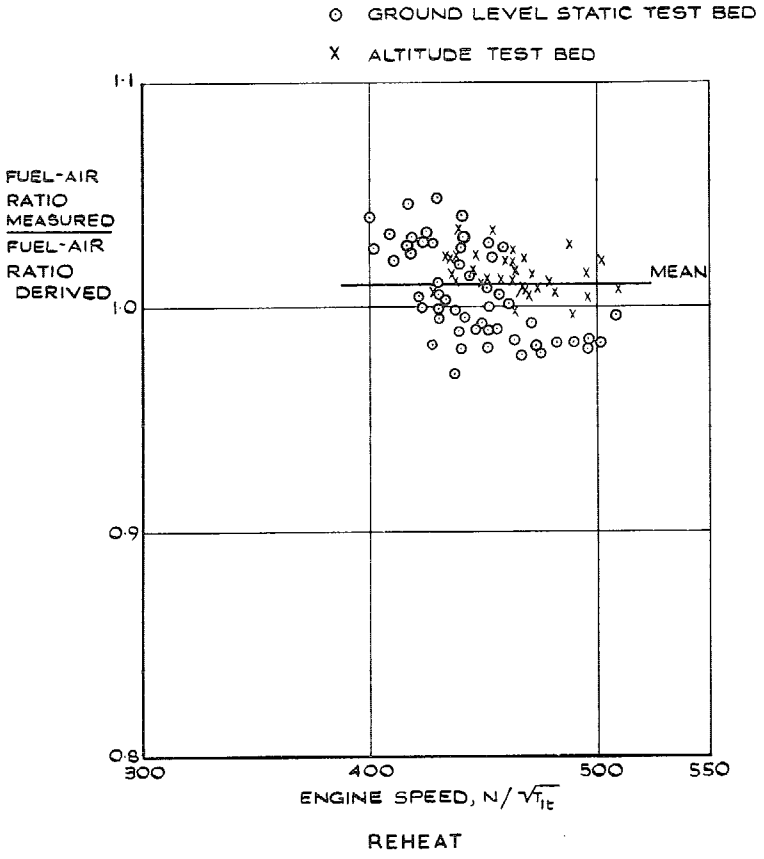


FIG. 19b. Comparison of fuel-air ratios measured and derived.

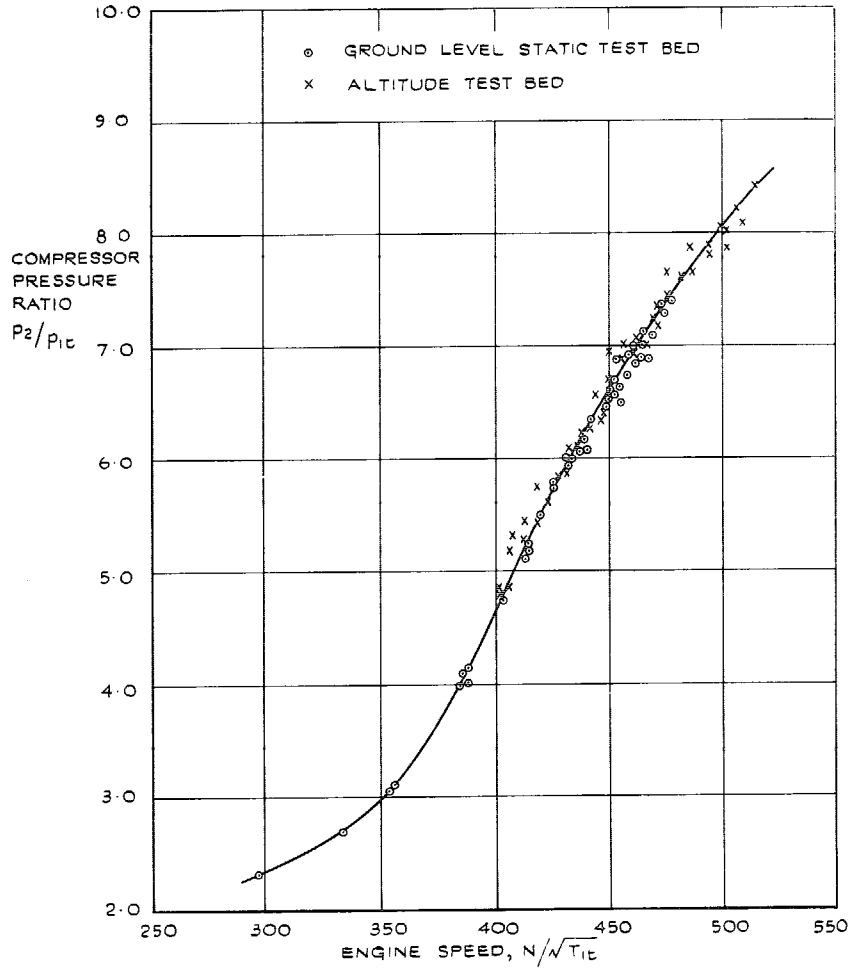


FIG. 20. Variation of compressor pressure ratio with engine speed.

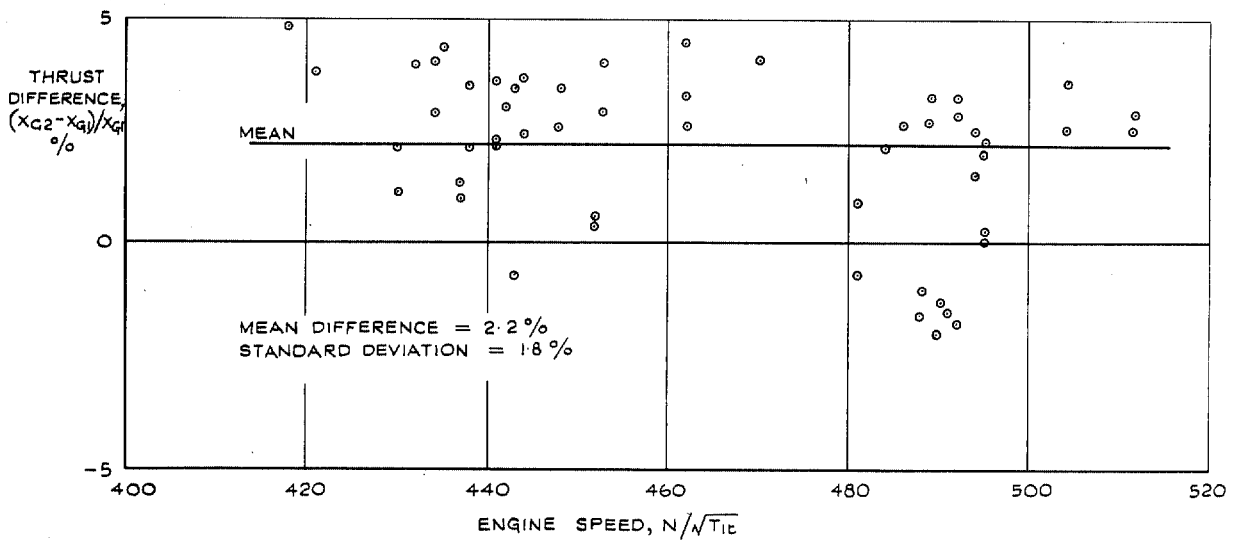


FIG. 21a. Comparison of thrust measurements in flight.

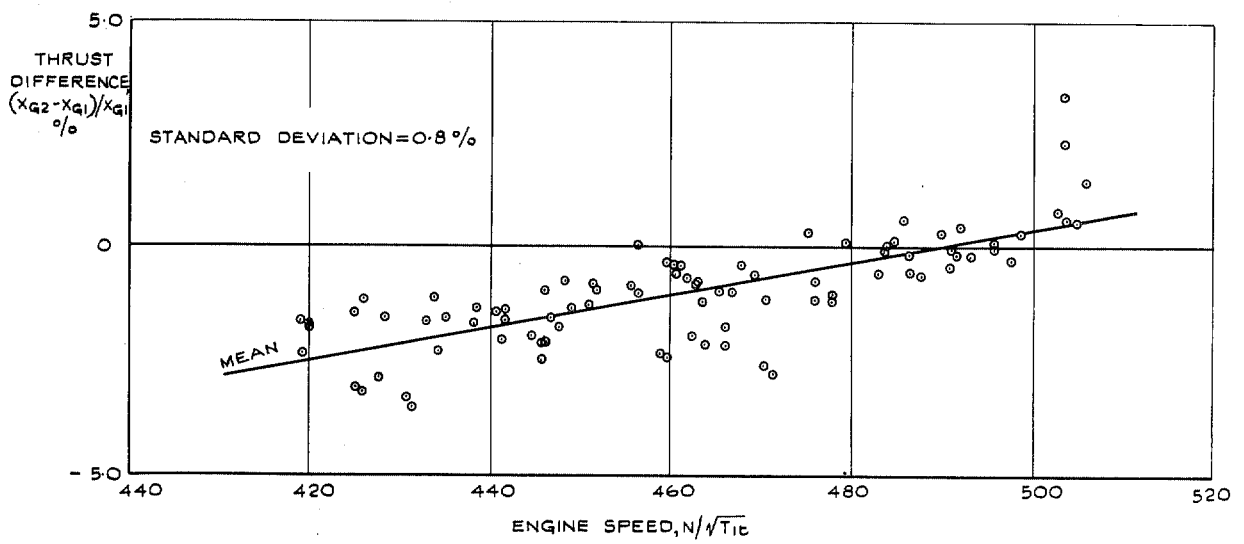


FIG. 21b. Comparison of thrust measurements in flight.

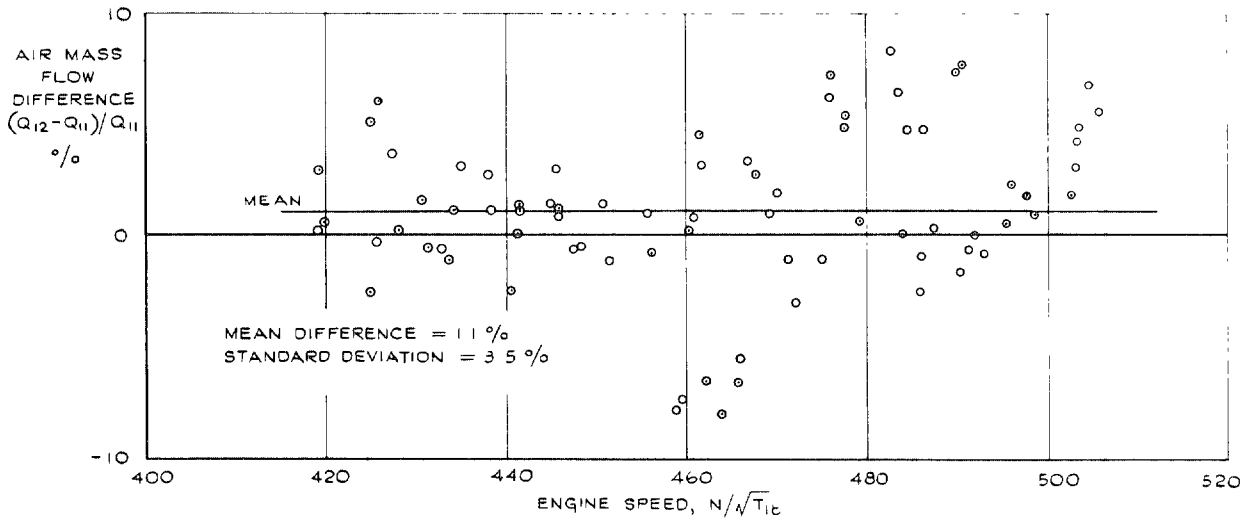


TURBINE NOZZLE GUIDE VANE, $Q_{12}$ AND TRANSITION PIPE, $Q_{11}$, METHODS

FIG. 22a. Comparison of air mass-flow measurements in flight.

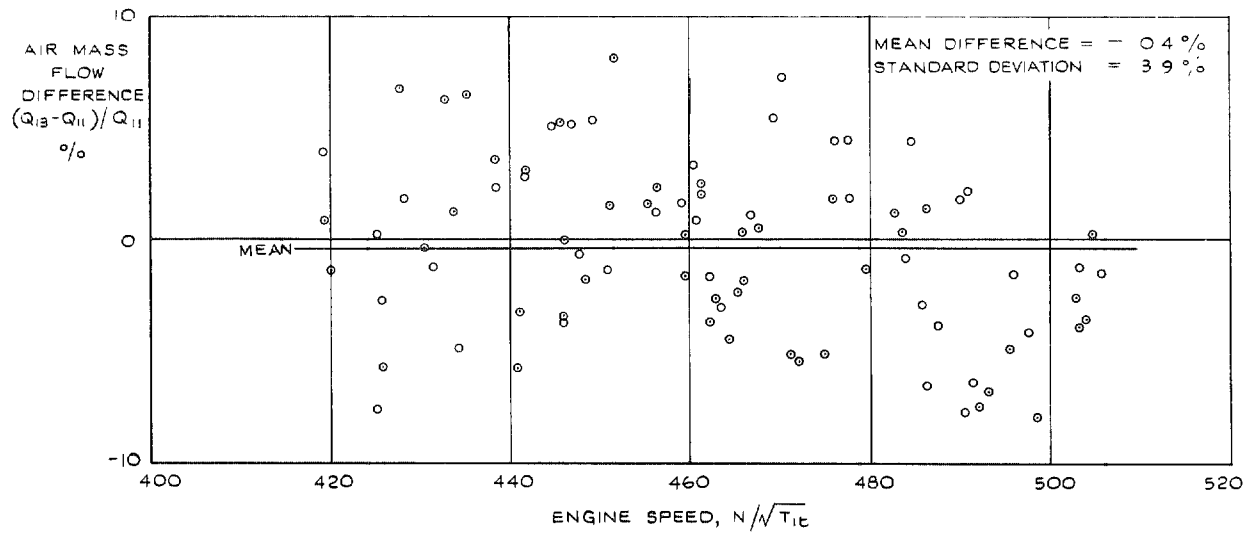


FUEL-AIR RATIO, $Q_{13}$, AND TRANSITION PIPE, $Q_{11}$, METHODS

FIG. 22b. Comparison of air mass-flow measurements in flight.

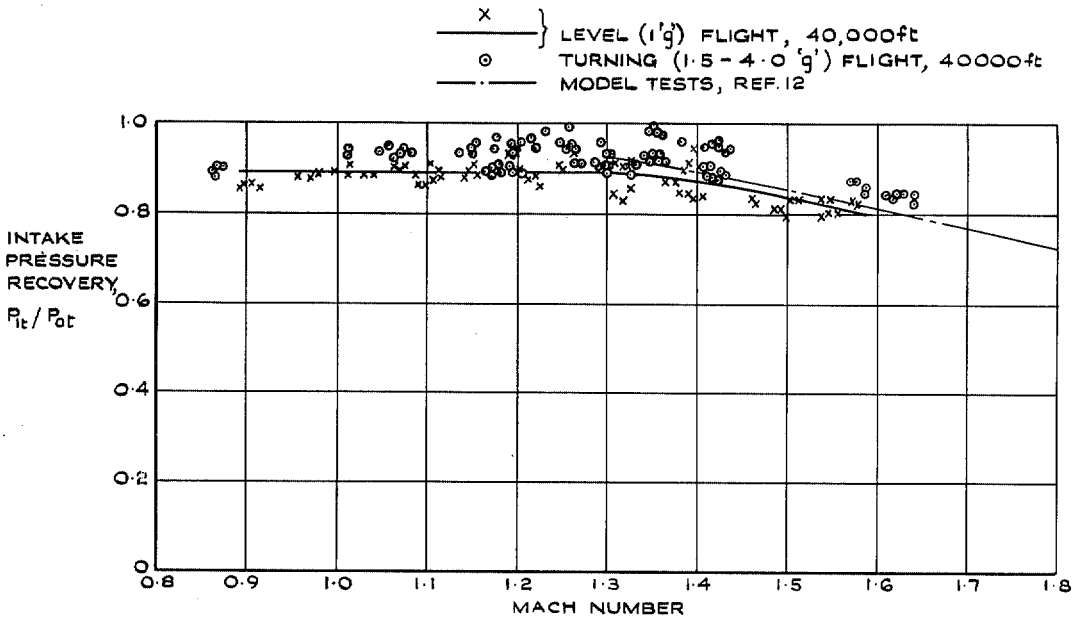


FIG. 23. Variation of intake pressure recovery in flight.

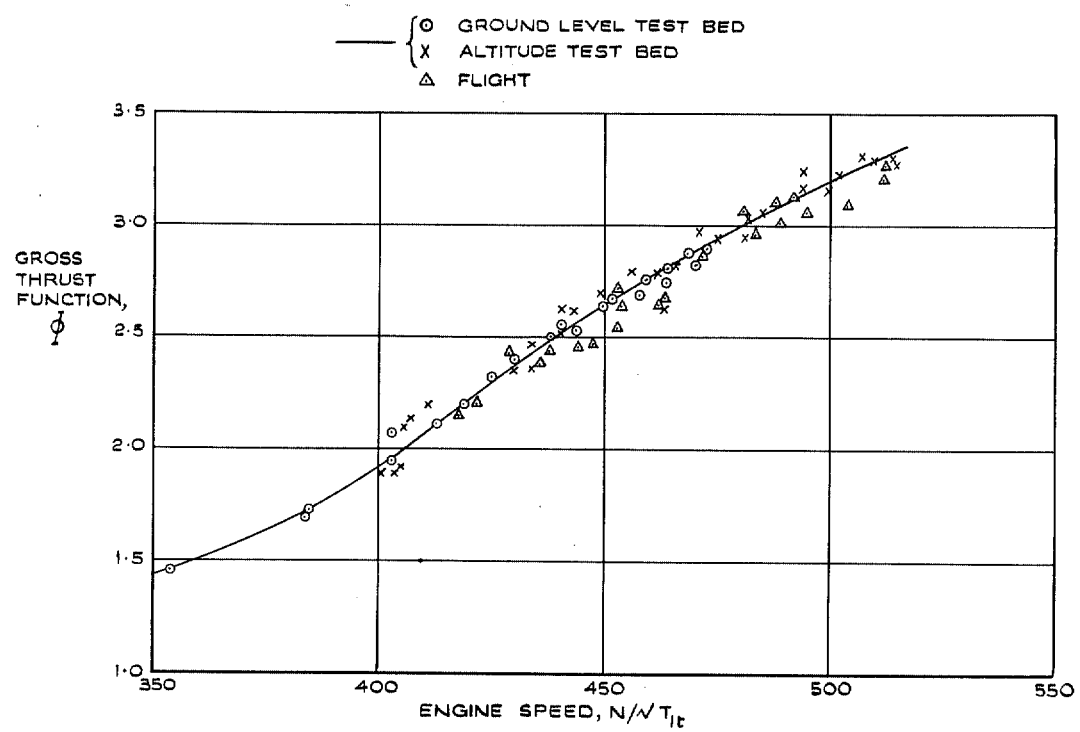


FIG. 24. Gross thrust function—non-reheat.

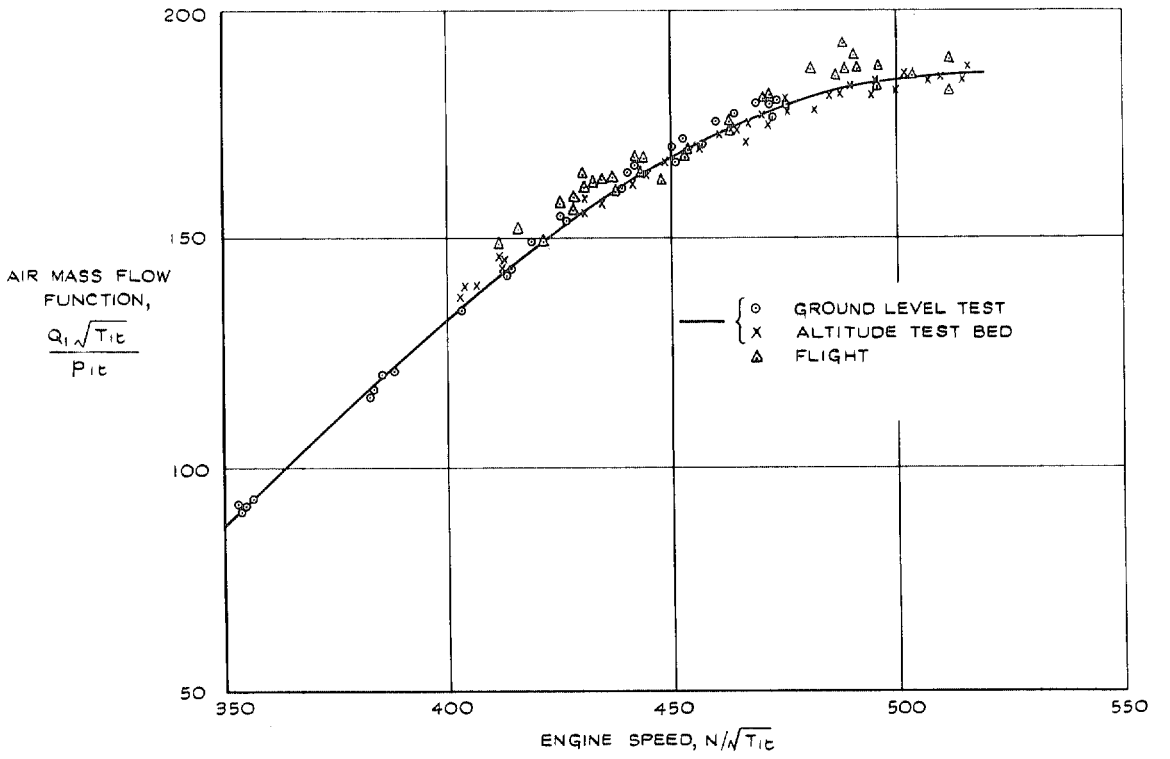


FIG. 25. Air mass-flow function—non-reheat.

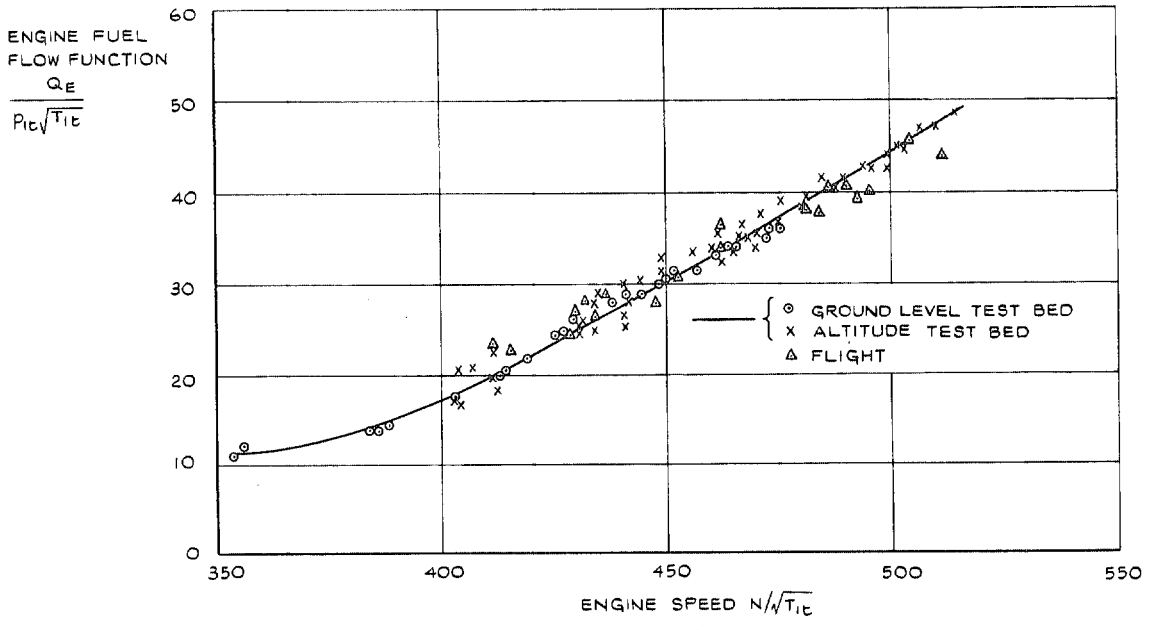


FIG. 26. Engine fuel flow function—non-reheat.

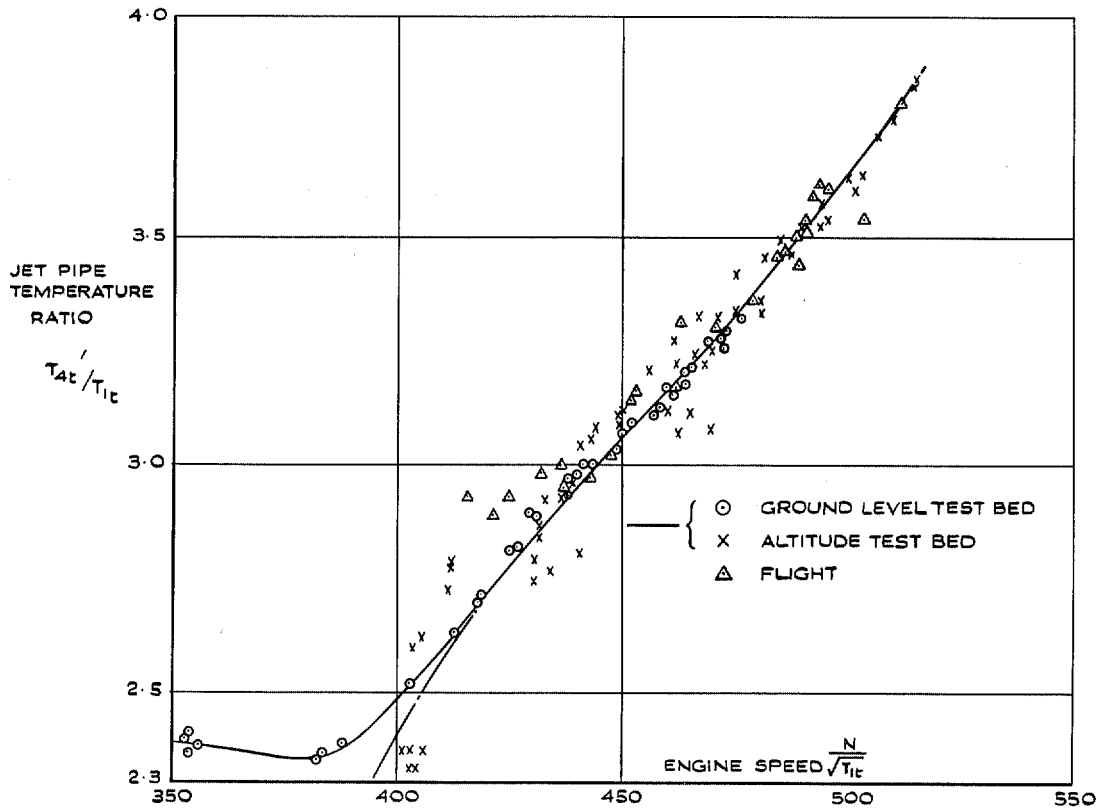


FIG. 27. Jet-pipe temperature ratio—non-reheat.

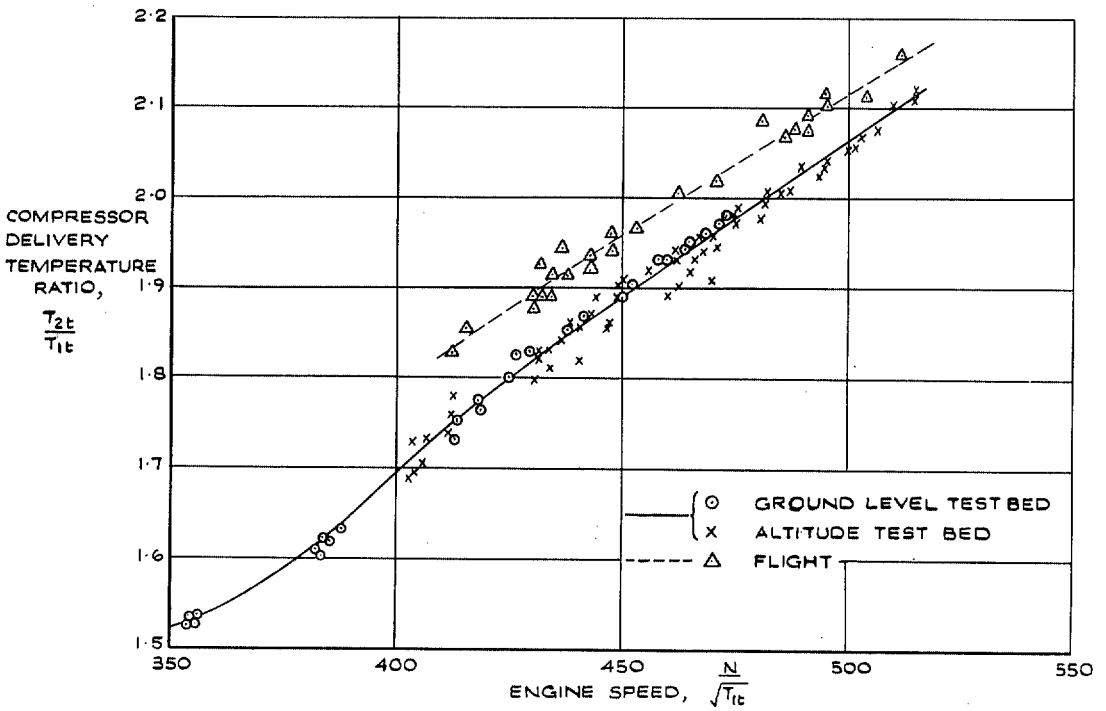


FIG. 28. Compressor delivery temperature ratio—non-reheat.

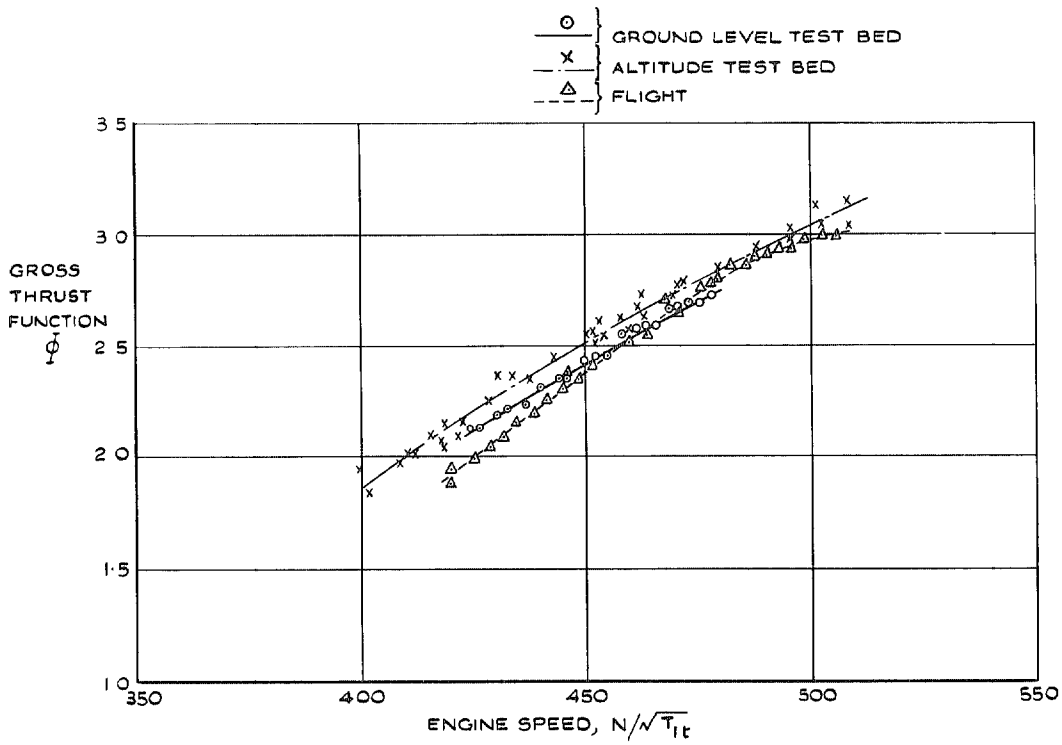


FIG. 29. Gross thrust function—reheat, $p_2/p'_4 = 3{\cdot}43$.

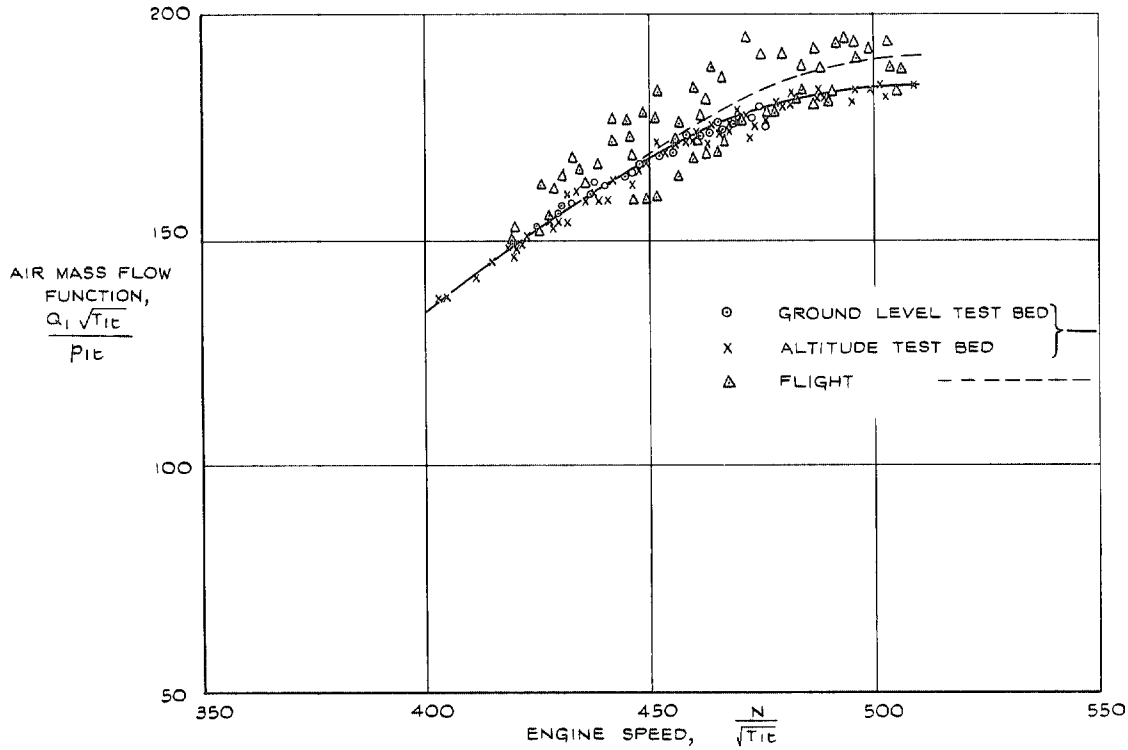


FIG. 30. Air mass-flow function—reheat, $p_2/p'_4 = 3{\cdot}43$.

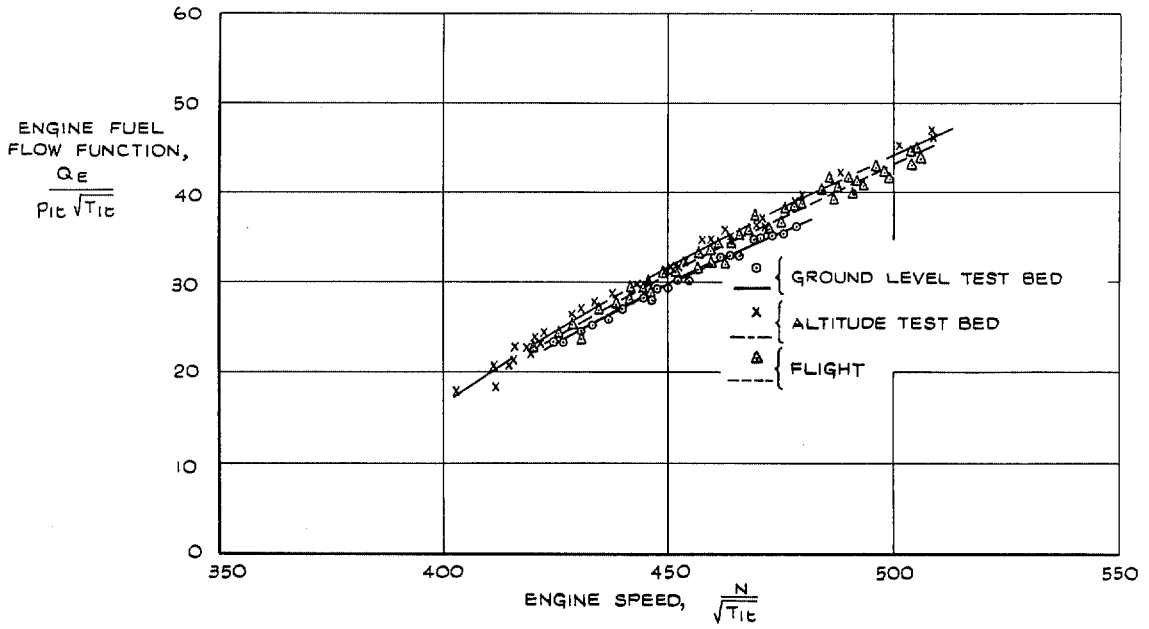


FIG. 31. Engine fuel-flow function—reheat, $p_2/p'_4 = 3{\cdot}43$.

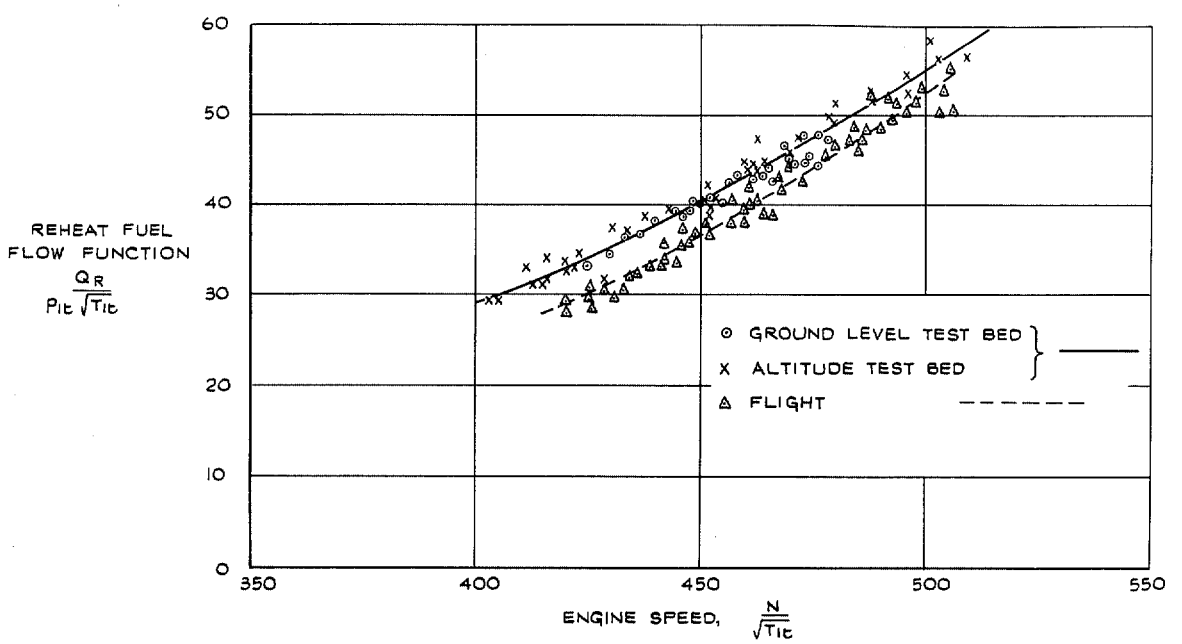


FIG. 32. Reheat fuel-flow function, $p_2/p'_4 = 3{\cdot}43$.

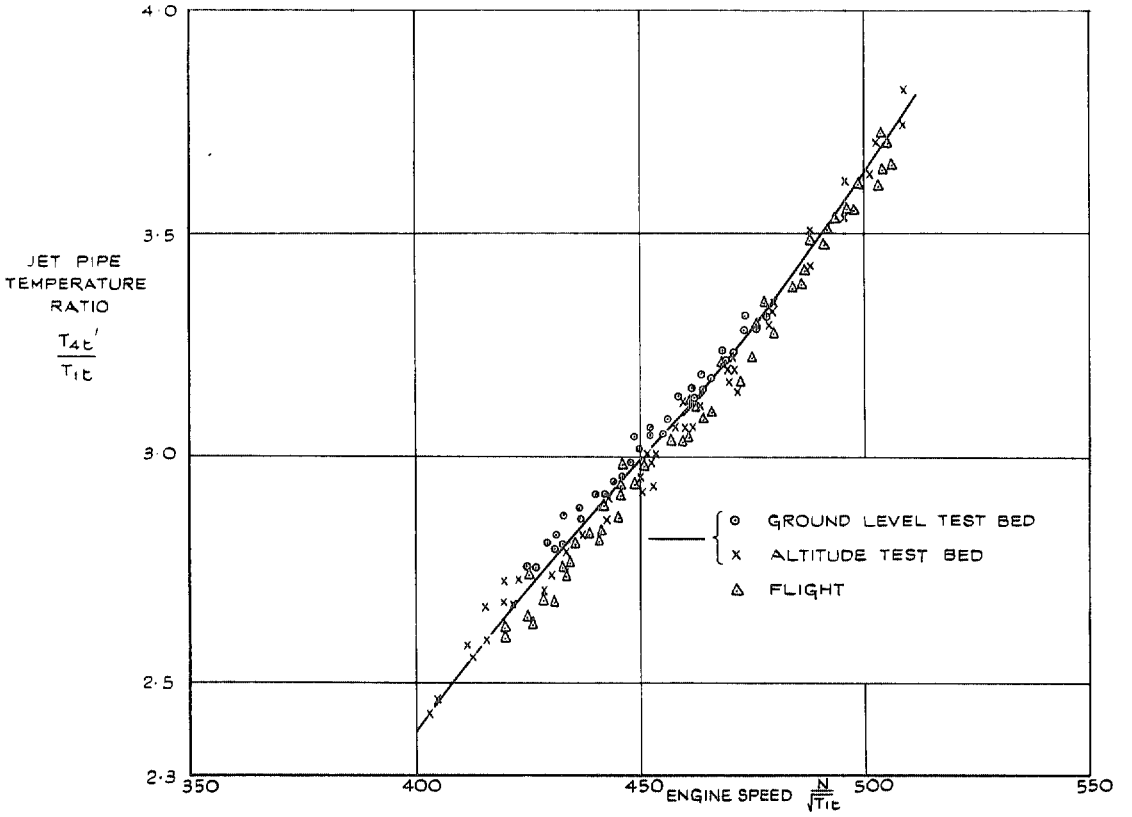


FIG. 33. Jet-pipe temperature ratio—reheat, $p_2/p_4' = 3{\cdot}43$.

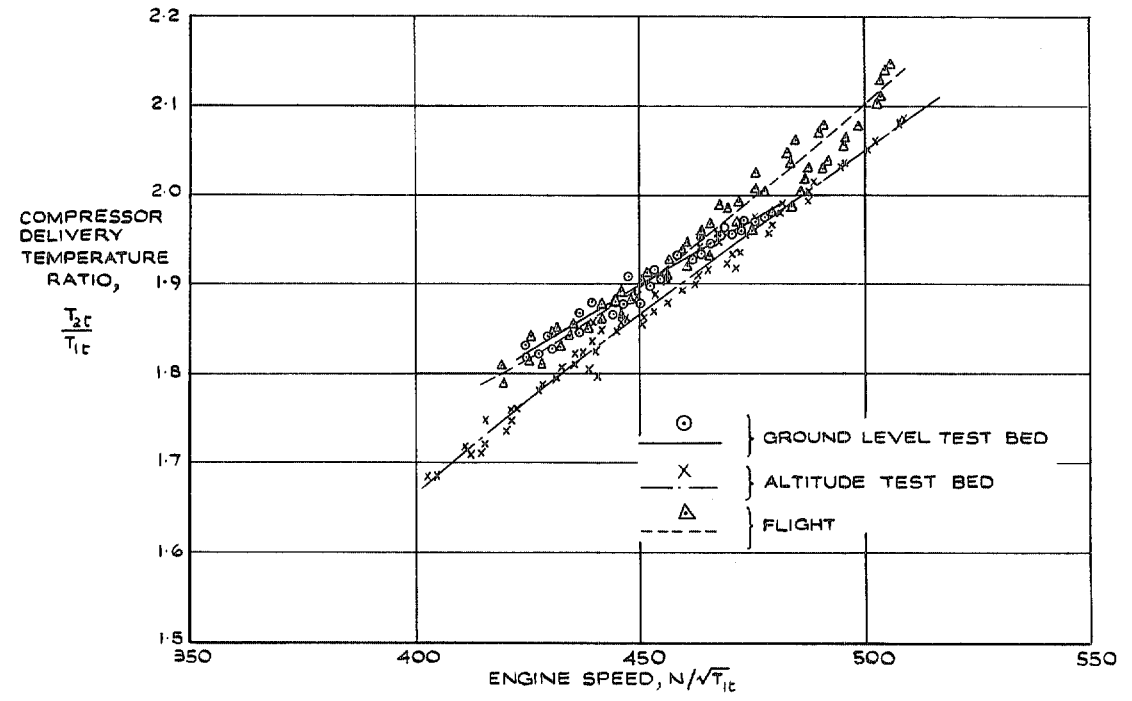


FIG. 34. Compressor delivery temperature ratio—reheat, $p_2/p_4' = 3{\cdot}43$.

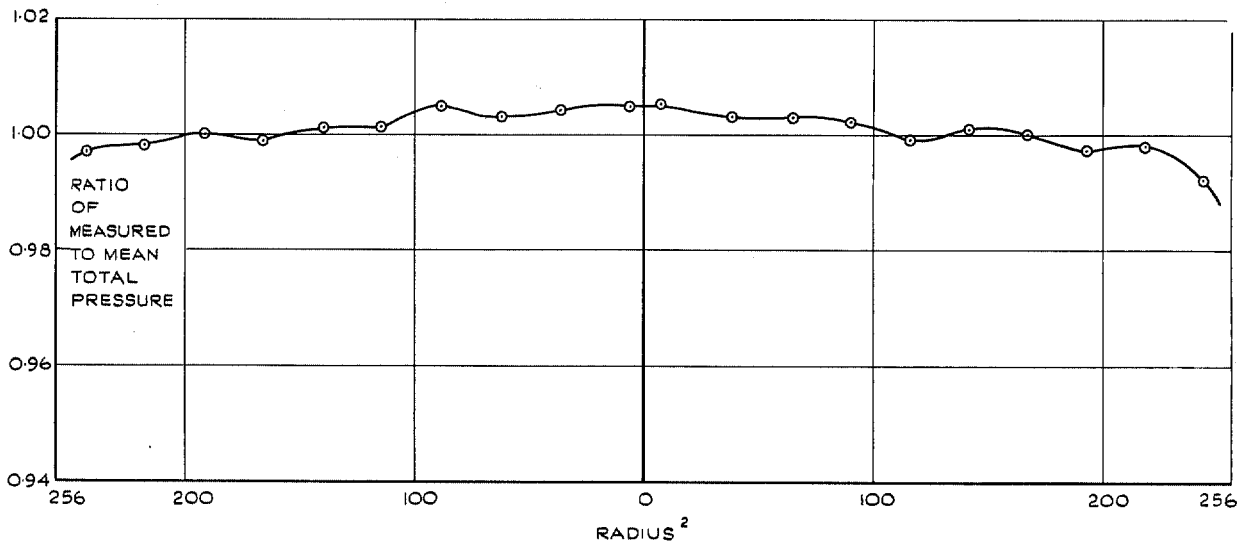


FIG. 35. Typical intake total-pressure distribution for the altitude test bed.

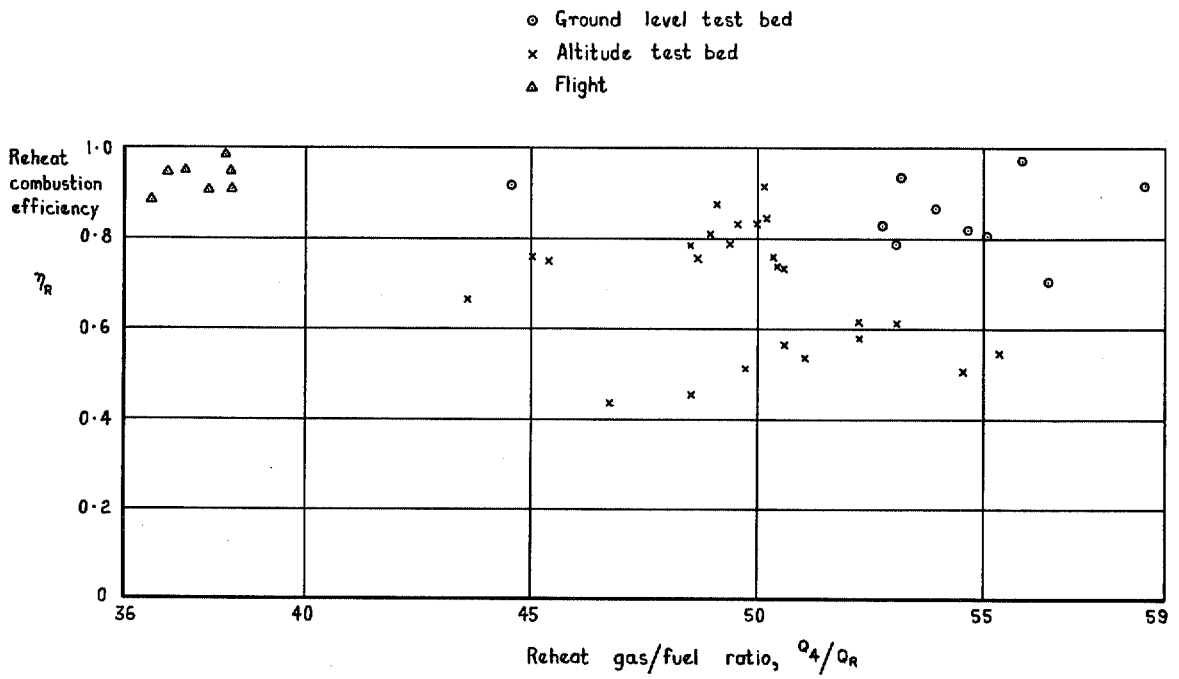


FIG. 36. Reheat combustion efficiency.

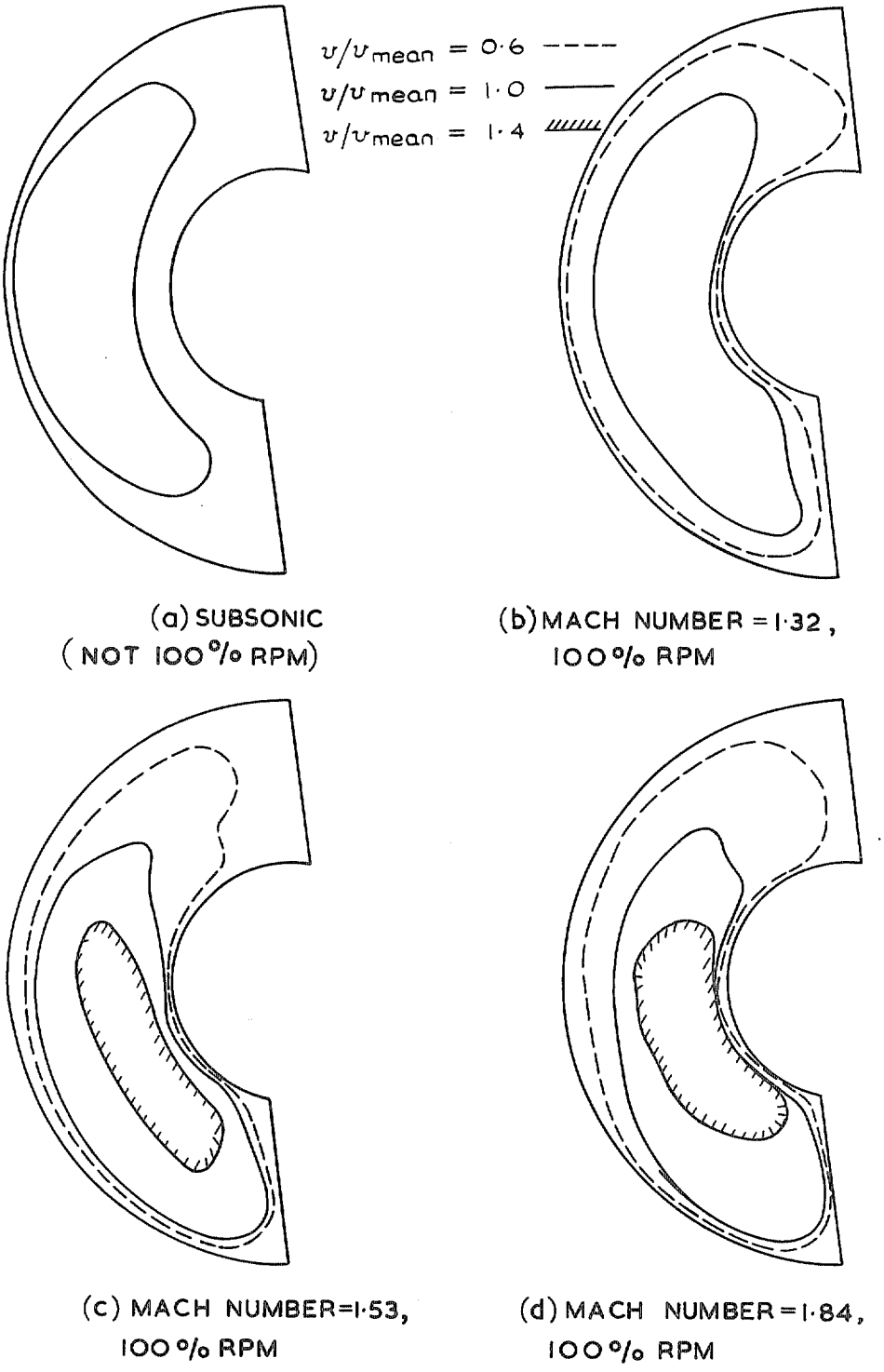


FIG. 37a to d. Fairey Delta 2 intakes. Typical velocity distributions at compressor entry for various flight Mach numbers (model tests, Ref. 12).

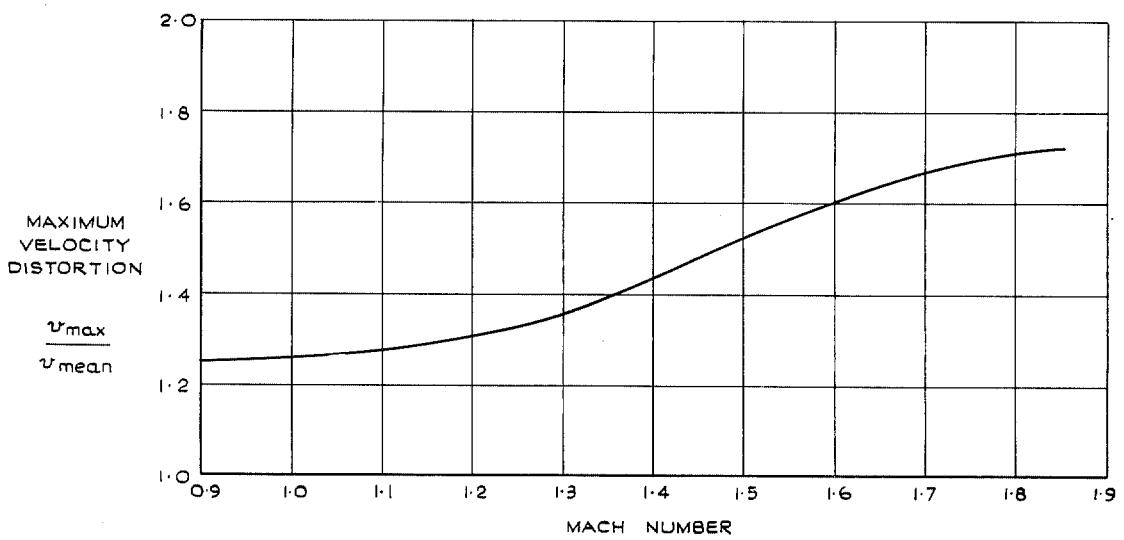


FIG. 38. Fairey Delta 2 intakes. Maximum velocity distortion at compressor entry (model tests, Ref. 12).

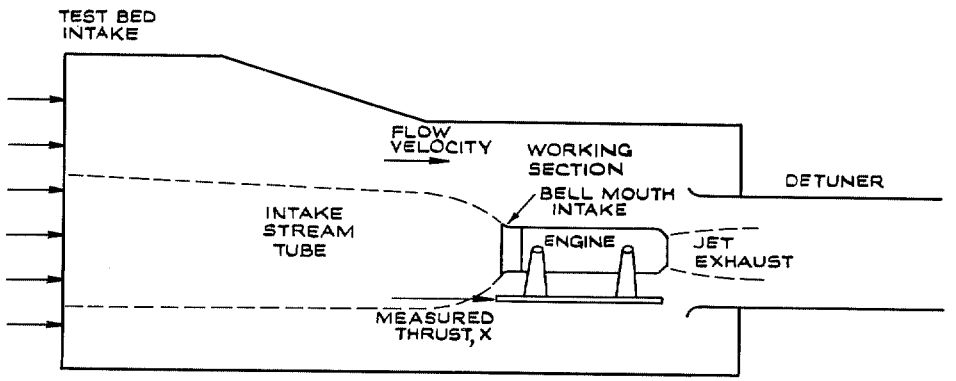


FIG. 39. Schematic arrangement of an engine in the ground-level static test bed.

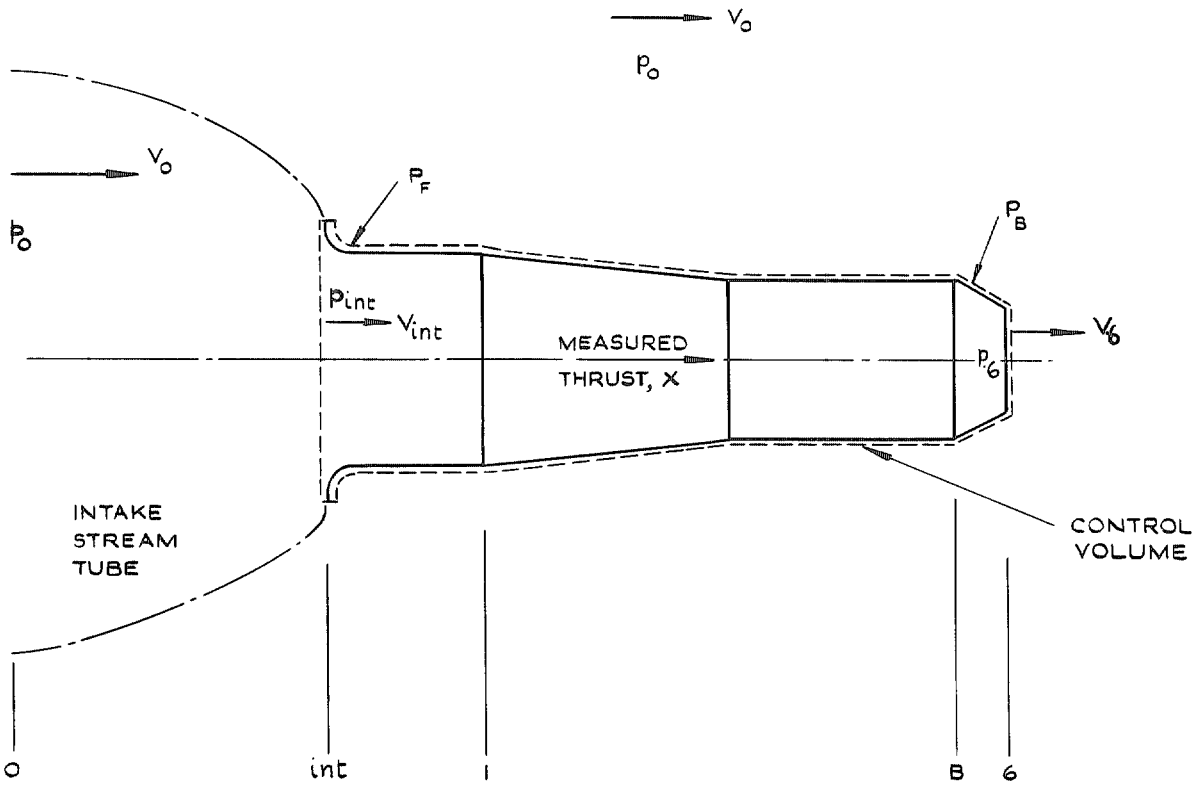


FIG. 40. Control volume, forces and velocities for an engine on a ground-level static test bed.

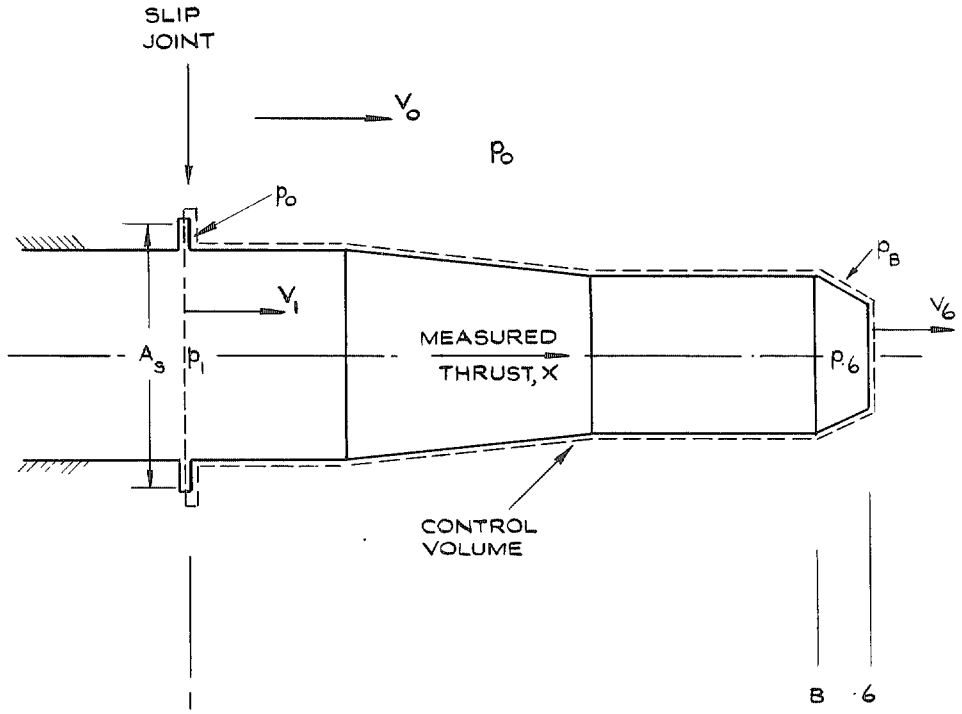


FIG. 41. Control volume, forces and velocities for an engine in a connected intake altitude test bed.

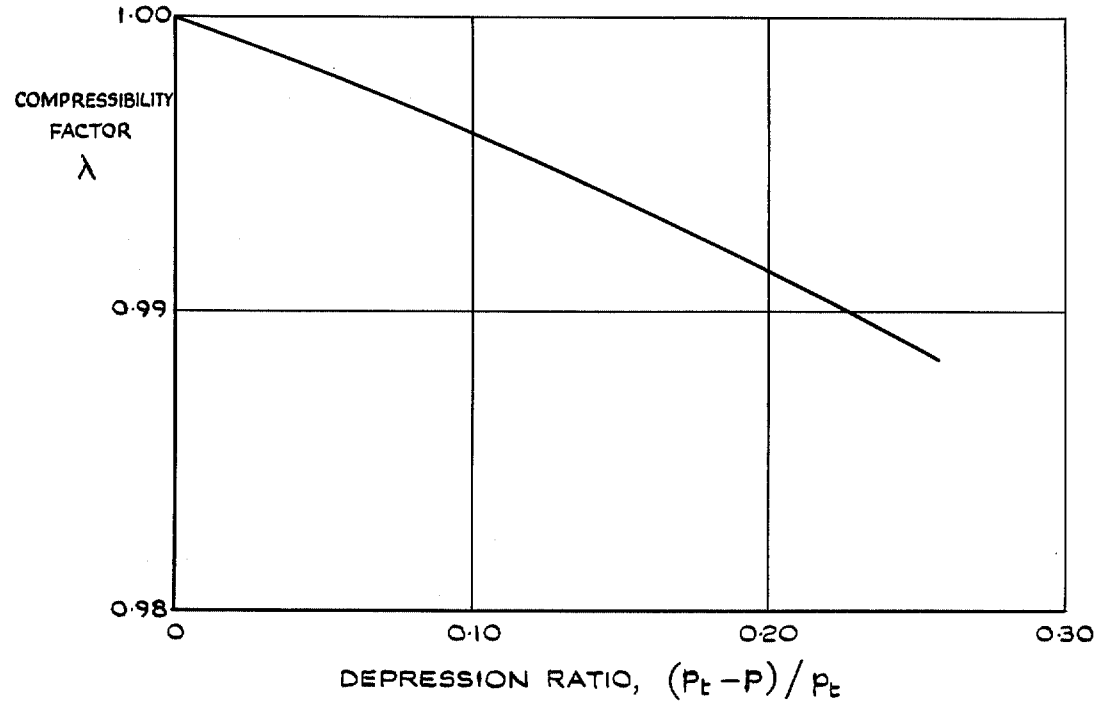


FIG. 42. Variation of the compressibility factor, $\lambda$, with depression ratio, $(p_t - p)/p_t$, $\gamma = 1{\cdot}40$.

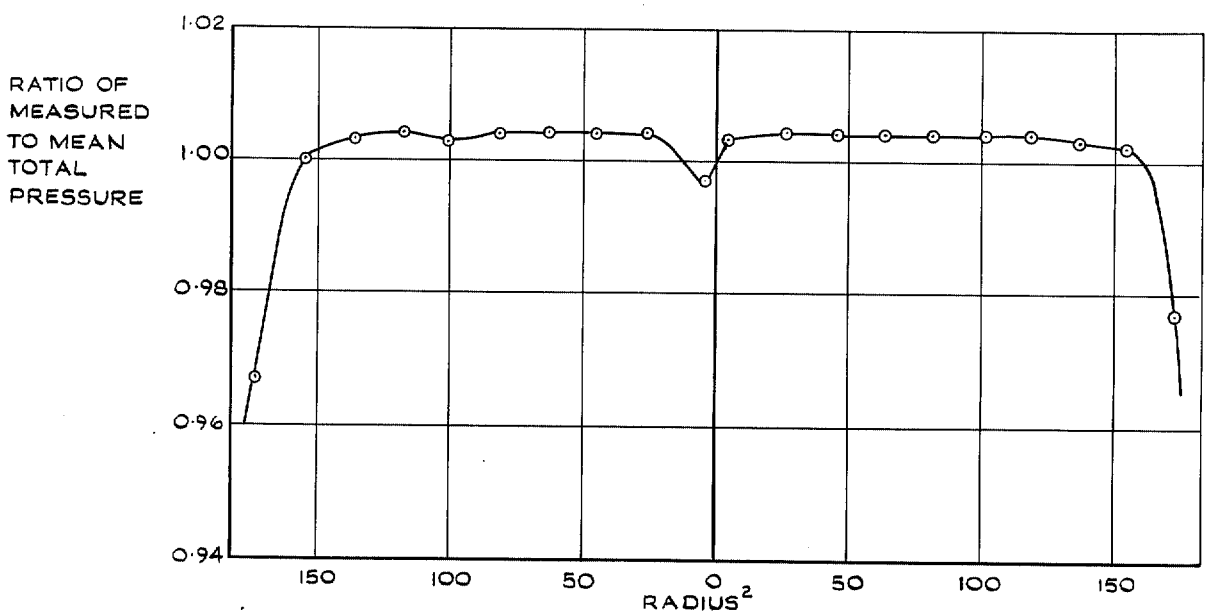


FIG. 43. Typical total-pressure distribution in the air mass-flow measuring section—altitude test bed.

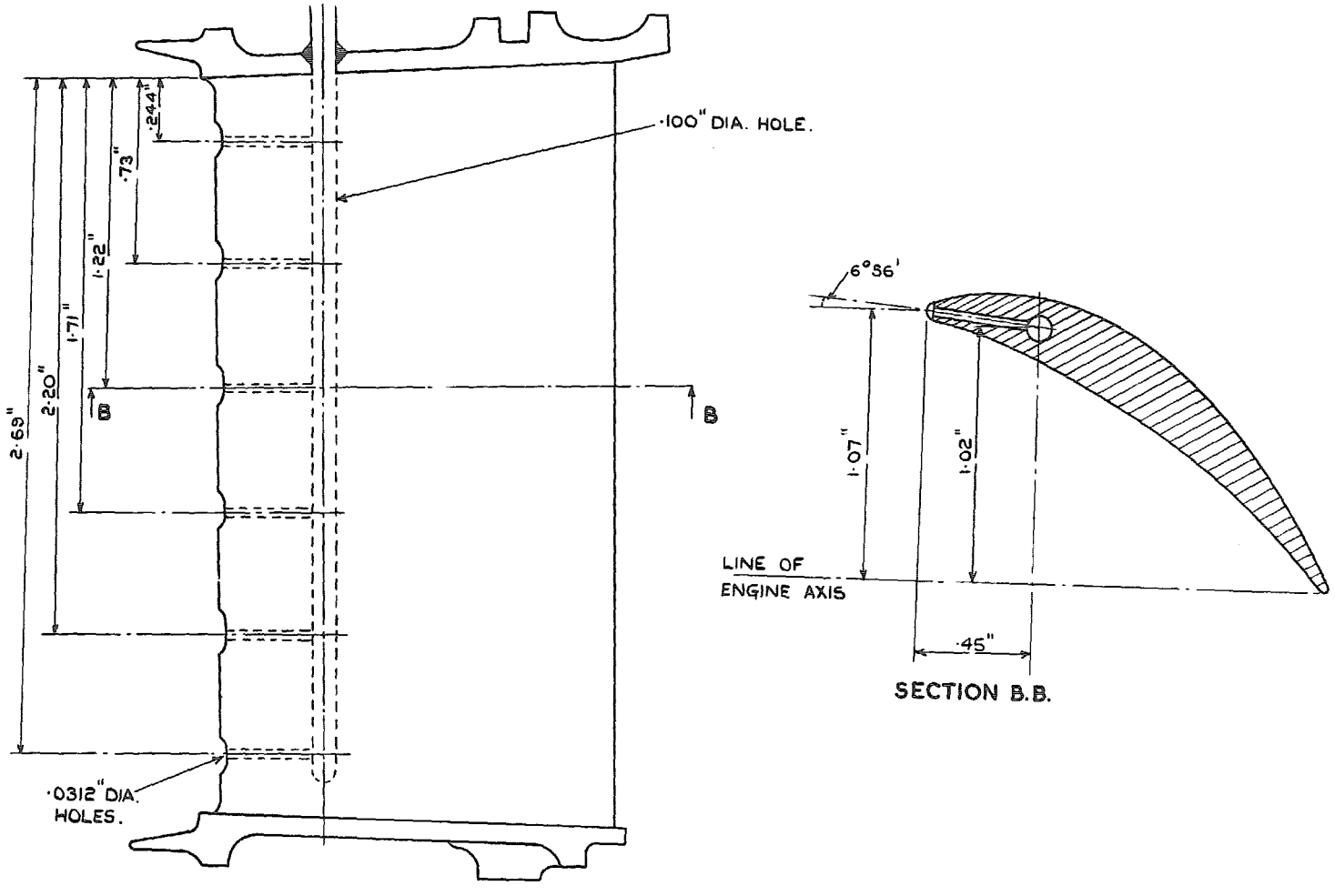


FIG. 44. Modification of nozzle guide vanes to measure total head pressure.

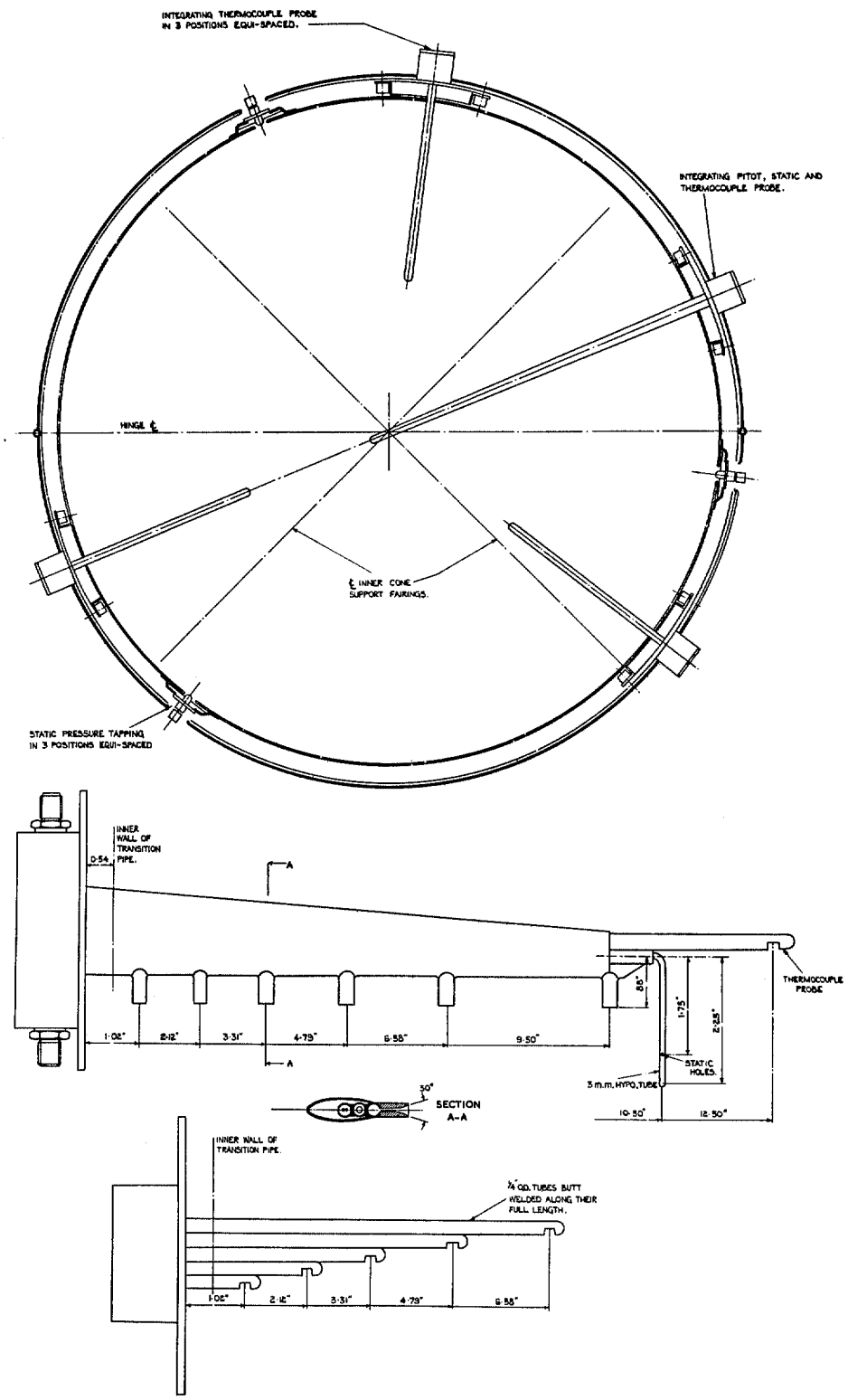


FIG. 45. Layout of transition section instrumentation.

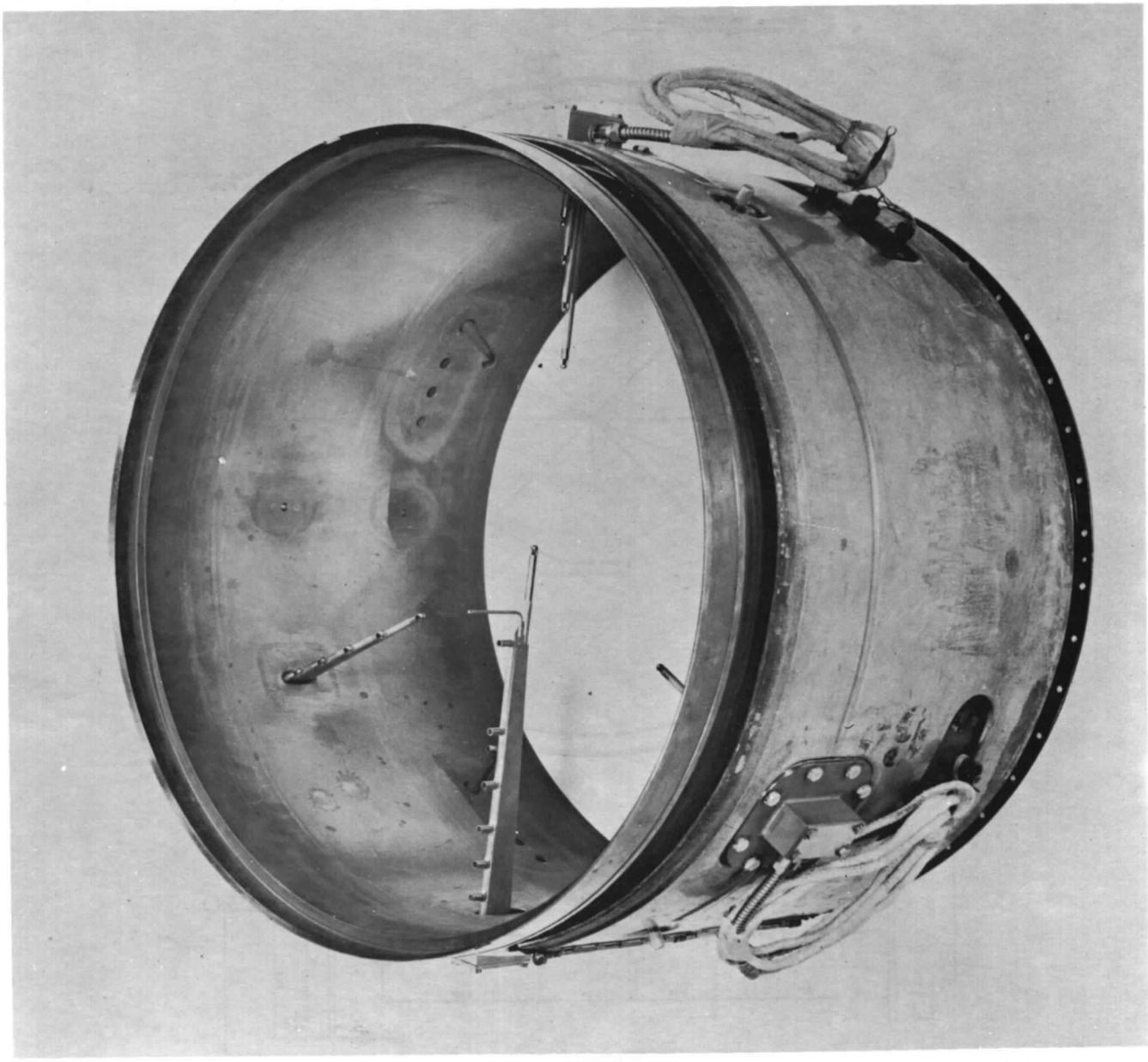

FIG. 46. Instrumented transition section.

Printed in Wales for Her Majesty's Stationery Office by Allens Printers (Wales) Ltd.

Dd.129527 K5

Published by
HER MAJESTY'S STATIONERY OFFICE

To be purchased from
49 High Holborn, London W.C.1
423 Oxford Street, London W.1
13A Castle Street, Edinburgh 2
109 St. Mary Street, Cardiff CF1 1JW
Brazennose Street, Manchester 2
50 Fairfax Street, Bristol 1
258-259 Broad Street, Birmingham 1
7-11 Linenhall Street, Belfast BT2 8AY
or through any bookseller



S.O. Code No. 23-3538